

A Joint *Fermi*-GBM and *Swift*-BAT Analysis of Gravitational-Wave Candidates from the Third Gravitational-wave Observing Run

C. FLETCHER,¹ J. WOOD,² R. HAMBURG,^{3,4,5} P. VERES,^{3,4} C. M. HUI,² E. BISSALDI,^{6,7} M. S. BRIGGS,^{3,4} E. BURNS,⁸
W. H. CLEVELAND,¹ M. M. GILES,⁹ A. GOLDSTEIN,¹ B. A. HRISTOV,¹⁰ D. KOCEVSKI,² S. LESAGE,^{11,4} B. MAILYAN,¹²
C. MALACARIA,¹³ S. POOLAKKIL,^{3,4} A. VON KIENLIN,¹⁴ AND C. A. WILSON-HODGE²
Fermi GAMMA-RAY BURST MONITOR TEAM

M. CRNOGORČEVIĆ,^{15,16,17} J. DELAUNAY,^{18,19,20} A. TOHUVAVOHU,²¹ R. CAPUTO,²² S. B. CENKO,^{22,23} S. LAHA,^{16,24,25} AND
T. PARSOTAN^{16,24,25}

R. ABBOTT,²⁶ H. ABE,²⁷ F. ACERNESE,^{28,29} K. ACKLEY,³⁰ N. ADHIKARI,³¹ R. X. ADHIKARI,²⁶ V. K. ADKINS,³²
V. B. ADYA,³³ C. AFFELDT,^{34,35} D. AGARWAL,³⁶ M. AGATHOS,^{37,38} K. AGATSUMA,³⁹ N. AGGARWAL,⁴⁰ O. D. AGUIAR,⁴¹
L. AIELLO,⁴² A. AIN,⁴³ P. AJITH,⁴⁴ T. AKUTSU,^{45,46} S. ALBANESI,^{47,48} R. A. ALFAIDI,⁴⁹ A. ALLOCCA,^{50,29} P. A. ALTIN,³³
A. AMATO,⁵¹ C. ANAND,³⁰ S. ANAND,²⁶ A. ANANYEVA,²⁶ S. B. ANDERSON,²⁶ W. G. ANDERSON,³¹ M. ANDO,^{52,53}
T. ANDRADE,⁵⁴ N. ANDRES,⁵⁵ M. ANDRÉS-CARCASONA,⁵⁶ T. ANDRIĆ,⁵⁷ S. V. ANGELOVA,⁵⁸ S. ANSOLDI,^{59,60}
J. M. ANTELS,⁶¹ S. ANTIER,^{62,63} T. APOSTOLATOS,⁶⁴ E. Z. APPAVURAVTHER,^{65,66} S. APPERT,²⁶ S. K. APPLE,⁶⁷ K. ARAI,²⁶
A. ARAYA,⁶⁸ M. C. ARAYA,²⁶ J. S. AREEDA,⁶⁹ M. ARÈNE,⁷⁰ N. ARITOMI,⁴⁵ N. ARNAUD,^{71,72} M. AROGETI,⁷³
S. M. ARONSON,³² K. G. ARUN,⁷⁴ H. ASADA,⁷⁵ Y. ASALI,⁷⁶ G. ASHTON,⁷⁷ Y. ASO,^{78,79} M. ASSIDUO,^{80,81}
S. ASSIS DE SOUZA MELO,⁷² S. M. ASTON,⁸² P. ASTONE,⁸³ F. AUBIN,⁸¹ K. AULTONEAL,⁶¹ C. AUSTIN,³² S. BABAK,⁷⁰
F. BADARACCO,⁸⁴ M. K. M. BADER,⁸⁵ C. BADGER,⁸⁶ S. BAE,⁸⁷ Y. BAE,⁸⁸ A. M. BAER,⁸⁹ S. BAGNASCO,⁴⁸ Y. BAI,²⁶
J. BAIRD,⁷⁰ R. BAJPAI,⁹⁰ T. BAKA,⁹¹ M. BALL,⁹² G. BALLARDIN,⁷² S. W. BALLMER,⁹³ A. BALSAMO,⁸⁹ G. BALTUS,⁹⁴
S. BANAGIRI,⁴⁰ B. BANERJEE,⁵⁷ D. BANKAR,³⁶ J. C. BARAYOGA,²⁶ C. BARBIERI,^{95,96,97} B. C. BARISH,²⁶ D. BARKER,⁹⁸
P. BARNEO,⁵⁴ F. BARONE,^{99,29} B. BARR,⁴⁹ L. BARSOTTI,¹⁰⁰ M. BARSUGLIA,⁷⁰ D. BARTA,¹⁰¹ J. BARTLETT,⁹⁸
M. A. BARTON,⁴⁹ I. BARTOS,¹⁰² S. BASAK,⁴⁴ R. BASSIRI,¹⁰³ A. BASTI,^{104,43} M. BAWAJ,^{65,105} J. C. BAYLEY,⁴⁹
M. BAZZAN,^{106,107} B. R. BECHER,¹⁰⁸ B. BÉCSY,¹⁰⁹ V. M. BEDAKIHALE,¹¹⁰ F. BEIRNAERT,¹¹¹ M. BEJGER,¹¹²
I. BELAHCENE,⁷¹ V. BENEDETTO,¹¹³ D. BENIWAL,¹¹⁴ M. G. BENJAMIN,¹¹⁵ T. F. BENNETT,¹¹⁶ J. D. BENTLEY,³⁹
M. BENYAALA,⁵⁸ S. BERA,³⁶ M. BERBEL,¹¹⁷ F. BERGAMIN,^{34,35} B. K. BERGER,¹⁰³ S. BERNUZZI,³⁸ C. P. L. BERRY,⁴⁹
D. BERSANETTI,¹¹⁸ A. BERTOLINI,⁸⁵ J. BETZWIESER,⁸² D. BEVERIDGE,¹¹⁹ R. BHANDARE,¹²⁰ A. V. BHANDARI,³⁶
U. BHARDWAJ,^{63,85} R. BHATT,²⁶ D. BHATTACHARJEE,¹²¹ S. BHAUMIK,¹⁰² A. BIANCHI,^{85,122} I. A. BILENKO,¹²³
G. BILLINGSLEY,²⁶ S. BINI,^{124,125} R. BIRNEY,¹²⁶ O. BIRNHOLTZ,¹²⁷ S. BISCANS,^{26,100} M. BISCHI,^{80,81} S. BISCOVEANU,¹⁰⁰
A. BISHT,^{34,35} B. BISWAS,³⁶ M. BITOSSO,^{72,43} M.-A. BIZOUARD,⁶² J. K. BLACKBURN,²⁶ C. D. BLAIR,¹¹⁹ D. G. BLAIR,¹¹⁹
R. M. BLAIR,⁹⁸ F. BOBBA,^{128,129} N. BODE,^{34,35} M. BOËR,⁶² G. BOGAERT,⁶² M. BOLDRINI,^{130,83} G. N. BOLINGBROKE,¹¹⁴
L. D. BONAVENA,¹⁰⁶ F. BONDU,¹³¹ E. BONILLA,¹⁰³ R. BONNAND,⁵⁵ P. BOOKER,^{34,35} B. A. BOOM,⁸⁵ R. BORK,²⁶
V. BOSCHI,⁴³ N. BOSE,¹³² S. BOSE,³⁶ V. BOSSILKOV,¹¹⁹ V. BOUDART,⁹⁴ Y. BOUFFANAIS,^{106,107} A. BOZZI,⁷²
C. BRADASCHIA,⁴³ P. R. BRADY,³¹ A. BRAMLEY,⁸² A. BRANCH,⁸² M. BRANCHESI,^{57,133} J. E. BRAU,⁹² M. BRESCHI,³⁸
T. BRIANT,¹³⁴ J. H. BRIGGS,⁴⁹ A. BRILLET,⁶² M. BRINKMANN,^{34,35} P. BROCKILL,³¹ A. F. BROOKS,²⁶ J. BROOKS,⁷²
D. D. BROWN,¹¹⁴ S. BRUNETT,²⁶ G. BRUNO,⁸⁴ R. BRUNTZ,⁸⁹ J. BRYANT,³⁹ F. BUCCI,⁸¹ T. BULIK,¹³⁵ H. J. BULTEN,⁸⁵
A. BUONANNO,^{136,137} K. BURTNKY,⁹⁸ R. BUSCICCHIO,³⁹ D. BUSKULIC,⁵⁵ C. BUY,¹³⁸ R. L. BYER,¹⁰³
G. S. CABOURN DAVIES,⁷⁷ G. CABRAS,^{59,60} R. CABRITA,⁸⁴ L. CADONATI,⁷³ M. CAESAR,¹³⁹ G. CAGNOLI,⁵¹ C. CAHILLANE,⁹⁸
J. CALDERÓN BUSTILLO,¹⁴⁰ J. D. CALLAGHAN,⁴⁹ T. A. CALLISTER,^{141,142} E. CALLONI,^{50,29} J. CAMERON,¹¹⁹ J. B. CAMP,¹⁴³
M. CANEPA,^{144,118} S. CANEVAROLO,⁹¹ M. CANNACCIUOLO,¹²⁸ K. C. CANNON,⁵³ H. CAO,¹¹⁴ Z. CAO,¹⁴⁵ E. CAPOCASA,^{70,45}
E. CAPOTE,⁹³ G. CARAPPELLA,^{128,129} F. CARBOGNANI,⁷² M. CARLASSARA,^{34,35} J. B. CARLIN,¹⁴⁶ M. F. CARNEY,⁴⁰
M. CARPINELLI,^{147,148,72} G. CARRILLO,⁹² G. CARULLO,^{104,43} T. L. CARVER,⁴² J. CASANUEVA DIAZ,⁷² C. CASENTINI,^{149,150}
G. CASTALDI,¹⁵¹ S. CAUDILL,^{85,91} M. CAVAGLIÀ,¹²¹ F. CAVALIER,⁷¹ R. CAVALIERI,⁷² G. CELLA,⁴³ P. CERDÁ-DURÁN,¹⁵²
E. CESARINI,¹⁵⁰ W. CHAIBI,⁶² S. CHALATHADKA SUBRAHMANYA,¹⁵³ E. CHAMPION,¹⁵⁴ C.-H. CHAN,¹⁵⁵ C. CHAN,⁵³
C. L. CHAN,¹⁵⁶ K. CHAN,¹⁵⁶ M. CHAN,¹⁵⁷ K. CHANDRA,¹³² I. P. CHANG,¹⁵⁵ P. CHANIAL,⁷² S. CHAO,¹⁵⁵
C. CHAPMAN-BIRD,⁴⁹ P. CHARLTON,¹⁵⁸ E. A. CHASE,⁴⁰ E. CHASSANDE-MOTTIN,⁷⁰ C. CHATTERJEE,¹¹⁹
DEBARATI CHATTERJEE,³⁶ DEEP CHATTERJEE,³¹ M. CHATURVEDI,¹²⁰ S. CHATY,⁷⁰ C. CHEN,^{159,155} D. CHEN,⁷⁸
H. Y. CHEN,¹⁰⁰ J. CHEN,¹⁵⁵ K. CHEN,¹⁶⁰ X. CHEN,¹¹⁹ Y.-B. CHEN,¹⁶¹ Y.-R. CHEN,¹⁵⁵ Z. CHEN,⁴² H. CHENG,¹⁰²
C. K. CHEONG,¹⁵⁶ H. Y. CHEUNG,¹⁵⁶ H. Y. CHIA,¹⁰² F. CHIADINI,^{162,129} C.-Y. CHIANG,¹⁶³ G. CHIARINI,¹⁰⁷ R. CHERICI,¹⁶⁴
A. CHINCARINI,¹¹⁸ M. L. CHIOFALO,^{104,43} A. CHIUMMO,⁷² R. K. CHOUDHARY,¹¹⁹ S. CHOUDHARY,³⁶ N. CHRISTENSEN,⁶²
Q. CHU,¹¹⁹ Y.-K. CHU,¹⁶³ S. S. Y. CHUA,³³ K. W. CHUNG,⁸⁶ G. CIANI,^{106,107} P. CIECIELAG,¹¹² M. CIEŚLAR,¹¹²
M. CIFALDI,^{149,150} A. A. CIOBANU,¹¹⁴ R. CIOLFI,^{165,107} F. CIPRIANO,⁶² F. CLARA,⁹⁸ J. A. CLARK,^{26,73} P. CLEARWATER,¹⁶⁶
S. CLESSE,¹⁶⁷ F. CLEVA,⁶² E. COCCIA,^{57,133} E. CODAZZO,⁵⁷ P.-F. COHADON,¹³⁴ D. E. COHEN,⁷¹ M. COLLEONI,¹⁶⁸
C. G. COLLETTE,¹⁶⁹ A. COLOMBO,^{95,96} M. COLPI,^{95,96} C. M. COMPTON,⁹⁸ M. CONSTANCIO JR.,⁴¹ L. CONTI,¹⁰⁷
S. J. COOPER,³⁹ P. CORBAN,⁸² T. R. CORBITT,³² I. CORDERO-CARRIÓN,¹⁷⁰ S. COREZZI,^{105,65} K. R. CORLEY,⁷⁶
N. J. CORNISH,¹⁰⁹ D. CORRE,⁷¹ A. CORSI,¹⁷¹ S. CORTESE,⁷² C. A. COSTA,⁴¹ R. COTESTA,¹³⁷ R. COTTINGHAM,⁸²

- M. W. COUGHLIN,¹⁷² J.-P. COULON,⁶² S. T. COUNTRYMAN,⁷⁶ B. COUSINS,¹⁷³ P. COUVARES,²⁶ D. M. COWARD,¹¹⁹
M. J. COWART,⁸² D. C. COYNE,²⁶ R. COYNE,¹⁷⁴ J. D. E. CREIGHTON,³¹ T. D. CREIGHTON,¹¹⁵ A. W. CRISWELL,¹⁷²
M. CROQUETTE,¹³⁴ S. G. CROWDER,¹⁷⁵ J. R. CUDELL,⁹⁴ T. J. CULLEN,³² A. CUMMING,⁴⁹ R. CUMMINGS,⁴⁹
L. CUNNINGHAM,⁴⁹ E. CUOCO,^{72,176,43} M. CURYŁO,¹³⁵ P. DABADIE,⁵¹ T. DAL CANTON,⁷¹ S. DALL'OSSO,⁵⁷ G. DÁLYA,^{111,177}
A. DANA,¹⁰³ B. D'ANGELO,^{144,118} S. DANILISHIN,^{178,85} S. D'ANTONIO,¹⁵⁰ K. DANZMANN,^{34,35} C. DARSOW-FROMM,¹⁵³
A. DASGUPTA,¹¹⁰ L. E. H. DATRIER,⁴⁹ SAYAK DATTA,³⁶ SAYANTANI DATTA,⁷⁴ V. DATTILO,⁷² I. DAVE,¹²⁰ M. DAVIER,⁷¹
D. DAVIS,²⁶ M. C. DAVIS,¹³⁹ E. J. DAW,¹⁷⁹ R. DEAN,¹³⁹ D. DEBRA,¹⁰³ M. DEENADAYALAN,³⁶ J. DEGALLAIX,¹⁸⁰
M. DE LAURENTIS,^{50,29} S. DELÉGLISE,¹³⁴ V. DEL FAVERO,¹⁵⁴ F. DE LILLO,⁸⁴ N. DE LILLO,⁴⁹ D. DELL'AQUILA,¹⁴⁷
W. DEL POZZO,^{104,43} L. M. DEMARCHI,⁴⁰ F. DE MATTEIS,^{149,150} V. D'EMILIO,⁴² N. DEMOS,¹⁰⁰ T. DENT,¹⁴⁰ A. DEPASSE,⁸⁴
R. DE PIETRI,^{181,182} R. DE ROSA,^{50,29} C. DE ROSSI,⁷² R. DESALVO,^{151,183} R. DE SIMONE,¹⁶² S. DHURANDHAR,³⁶
M. C. DÍAZ,¹¹⁵ N. A. DIDIO,⁹³ T. DIETRICH,¹³⁷ L. DI FIORE,²⁹ C. DI FRONZO,³⁹ C. DI GIORGIO,^{128,129} F. DI GIOVANNI,¹⁵²
M. DI GIOVANNI,⁵⁷ T. DI GIROLAMO,^{50,29} A. DI LIETO,^{104,43} A. DI MICHELE,¹⁰⁵ B. DING,¹⁶⁹ S. DI PACE,^{130,83}
I. DI PALMA,^{130,83} F. DI RENZO,^{104,43} A. K. DIVAKARLA,¹⁰² A. DMITRIEV,³⁹ Z. DOCTOR,⁴⁰ L. DONAHUE,¹⁸⁴
L. D'ONOFRIO,^{50,29} F. DONOVAN,¹⁰⁰ K. L. DOOLEY,⁴² S. DORAVARI,³⁶ M. DRAGO,^{130,83} J. C. DRIGGERS,⁹⁸ Y. DRORI,²⁶
J.-G. DUCOIN,⁷¹ P. DUPEJ,⁴⁹ U. DUPLETSYA,^{128,129} O. DURANTE,^{128,129} D. D'URSO,^{147,148} P.-A. DUVERNE,⁷¹ S. E. DWYER,⁹⁸
C. EASSA,⁹⁸ P. J. EASTER,³⁰ M. EBERSOLD,¹⁸⁵ T. ECKHARDT,¹⁵³ G. EDDOLLS,⁴⁹ B. EDELMAN,⁹² T. B. EDO,²⁶ O. EDY,⁷⁷
A. EFFLER,⁸² S. EGUCHI,¹⁵⁷ J. EICHHOLZ,³³ S. S. EIKENBERRY,¹⁰² M. EISENMANN,^{55,45} R. A. EISENSTEIN,¹⁰⁰ A. EJLLI,⁴²
E. ENGELBY,⁶⁹ Y. ENOMOTO,⁵² L. ERRICO,^{50,29} R. C. ESSICK,¹⁸⁶ H. ESTELLÉS,¹⁶⁸ D. ESTEVEZ,¹⁸⁷ Z. ETIENNE,¹⁸⁸
T. ETZEL,²⁶ M. EVANS,¹⁰⁰ T. M. EVANS,⁸² T. EVSTAFYEVA,³⁷ B. E. EWING,¹⁷³ F. FABRIZI,^{80,81} F. FAEDI,⁸¹
V. FAFONE,^{149,150,57} H. FAIR,⁹³ S. FAIRHURST,⁴² P. C. FAN,¹⁸⁴ A. M. FARAH,¹⁸⁹ S. FARINON,¹¹⁸ B. FARR,⁹²
W. M. FARR,^{141,142} E. J. FAUCHON-JONES,⁴² G. FAVARO,¹⁰⁶ M. FAVATA,¹⁹⁰ M. FAYS,⁹⁴ M. FAZIO,¹⁹¹ J. FEICHT,²⁶
M. M. FEJER,¹⁰³ E. FENYVESI,^{101,192} D. L. FERGUSON,¹⁹³ A. FERNANDEZ-GALIANA,¹⁰⁰ I. FERRANTE,^{104,43}
T. A. FERREIRA,⁴¹ F. FIDECARO,^{104,43} P. FIGURA,¹³⁵ A. FIORI,^{43,104} I. FIORI,⁷² M. FISHBACH,⁴⁰ R. P. FISHER,⁸⁹
R. FITTIPALDI,^{194,129} V. FIUMARA,^{195,129} R. FLAMINIO,^{55,45} E. FLODEN,¹⁷² H. K. FONG,⁵³ J. A. FONT,^{152,196} B. FORMAL,¹⁸³
P. W. F. FORSYTH,³³ A. FRANKE,¹⁵³ S. FRASCA,^{130,83} F. FRASCONI,⁴³ J. P. FREED,⁶¹ Z. FREI,¹⁷⁷ A. FREISE,^{85,122}
O. FREITAS,¹⁹⁷ R. FREY,⁹² P. FRITSCHER,¹⁰⁰ V. V. FROLOV,⁸² G. G. FRONZÉ,⁴⁸ Y. FUJII,¹⁹⁸ Y. FUJIKAWA,¹⁹⁹
Y. FUJIMOTO,²⁰⁰ P. FULDA,¹⁰² M. FYFFE,⁸² H. A. GABBARD,⁴⁹ W. E. GABELLA,²⁰¹ B. U. GADRE,¹³⁷ J. R. GAIR,¹³⁷
J. GAIS,¹⁵⁶ S. GALAUDAGE,³⁰ R. GAMBA,³⁸ D. GANAPATHY,¹⁰⁰ A. GANGULY,³⁶ D. GAO,²⁰² S. G. GAONKAR,³⁶
B. GARAVENTA,^{118,144} C. GARCÍA NÚÑEZ,¹²⁶ C. GARCÍA-QUIRÓS,¹⁶⁸ F. GARUFI,^{50,29} B. GATELEY,⁹⁸ V. GAYATHRI,¹⁰²
G.-G. GE,²⁰² G. GEMME,¹¹⁸ A. GENNAI,⁴³ J. GEORGE,¹²⁰ O. GERBERDING,¹⁵³ L. GERGELY,²⁰³ P. GEWECKE,¹⁵³
S. GHONGE,⁷³ ABHIRUP GHOSH,¹³⁷ ARCHISHMAN GHOSH,¹¹¹ SHAON GHOSH,¹⁹⁰ SHROBANA GHOSH,⁴² TATHAGATA GHOSH,³⁶
B. GIACOMAZZO,^{95,96,97} L. GIACOPPO,^{130,83} J. A. GIAIME,^{32,82} K. D. GIARDINA,⁸² D. R. GIBSON,¹²⁶ C. GIER,⁵⁸
M. GIESLER,²⁰⁴ P. GIRI,^{43,104} F. GISSI,¹¹³ S. GKAITATZIS,^{43,104} J. GLANZER,³² A. E. GLECKL,⁶⁹ P. GODWIN,¹⁷³
E. GOETZ,²⁰⁵ R. GOETZ,¹⁰² N. GOHLKE,^{34,35} J. GOLOMB,²⁶ B. GONCHAROV,⁵⁷ G. GONZÁLEZ,³² M. GOSSELIN,⁷²
R. GOUATY,⁵⁵ D. W. GOULD,³³ S. GOYAL,⁴⁴ B. GRACE,³³ A. GRADO,^{206,29} V. GRAHAM,⁴⁹ M. GRANATA,¹⁸⁰ V. GRANATA,¹²⁸
A. GRANT,⁴⁹ S. GRAS,¹⁰⁰ P. GRASSIA,²⁶ C. GRAY,⁹⁸ R. GRAY,⁴⁹ G. GRECO,⁶⁵ A. C. GREEN,¹⁰² R. GREEN,⁴²
A. M. GRETARSSON,⁶¹ E. M. GRETARSSON,⁶¹ D. GRIFFITH,²⁶ W. L. GRIFFITHS,⁴² H. L. GRIGGS,⁷³ G. GRIGNANI,^{105,65}
A. GRIMALDI,^{124,125} E. GRIMES,⁶¹ S. J. GRIMM,^{57,133} H. GROTE,⁴² S. GRUNEWALD,¹³⁷ P. GRUNING,⁷¹ A. S. GRUSON,⁶⁹
D. GUERRA,¹⁵² G. M. GUIDI,^{80,81} A. R. GUIMARAES,³² G. GUIXÉ,⁵⁴ H. K. GULATI,¹¹⁰ A. M. GUNNY,¹⁰⁰ H.-K. GUO,¹⁸³
Y. GUO,⁸⁵ ANCHAL GUPTA,²⁶ ANURADHA GUPTA,²⁰⁷ I. M. GUPTA,¹⁷³ P. GUPTA,^{85,91} S. K. GUPTA,¹³² R. GUSTAFSON,²⁰⁸
F. GUZMAN,²⁰⁹ S. HA,²¹⁰ I. P. W. HADIPUTRAWAN,¹⁶⁰ L. HAEGEL,⁷⁰ S. HAINO,¹⁶³ O. HALIM,⁶⁰ E. D. HALL,¹⁰⁰
E. Z. HAMILTON,¹⁸⁵ G. HAMMOND,⁴⁹ W.-B. HAN,²¹¹ M. HANEY,¹⁸⁵ J. HANKS,⁹⁸ C. HANNA,¹⁷³ M. D. HANNAM,⁴²
O. HANNUKSELA,^{91,85} H. HANSEN,⁹⁸ T. J. HANSEN,⁶¹ J. HANSON,⁸² T. HARDER,⁶² K. HARIS,^{85,91} J. HARMS,^{57,133}
G. M. HARRY,⁶⁷ I. W. HARRY,⁷⁷ D. HARTWIG,¹⁵³ K. HASEGAWA,²¹² B. HASKELL,¹¹² C.-J. HASTER,¹⁰⁰ J. S. HATHAWAY,¹⁵⁴
K. HATTORI,²¹³ K. HAUGHIAN,⁴⁹ H. HAYAKAWA,²¹⁴ K. HAYAMA,¹⁵⁷ F. J. HAYES,⁴⁹ J. HEALY,¹⁵⁴ A. HEIDMANN,¹³⁴
A. HEIDT,^{34,35} M. C. HEINTZE,⁸² J. HEINZE,^{34,35} J. HEINZEL,¹⁰⁰ H. HEITMANN,⁶² F. HELLMAN,²¹⁵ P. HELLO,⁷¹
A. F. HELMLING-CORNELL,⁹² G. HEMMING,⁷² M. HENDRY,⁴⁹ I. S. HENG,⁴⁹ E. HENNES,⁸⁵ J. HENNIG,²¹⁶ M. H. HENNIG,²¹⁶
C. HENSHAW,⁷³ A. G. HERNANDEZ,¹¹⁶ F. HERNANDEZ VIVANCO,³⁰ M. HEURS,^{34,35} A. L. HEWITT,²¹⁷ S. HIGGINBOTHAM,⁴²
S. HILD,^{178,85} P. HILL,⁵⁸ Y. HIMEMOTO,²¹⁸ A. S. HINES,²⁰⁹ N. HIRATA,⁴⁵ C. HIROSE,¹⁹⁹ T.-C. HO,¹⁶⁰ S. HOCHHEIM,^{34,35}
D. HOFMAN,¹⁸⁰ J. N. HOHMANN,¹⁵³ D. G. HOLCOMB,¹³⁹ N. A. HOLLAND,³³ I. J. HOLLOWES,¹⁷⁹ Z. J. HOLMES,¹¹⁴ K. HOLT,⁸²
D. E. HOLZ,¹⁸⁹ Q. HONG,¹⁵⁵ J. HOUGH,⁴⁹ S. HOURIHANE,²⁶ E. J. HOWELL,¹¹⁹ C. G. HOY,⁴² D. HOYLAND,³⁹ A. HREIBI,^{34,35}
B.-H. HSIEH,²¹² H.-F. HSIEH,¹⁵⁵ C. HSIUNG,¹⁵⁹ Y. HSU,¹⁵⁵ H.-Y. HUANG,¹⁶³ P. HUANG,²⁰² Y.-C. HUANG,¹⁵⁵ Y.-J. HUANG,¹⁶³
YITING HUANG,¹⁷⁵ YIWEN HUANG,¹⁰⁰ M. T. HÜBNER,³⁰ A. D. HUDDART,²¹⁹ B. HUGHEY,⁶¹ D. C. Y. HUI,²²⁰ V. HUI,⁵⁵
S. HUSA,¹⁶⁸ S. H. HUTTNER,⁴⁹ R. HUXFORD,¹⁷³ T. HUYNH-DINH,⁸² S. IDE,²²¹ B. IDZKOWSKI,¹³⁵ A. IESS,^{149,150}
K. INAYOSHI,²²² Y. INOUE,¹⁶⁰ P. IOSIF,²²³ M. ISI,¹⁰⁰ K. ISLEIF,¹⁵³ K. ITO,²²⁴ Y. ITOH,^{200,225} B. R. IYER,⁴⁴
V. JABERIANHAMEDAN,¹¹⁹ T. JACQMIN,¹³⁴ P.-E. JACQUET,¹³⁴ S. J. JADHAV,²²⁶ S. P. JADHAV,³⁶ T. JAIN,³⁷ A. L. JAMES,⁴²
A. Z. JAN,¹⁹³ K. JANI,²⁰¹ J. JANQUART,^{91,85} K. JANSSENS,^{227,62} N. N. JANTHALUR,²²⁶ P. JARANOWSKI,²²⁸ D. JARIWALA,¹⁰²
R. JAUME,¹⁶⁸ A. C. JENKINS,⁸⁶ K. JENNER,¹¹⁴ C. JEON,²²⁹ W. JIA,¹⁰⁰ J. JIANG,¹⁰² H.-B. JIN,^{230,231} G. R. JOHNS,⁸⁹
R. JOHNSTON,⁴⁹ A. W. JONES,¹¹⁹ D. I. JONES,²³² P. JONES,³⁹ R. JONES,⁴⁹ P. JOSHI,¹⁷³ L. JU,¹¹⁹ A. JUE,¹⁸³ P. JUNG,⁸⁸
K. JUNG,²¹⁰ J. JUNKER,^{34,35} V. JUSTE,¹⁸⁷ K. KAIHOTSU,²²⁴ T. KAJITA,²³³ M. KAKIZAKI,²¹³ C. V. KALAGHATGI,^{42,91,85,234}
V. KALOGERA,⁴⁰ B. KAMAI,²⁶ M. KAMIIZUMI,²¹⁴ N. KANDA,^{200,225} S. KANDHASAMY,³⁶ G. KANG,²³⁵ J. B. KANNER,²⁶
Y. KAO,¹⁵⁵ S. J. KAPADIA,⁴⁴ D. P. KAPASI,³³ C. KARATHANASIS,⁵⁶ S. KARKI,¹²¹ R. KASHYAP,¹⁷³ M. KASPRZACK,²⁶

- W. KASTAUN,^{34,35} T. KATO,²¹² S. KATSANEVAS,⁷² E. KATSAVOUNIDIS,¹⁰⁰ W. KATZMAN,⁸² T. KAUR,¹¹⁹ K. KAWABE,⁹⁸
 K. KAWAGUCHI,²¹² F. KÉFÉLIAN,⁶² D. KEITEL,¹⁶⁸ J. S. KEY,²³⁶ S. KHADKA,¹⁰³ F. Y. KHALILI,¹²³ S. KHAN,⁴²
 T. KHANAM,¹⁷¹ E. A. KHAZANOV,²³⁷ N. KHETAN,^{57,133} M. KHURSHED,¹²⁰ N. KIJBUNCHOO,³³ A. KIM,⁴⁰ C. KIM,²²⁹
 J. C. KIM,²³⁸ J. KIM,²³⁹ K. KIM,²²⁹ W. S. KIM,⁸⁸ Y.-M. KIM,²¹⁰ C. KIMBALL,⁴⁰ N. KIMURA,²¹⁴ M. KINLEY-HANLON,⁴⁹
 R. KIRCHHOFF,^{34,35} J. S. KISSEL,⁹⁸ S. KLIMENKO,¹⁰² T. KLINGER,³⁷ A. M. KNEE,²⁰⁵ T. D. KNOWLES,¹⁸⁸ N. KNUST,^{34,35}
 E. KNYAZEV,¹⁰⁰ Y. KOBAYASHI,²⁰⁰ P. KOCH,^{34,35} G. KOEKOEK,^{85,178} K. KOHRI,²⁴⁰ K. KOKEYAMA,²⁴¹ S. KOLEY,⁵⁷
 P. KOLITSIDOU,⁴² M. KOLSTEIN,⁵⁶ K. KOMORI,¹⁰⁰ V. KONDRASHOV,²⁶ A. K. H. KONG,¹⁵⁵ A. KONTOS,¹⁰⁸ N. KOPER,^{34,35}
 M. KOROBKO,¹⁵³ M. KOVALAM,¹¹⁹ N. KOYAMA,¹⁹⁹ D. B. KOZAK,²⁶ C. KOZAKAI,⁷⁸ V. KRINGEL,^{34,35}
 N. V. KRISHNENDU,^{34,35} A. KRÓLAK,^{242,243} G. KUEHN,^{34,35} F. KUEI,¹⁵⁵ P. KULJER,⁸⁵ S. KULKARNI,²⁰⁷ A. KUMAR,²²⁶
 PRAYUSH KUMAR,⁴⁴ RAHUL KUMAR,⁹⁸ RAKESH KUMAR,¹¹⁰ J. KUME,⁵³ K. KUNS,¹⁰⁰ Y. KUROMIYA,²²⁴ S. KUROYANAGI,^{244,245}
 K. KWAK,²¹⁰ G. LACAILLE,⁴⁹ P. LAGABBE,⁵⁵ D. LAGHI,¹³⁸ E. LALANDE,²⁴⁶ M. LALLEMAN,²²⁷ T. L. LAM,¹⁵⁶
 A. LAMBERTS,^{62,247} M. LANDRY,⁹⁸ B. B. LANE,¹⁰⁰ R. N. LANG,¹⁰⁰ J. LANGE,¹⁹³ B. LANTZ,¹⁰³ I. LA ROSA,⁵⁵
 A. LARTAUX-VOLLARD,⁷¹ P. D. LASKY,³⁰ M. LAXEN,⁸² A. LAZZARINI,²⁶ C. LAZZARO,^{106,107} P. LEACI,^{130,83} S. LEAVEY,^{34,35}
 S. LEBOHEC,¹⁸³ Y. K. LECOEUQUE,²⁰⁵ E. LEE,²¹² H. M. LEE,²⁴⁸ H. W. LEE,²³⁸ K. LEE,²⁴⁹ R. LEE,¹⁵⁵ I. N. LEGRED,²⁶
 J. LEHMANN,^{34,35} A. LEMÂITRE,²⁵⁰ M. LENTI,^{81,251} M. LEONARDI,⁴⁵ E. LEONOVA,⁶³ N. LEROY,⁷¹ N. LETENDRE,⁵⁵
 C. LEVESQUE,²⁴⁶ Y. LEVIN,³⁰ J. N. LEVITON,²⁰⁸ K. LEYDE,⁷⁰ A. K. Y. LI,²⁶ B. LI,¹⁵⁵ J. LI,⁴⁰ K. L. LI,²⁵² P. LI,²⁵³
 T. G. F. LI,¹⁵⁶ X. LI,¹⁶¹ C.-Y. LIN,²⁵⁴ E. T. LIN,¹⁵⁵ F.-K. LIN,¹⁶³ F.-L. LIN,²⁵⁵ H. L. LIN,¹⁶⁰ L. C.-C. LIN,²⁵² F. LINDE,^{234,85}
 S. D. LINKER,^{151,116} J. N. LINLEY,⁴⁹ T. B. LITTENBERG,²⁵⁶ G. C. LIU,¹⁵⁹ J. LIU,¹¹⁹ K. LIU,¹⁵⁵ X. LIU,³¹ F. LLAMAS,¹¹⁵
 R. K. L. LO,²⁶ T. LO,¹⁵⁵ L. T. LONDON,^{63,100} A. LONGO,²⁵⁷ D. LOPEZ,¹⁸⁵ M. LOPEZ PORTILLA,⁹¹ M. LORENZINI,^{149,150}
 V. LORIETTE,²⁵⁸ M. LORMAND,⁸² G. LOSURDO,⁴³ T. P. LOTT,⁷³ J. D. LOUGH,^{34,35} C. O. LOUSTO,¹⁵⁴ G. LOVELACE,⁶⁹
 J. F. LUCACCIONI,²⁵⁹ H. LÜCK,^{34,35} D. LUMACA,^{149,150} A. P. LUNDGREN,⁷⁷ L.-W. LUO,¹⁶³ J. E. LYNAM,⁸⁹ M. MA'ARIF,¹⁶⁰
 R. MACAS,⁷⁷ J. B. MACHTINGER,⁴⁰ M. MACINNIS,¹⁰⁰ D. M. MACLEOD,⁴² I. A. O. MACMILLAN,²⁶ A. MACQUET,⁶²
 I. MAGAÑA HERNANDEZ,³¹ C. MAGAZZÙ,⁴³ R. M. MAGEE,²⁶ R. MAGGIORE,³⁹ M. MAGNOZZI,^{118,144} S. MAHESH,¹⁸⁸
 E. MAJORANA,^{130,83} I. MAKSIMOVIC,²⁵⁸ S. MALIAKAL,²⁶ A. MALIK,¹²⁰ N. MAN,⁶² V. MANDIC,¹⁷² V. MANGANO,^{130,83}
 G. L. MANSSELL,^{98,100} M. MANSKE,³¹ M. MANTOVANI,⁷² M. MAPELLI,^{106,107} F. MARCHESONI,^{66,65,260} D. MARÍN PINA,⁵⁴
 F. MARION,⁵⁵ Z. MARK,¹⁶¹ S. MÁRKA,⁷⁶ Z. MÁRKA,⁷⁶ C. MARKAKIS,³⁷ A. S. MARKOSYAN,¹⁰³ A. MARKOWITZ,²⁶
 E. MAROS,²⁶ A. MARQUINA,¹⁷⁰ S. MARSAT,⁷⁰ F. MARTELLI,^{80,81} I. W. MARTIN,⁴⁹ R. M. MARTIN,¹⁹⁰ M. MARTINEZ,⁵⁶
 V. A. MARTINEZ,¹⁰² V. MARTINEZ,⁵¹ K. MARTINOVIC,⁸⁶ D. V. MARTYNOV,³⁹ E. J. MARX,¹⁰⁰ H. MASALEHDAN,¹⁵³
 K. MASON,¹⁰⁰ E. MASSERA,¹⁷⁹ A. MASSEROT,⁵⁵ M. MASSO-REID,⁴⁹ S. MASTROGIOVANNI,⁷⁰ A. MATAS,¹³⁷
 M. MATEU-LUCENA,¹⁶⁸ F. MATICHARD,^{26,100} M. MATUSHECHKINA,^{34,35} N. MAVALVALA,¹⁰⁰ J. J. McCANN,¹¹⁹
 R. MCCARTHY,⁹⁸ D. E. MCCLELLAND,³³ P. K. McCLINCY,¹⁷³ S. McCORMICK,⁸² L. McCULLER,¹⁰⁰ G. I. MCGHEE,⁴⁹
 S. C. MCGUIRE,⁸² C. McISAAC,⁷⁷ J. McIVER,²⁰⁵ T. McRAE,³³ S. T. McWILLIAMS,¹⁸⁸ D. MEACHER,³¹ M. MEHMET,^{34,35}
 A. K. MEHTA,¹³⁷ Q. MEIJER,⁹¹ A. MELATOS,¹⁴⁶ D. A. MELCHOR,⁶⁹ G. MENDELL,⁹⁸ A. MENENDEZ-VAZQUEZ,⁵⁶
 C. S. MENONI,¹⁹¹ R. A. MERCER,³¹ L. MERENI,¹⁸⁰ K. MERFELD,⁹² E. L. MERILH,⁸² J. D. MERRITT,⁹² M. MERZOUGUI,⁶²
 S. MESHKOV,²⁶ * C. MESSENGER,⁴⁹ C. MESSICK,¹⁰⁰ P. M. MEYERS,¹⁴⁶ F. MEYLAHN,^{34,35} A. MHASKE,³⁶ A. MIANI,^{124,125}
 H. MIAO,³⁹ I. MICHALOLIAKOS,¹⁰² C. MICHEL,¹⁸⁰ Y. MICHIMURA,⁵² H. MIDDLETON,¹⁴⁶ D. P. MIHAYLOV,¹³⁷ L. MILANO,⁵⁰ †
 A. L. MILLER,⁸⁴ A. MILLER,¹¹⁶ B. MILLER,^{63,85} M. MILLHOUSE,¹⁴⁶ J. C. MILLS,⁴² E. MILOTTI,^{261,60} Y. MINENKOV,¹⁵⁰
 N. MIO,²⁶² LL. M. MIR,⁵⁶ M. MIRAVET-TENÉS,¹⁵² A. MISHKIN,¹⁰² C. MISHRA,²⁶³ T. MISHRA,¹⁰² T. MISTRY,¹⁷⁹ S. MITRA,³⁶
 V. P. MITROFANOV,¹²³ G. MITSSELMAKHER,¹⁰² R. MITTLEMAN,¹⁰⁰ O. MIYAKAWA,²¹⁴ K. MIYO,²¹⁴ S. MIYOKI,²¹⁴
 GEOFFREY MO,¹⁰⁰ L. M. MODAFFERI,¹⁶⁸ E. MOGUEL,²⁵⁹ K. MOGUSHI,¹²¹ S. R. P. MOHAPATRA,¹⁰⁰ S. R. MOHITE,³¹
 I. MOLINA,⁶⁹ M. MOLINA-RUIZ,²¹⁵ M. MONDIN,¹¹⁶ M. MONTANI,^{80,81} C. J. MOORE,³⁹ J. MORAGUES,¹⁶⁸ D. MORARU,⁹⁸
 F. MORAWSKI,¹¹² A. MORE,³⁶ C. MORENO,⁶¹ G. MORENO,⁹⁸ Y. MORI,²²⁴ S. MORISAKI,³¹ N. MORISUE,²⁰⁰ Y. MORIWAKI,²¹³
 B. MOURS,¹⁸⁷ C. M. MOW-LOWRY,^{85,122} S. MOZZON,⁷⁷ F. MUCIACCIA,^{130,83} ARUNAVA MUKHERJEE,²⁶⁴ D. MUKHERJEE,¹⁷³
 SOMA MUKHERJEE,¹¹⁵ SUBROTO MUKHERJEE,¹¹⁰ SUVODIP MUKHERJEE,^{186,63} N. MUKUND,^{34,35} A. MULLAVEY,⁸²
 J. MUNCH,¹¹⁴ E. A. MUÑIZ,⁹³ P. G. MURRAY,⁴⁹ R. MUSENICH,^{118,144} S. MUUSSE,¹¹⁴ S. L. NADJI,^{34,35} K. NAGANO,²⁶⁵
 A. NAGAR,^{48,266} K. NAKAMURA,⁴⁵ H. NAKANO,²⁶⁷ M. NAKANO,²¹² Y. NAKAYAMA,²²⁴ V. NAPOLANO,⁷²
 I. NARDECCHIA,^{149,150} H. NAROLA,⁹¹ L. NATICCHIONI,⁸³ B. NAYAK,¹¹⁶ R. K. NAYAK,²⁶⁸ B. F. NEIL,¹¹⁹ J. NEILSON,^{113,129}
 A. NELSON,²⁰⁹ T. J. N. NELSON,⁸² M. NERY,^{34,35} P. NEUBAUER,²⁵⁹ A. NEUNZERT,²³⁶ K. Y. NG,¹⁰⁰ S. W. S. NG,¹¹⁴
 C. NGUYEN,⁷⁰ P. NGUYEN,⁹² T. NGUYEN,¹⁰⁰ L. NGUYEN QUYNH,²⁶⁹ J. NI,¹⁷² W.-T. NI,^{230,202,155} S. A. NICHOLS,³²
 T. NISHIMOTO,²¹² A. NISHIZAWA,⁵³ S. NISSANKE,^{63,85} E. NITOGIA,¹⁶⁴ F. NOCERA,⁷² M. NORMAN,⁴² C. NORTH,⁴²
 S. NOZAKI,²¹³ G. NURBEK,¹¹⁵ L. K. NUTTALL,⁷⁷ Y. OBAYASHI,²¹² J. OBERLING,⁹⁸ B. D. O'BRIEN,¹⁰² J. O'DELL,²¹⁹
 E. OELKER,⁴⁹ W. OGAKI,²¹² G. OGANESYAN,^{57,133} J. J. OH,⁸⁸ K. OH,²²⁰ S. H. OH,⁸⁸ M. OHASHI,²¹⁴ T. OHASHI,²⁰⁰
 M. OHKAWA,¹⁹⁹ F. OHME,^{34,35} H. OHTA,⁵³ M. A. OKADA,⁴¹ Y. OKUTANI,²²¹ C. OLIVETTO,⁷² K. OOHARA,^{212,270}
 R. ORAM,⁸² B. O'REILLY,⁸² R. G. ORMISTON,¹⁷² N. D. ORMSBY,⁸⁹ R. O'SHAUGHNESSY,¹⁵⁴ E. O'SHEA,²⁰⁴ S. OSHINO,²¹⁴
 S. OSSOKINE,¹³⁷ C. OSTHELDER,²⁶ S. OTABE,²⁷ D. J. OTTAWAY,¹¹⁴ H. OVERMIER,⁸² A. E. PACE,¹⁷³ G. PAGANO,^{104,43}
 R. PAGANO,³² M. A. PAGE,¹¹⁹ G. PAGLIAROLI,^{57,133} A. PAI,¹³² S. A. PAI,¹²⁰ S. PAL,²⁶⁸ J. R. PALAMOS,⁹² O. PALASHOV,²³⁷
 C. PALOMBA,⁸³ H. PAN,¹⁵⁵ K.-C. PAN,¹⁵⁵ P. K. PANDA,²²⁶ P. T. H. PANG,^{85,91} C. PANKOW,⁴⁰ F. PANNARALE,^{130,83}
 B. C. PANT,¹²⁰ F. H. PANTHER,¹¹⁹ F. PAOLETTI,⁴³ A. PAOLI,⁷² A. PAOLONE,^{83,271} G. PAPPAS,²²³ A. PARISI,¹⁵⁹ H. PARK,³¹
 J. PARK,²⁷² W. PARKER,⁸² D. PASCUCCI,^{85,111} A. PASQUALETTI,⁷² R. PASSAQUIETI,^{104,43} D. PASSUELLO,⁴³ M. PATEL,⁸⁹
 M. PATHAK,¹¹⁴ B. PATRICELLI,^{72,43} A. S. PATRON,³² S. PAUL,⁹² E. PAYNE,³⁰ M. PEDRAZA,²⁶ R. PEDURAND,¹²⁹
 M. PEGORARO,¹⁰⁷ A. PELE,⁸² F. E. PEÑA ARELLANO,²¹⁴ S. PENANO,¹⁰³ S. PENN,²⁷³ A. PEREGO,^{124,125} A. PEREIRA,⁵¹
 T. PEREIRA,²⁷⁴ C. J. PEREZ,⁹⁸ C. PÉRIGOIS,⁵⁵ C. C. PERKINS,¹⁰² A. PERRECA,^{124,125} S. PERRIÈS,¹⁶⁴ D. PESIOS,²²³

- J. PETERMANN,¹⁵³ D. PETTERSON,²⁶ H. P. PFEIFFER,¹³⁷ H. PHAM,⁸² K. A. PHAM,¹⁷² K. S. PHUKON,^{85, 234}
H. PHURAILATPAM,¹⁵⁶ O. J. PICCINI,⁸³ M. PICHOT,⁶² M. PIENDIBENE,^{104, 43} F. PIERGIOVANNI,^{80, 81} L. PIERINI,^{130, 83}
V. PIERRO,^{113, 129} G. PILLANT,⁷² M. PILLAS,⁷¹ F. PILO,⁴³ L. PINARD,¹⁸⁰ C. PINEDA-BOSQUE,¹¹⁶ I. M. PINTO,^{113, 129, 275}
M. PINTO,⁷² B. J. PIOTRZKOWSKI,³¹ K. PIOTRZKOWSKI,⁸⁴ M. PIRELLO,⁹⁸ M. D. PITKIN,²¹⁷ A. PLACIDI,^{65, 105}
E. PLACIDI,^{130, 83} M. L. PLANAS,¹⁶⁸ W. PLASTINO,^{276, 257} C. PLUCHAR,²⁷⁷ R. POGGIANI,^{104, 43} E. POLINI,⁵⁵
D. Y. T. PONG,¹⁵⁶ S. PONRATHNAM,³⁶ E. K. PORTER,⁷⁰ R. POULTON,⁷² A. POVERMAN,¹⁰⁸ J. POWELL,¹⁶⁶ M. PRACCHIA,⁵⁵
T. PRADIER,¹⁸⁷ A. K. PRAJAPATI,¹¹⁰ K. PRASAI,¹⁰³ R. PRASANNA,²²⁶ G. PRATTEN,³⁹ M. PRINCIPE,^{113, 275, 129}
G. A. PRODI,^{278, 125} L. PROKHOROV,³⁹ P. PROSPITO,^{149, 150} L. PRUDENZI,¹³⁷ A. PUECHER,^{85, 91} M. PUNTURO,⁶⁵
F. PUOSI,^{43, 104} P. PUPPO,⁸³ M. PÜRRE, ¹³⁷ H. QI,⁴² N. QUARTEY,⁸⁹ V. QUETSCHKE,¹¹⁵ P. J. QUINONEZ,⁶¹
R. QUITZOW-JAMES,¹²¹ F. J. RAAB,⁹⁸ G. RAALMAKERS,^{63, 85} H. RADKINS,⁹⁸ N. RADULESCO,⁶² P. RAFFAI,¹⁷⁷ S. X. RAIL,²⁴⁶
S. RAJA,¹²⁰ C. RAJAN,¹²⁰ K. E. RAMIREZ,⁸² T. D. RAMIREZ,⁶⁹ A. RAMOS-BUADES,¹³⁷ J. RANA,¹⁷³ P. RAPAGNANI,^{130, 83}
A. RAY,³¹ V. RAYMOND,⁴² N. RAZA,²⁰⁵ M. RAZZANO,^{104, 43} J. READ,⁶⁹ L. A. REES,⁶⁷ T. REGIMBAU,⁵⁵ L. REI,¹¹⁸ S. REID,⁵⁸
S. W. REID,⁸⁹ D. H. REITZE,^{26, 102} P. RELTON,⁴² A. RENZINI,²⁶ P. RETTEGNO,^{47, 48} B. REVENU,⁷⁰ A. REZA,⁸⁵ M. REZAC,⁶⁹
F. RICCI,^{130, 83} D. RICHARDS,²¹⁹ J. W. RICHARDSON,²⁷⁹ L. RICHARDSON,²⁰⁹ G. RIEMENSCHNEIDER,^{47, 48} K. RILES,²⁰⁸
S. RINALDI,^{104, 43} K. RINK,²⁰⁵ N. A. ROBERTSON,²⁶ R. ROBIE,²⁶ F. ROBINET,⁷¹ A. ROCCHI,¹⁵⁰ S. RODRIGUEZ,⁶⁹
L. ROLLAND,⁵⁵ J. G. ROLLINS,²⁶ M. ROMANELLI,¹³¹ R. ROMANO,^{28, 29} C. L. ROMEL,⁹⁸ A. ROMERO,⁵⁶
I. M. ROMERO-SHAW,³⁰ J. H. ROMIE,⁸² S. RONCHINI,^{57, 133} L. ROSA,^{29, 50} C. A. ROSE,³¹ D. ROSIŃSKA,¹³⁵ M. P. ROSS,²⁸⁰
S. ROWAN,⁴⁹ S. J. ROWLINSON,³⁹ S. ROY,⁹¹ SANTOSH ROY,³⁶ SOUMEN ROY,²⁸¹ D. ROZZA,^{147, 148} P. RUGGI,⁷²
K. RUIZ-ROCHA,²⁰¹ K. RYAN,⁹⁸ S. SACHDEV,¹⁷³ T. SADECKI,⁹⁸ J. SADIQ,¹⁴⁰ S. SAHA,¹⁵⁵ Y. SAITO,²¹⁴ K. SAKAI,²⁸²
M. SAKELLARIADOU,⁸⁶ S. SAKON,¹⁷³ O. S. SALAFIA,^{97, 96, 95} F. SALCES-CARCOBA,²⁶ L. SALCONI,⁷² M. SALEEM,¹⁷²
F. SALEMI,^{124, 125} A. SAMAJDAR,⁹⁶ E. J. SANCHEZ,²⁶ J. H. SANCHEZ,⁶⁹ L. E. SANCHEZ,²⁶ N. SANCHIS-GUAL,²⁸³
J. R. SANDERS,²⁸⁴ A. SANUY,⁵⁴ T. R. SARAVANAN,³⁶ N. SARIN,³⁰ B. SASSOLAS,¹⁸⁰ H. SATARI,^{119, 42} O. SAUTER,¹⁰²
R. L. SAVAGE,⁹⁸ V. SAVANT,³⁶ T. SAWADA,²⁰⁰ H. L. SAWANT,³⁶ S. SAYAH,¹⁸⁰ D. SCHAETZL,²⁶ M. SCHEEL,¹⁶¹ J. SCHEUER,⁴⁰
M. G. SCHIWORSKI,¹¹⁴ P. SCHMIDT,³⁹ S. SCHMIDT,⁹¹ R. SCHNABEL,¹⁵³ M. SCHNEEWIND,^{34, 35} R. M. S. SCHOFIELD,⁹²
A. SCHÖNBECK,¹⁵³ B. W. SCHULTE,^{34, 35} B. F. SCHUTZ,^{42, 34, 35} E. SCHWARTZ,⁴² J. SCOTT,⁴⁹ S. M. SCOTT,³³
M. SEGLAR-ARROYO,⁵⁵ Y. SEKIGUCHI,²⁸⁵ D. SELERS,⁸² A. S. SENGUPTA,²⁸¹ D. SENTENAC,⁷² E. G. SEO,¹⁵⁶
V. SEQUINO,^{50, 29} A. SERGEEV,²³⁷ Y. SETYAWATI,^{34, 35, 91} T. SHAFFER,⁹⁸ M. S. SHAHRIAR,⁴⁰ M. A. SHAIKH,⁴⁴ B. SHAMS,¹⁸³
L. SHAO,²²² A. SHARMA,^{57, 133} P. SHARMA,¹²⁰ P. SHAWHAN,¹³⁶ N. S. SHCHEBLANOV,²⁵⁰ A. SHEELA,²⁶³ Y. SHIKANO,^{286, 287}
M. SHIKAUCHI,⁵³ H. SHIMIZU,²⁸⁸ K. SHIMODE,²¹⁴ H. SHINKAI,²⁸⁹ T. SHISHIDO,⁷⁹ A. SHODA,⁴⁵ D. H. SHOEMAKER,¹⁰⁰
D. M. SHOEMAKER,¹⁹³ S. SHYAMSUNDAR,¹²⁰ M. SIENIAWSKA,⁸⁴ D. SIGG,⁹⁸ L. SILENZI,^{65, 66} L. P. SINGER,¹⁴³ D. SINGH,¹⁷³
M. K. SINGH,⁴⁴ N. SINGH,¹³⁵ A. SINGHA,^{178, 85} A. M. SINTES,¹⁶⁸ V. SIPALA,^{147, 148} V. SKLIRIS,⁴² B. J. J. SLAGMOLEN,³³
T. J. SLAVEN-BLAIR,¹¹⁹ J. SMETANA,³⁹ J. R. SMITH,⁶⁹ L. SMITH,⁴⁹ R. J. E. SMITH,³⁰ J. SOLDATESCHI,^{251, 290, 81}
S. N. SOMALA,²⁹¹ K. SOMIYA,²⁷ I. SONG,¹⁵⁵ K. SONI,³⁶ S. SONI,¹⁰⁰ V. SORDINI,¹⁶⁴ F. SORRENTINO,¹¹⁸ N. SORRENTINO,^{104, 43}
R. SOULARD,⁶² T. SOURADEEP,^{292, 36} E. SOWELL,¹⁷¹ V. SPAGNUOLO,^{178, 85} A. P. SPENCER,⁴⁹ M. SPERA,^{106, 107}
P. SPINICELLI,⁷² A. K. SRIVASTAVA,¹¹⁰ V. SRIVASTAVA,⁹³ K. STAATS,⁴⁰ C. STACHIE,⁶² F. STACHURSKI,⁴⁹ D. A. STEER,⁷⁰
J. STEINLECHNER,^{178, 85} S. STEINLECHNER,^{178, 85} N. STERGIOLAS,²²³ D. J. STOPS,³⁹ M. STOVER,²⁵⁹ K. A. STRAIN,⁴⁹
L. C. STRANG,¹⁴⁶ G. STRATTA,^{293, 83} M. D. STRONG,³² A. STRUNK,⁹⁸ R. STURANI,²⁷⁴ A. L. STUVER,¹³⁹ M. S. SUTCHENK,¹¹²
S. SUDHAGAR,³⁶ V. SUDHIR,¹⁰⁰ R. SUGIMOTO,¹⁹⁹ H. G. SUH,³¹ A. G. SULLIVAN,⁷⁶ T. Z. SUMMERSCALES,²⁹⁵ L. SUN,³³
S. SUNIL,¹¹⁰ A. SUR,¹¹² J. SURESH,⁵³ P. J. SUTTON,⁴² TAKAMASA SUZUKI,¹⁹⁹ TAKANORI SUZUKI,²⁷ TOSHIKAZU SUZUKI,²¹²
B. L. SWINKELS,⁸⁵ M. J. SZCZEPAŃCZYK,¹⁰² P. SZEWCZYK,¹³⁵ M. TACCA,⁸⁵ H. TAGOSHI,²¹² S. C. TAIT,⁴⁹ H. TAKAHASHI,²⁹⁶
R. TAKAHASHI,⁴⁵ S. TAKANO,⁵² H. TAKEDA,⁵² M. TAKEDA,²⁰⁰ C. J. TALBOT,⁵⁸ C. TALBOT,²⁶ K. TANAKA,²⁹⁷
TAIKI TANAKA,²¹² TAKAHIRO TANAKA,²⁹⁸ A. J. TANASIJCZUK,⁸⁴ S. TANIOKA,²¹⁴ D. B. TANNER,¹⁰² D. TAO,²⁶ L. TAO,¹⁰²
R. D. TAPIA,¹⁷³ E. N. TAPIA SAN MARTÍN,⁸⁵ C. TARANTO,¹⁴⁹ A. TARUYA,²⁹⁹ J. D. TASSON,¹⁸⁴ R. TENORIO,¹⁶⁸
J. E. S. TERHUNE,¹³⁹ L. TERKOWSKI,¹⁵³ M. P. THIRUGNANASAMBANDAM,³⁶ M. THOMAS,⁸² P. THOMAS,⁹⁸
E. E. THOMPSON,⁷³ J. E. THOMPSON,⁴² S. R. THONDAPU,¹²⁰ K. A. THORNE,⁸² E. THRANE,³⁰ SHUBHANSHU TIWARI,¹⁸⁵
SRISHTI TIWARI,³⁶ V. TIWARI,⁴² A. M. TOIVONEN,¹⁷² A. E. TOLLEY,⁷⁷ T. TOMARU,⁴⁵ T. TOMURA,²¹⁴ M. TONELLI,^{104, 43}
Z. TORNASI,⁴⁹ A. TORRES-FORNÉ,¹⁵² C. I. TORRIE,²⁶ I. TOSTA E MELO,¹⁴⁸ D. TÖYRÄ,³³ A. TRAPANANTI,^{66, 65}
F. TRAVASSO,^{65, 66} G. TRAYLOR,⁸² M. TREVOR,¹³⁶ M. C. TRINGALI,⁷² A. TRIPATHEE,²⁰⁸ L. TROIANO,^{300, 129} A. TROVATO,⁷⁰
L. TROZZO,^{29, 214} R. J. TRUDEAU,²⁶ D. TSAI,¹⁵⁵ K. W. TSANG,^{85, 301, 91} T. TSANG,³⁰² J-S. TSAO,²⁵⁵ M. TSE,¹⁰⁰ R. TSO,¹⁶¹
S. TSUCHIDA,²⁰⁰ L. TSUKADA,¹⁷³ D. TSUNA,⁵³ T. TSUTSUI,⁵³ K. TURBANG,^{303, 227} M. TURCONI,⁶² D. TUYENBAYEV,²⁰⁰
A. S. UBHI,³⁹ T. UCHIYAMA,²¹⁴ R. P. UDALL,²⁶ A. UEDA,³⁰⁴ T. UEHARA,^{305, 306} K. UENO,⁵³ G. UESHIMA,³⁰⁷
C. S. UNNIKRIISHNAN,³⁰⁸ A. L. URBAN,³² T. USHIBA,²¹⁴ A. UTINA,^{178, 85} G. VAJENTE,²⁶ A. VAJPEYI,³⁰ G. VALDES,²⁰⁹
M. VALENTINI,^{207, 124, 125} V. VALSAN,³¹ N. VAN BAKEL,⁸⁵ M. VAN BEUZEKOM,⁸⁵ M. VAN DAEL,^{85, 309}
J. F. J. VAN DEN BRAND,^{178, 122, 85} C. VAN DEN BROECK,^{91, 85} D. C. VANDER-HYDE,⁹³ H. VAN HAEVERMAET,²²⁷
J. V. VAN HEIJNINGEN,⁸⁴ M. H. P. M. VAN PUTTEN,³¹⁰ N. VAN REMORTEL,²²⁷ M. VARDARO,^{234, 85} A. F. VARGAS,¹⁴⁶
V. VARMA,¹³⁷ M. VASÚTH,¹⁰¹ A. VECCHIO,³⁹ G. VEDOVATO,¹⁰⁷ J. VEITCH,⁴⁹ P. J. VEITCH,¹¹⁴ J. VENNEBERG,^{34, 35}
G. VENUGOPALAN,²⁶ D. VERKINDT,⁵⁵ P. VERMA,²⁴³ Y. VERMA,¹²⁰ S. M. VERMEULEN,⁴² D. VESKE,⁷⁶ F. VETRANO,⁸⁰
A. VICERÉ,^{80, 81} S. VIDYANT,⁹³ A. D. VIETS,³¹¹ A. VIJAYKUMAR,⁴⁴ V. VILLA-ORTEGA,¹⁴⁰ J.-Y. VINET,⁶² A. VIRTUOSO,^{261, 60}
S. VITALE,¹⁰⁰ H. VOCCA,^{105, 65} E. R. G. VON REIS,⁹⁸ J. S. A. VON WRANGEL,^{34, 35} C. VORVICK,⁹⁸ S. P. VYATCHANIN,¹²³
L. E. WADE,²⁵⁹ M. WADE,²⁵⁹ K. J. WAGNER,¹⁵⁴ R. C. WALET,⁸⁵ M. WALKER,⁸⁹ G. S. WALLACE,⁵⁸ L. WALLACE,²⁶
J. WANG,²⁰² J. Z. WANG,²⁰⁸ W. H. WANG,¹¹⁵ R. L. WARD,³³ J. WARNER,⁹⁸ M. WAS,⁵⁵ T. WASHIMI,⁴⁵
N. Y. WASHINGTON,²⁶ J. WATCHI,¹⁶⁹ B. WEAVER,⁹⁸ C. R. WEAVING,⁷⁷ S. A. WEBSTER,⁴⁹ M. WEINERT,^{34, 35}

A. J. WEINSTEIN,²⁶ R. WEISS,¹⁰⁰ C. M. WELLER,²⁸⁰ R. A. WELLER,²⁰¹ F. WELLMANN,^{34,35} L. WEN,¹¹⁹ P. WESSELS,^{34,35}
 K. WETTE,³³ J. T. WHELAN,¹⁵⁴ D. D. WHITE,⁶⁹ B. F. WHITING,¹⁰² C. WHITTLE,¹⁰⁰ D. WILKEN,^{34,35} D. WILLIAMS,⁴⁹
 M. J. WILLIAMS,⁴⁹ A. R. WILLIAMSON,⁷⁷ J. L. WILLIS,²⁶ B. WILLKE,^{34,35} D. J. WILSON,²⁷⁷ C. C. WIPF,²⁶
 T. WLODARCZYK,¹³⁷ G. WOAN,⁴⁹ J. WOEHLER,^{34,35} J. K. WOFFORD,¹⁵⁴ D. WONG,²⁰⁵ I. C. F. WONG,¹⁵⁶ M. WRIGHT,⁴⁹
 C. WU,¹⁵⁵ D. S. WU,^{34,35} H. WU,¹⁵⁵ D. M. WYSOCKI,³¹ L. XIAO,²⁶ T. YAMADA,²⁸⁸ H. YAMAMOTO,²⁶ K. YAMAMOTO,²¹³
 T. YAMAMOTO,²¹⁴ K. YAMASHITA,²²⁴ R. YAMAZAKI,²²¹ F. W. YANG,¹⁸³ K. Z. YANG,¹⁷² L. YANG,¹⁹¹ Y.-C. YANG,¹⁵⁵
 Y. YANG,³¹² YANG YANG,¹⁰² M. J. YAP,³³ D. W. YEELES,⁴² S.-W. YEH,¹⁵⁵ A. B. YELIKAR,¹⁵⁴ M. YING,¹⁵⁵
 J. YOKOYAMA,^{53,52} T. YOKOZAWA,²¹⁴ J. YOO,²⁰⁴ T. YOSHIOKA,²²⁴ HANG YU,¹⁶¹ HAOCUN YU,¹⁰⁰ H. YUZURIHARA,²¹²
 A. ZADROŻNY,²⁴³ M. ZANOLIN,⁶¹ S. ZEIDLER,³¹³ T. ZELENKOVA,⁷² J.-P. ZENDRI,¹⁰⁷ M. ZEVIN,¹⁸⁹ M. ZHAN,²⁰² H. ZHANG,²⁵⁵
 J. ZHANG,¹¹⁹ L. ZHANG,²⁶ R. ZHANG,¹⁰² T. ZHANG,³⁹ Y. ZHANG,²⁰⁹ C. ZHAO,¹¹⁹ G. ZHAO,¹⁶⁹ Y. ZHAO,^{212,45} YUE ZHAO,¹⁸³
 R. ZHOU,²¹⁵ Z. ZHOU,⁴⁰ X. J. ZHU,³⁰ Z.-H. ZHU,^{145,253} A. B. ZIMMERMAN,¹⁹³ M. E. ZUCKER,^{26,100} AND J. ZWEIZIG²⁶
 THE LIGO SCIENTIFIC COLLABORATION, THE VIRGO COLLABORATION, AND THE KAGRA COLLABORATION

¹Science and Technology Institute, Universities Space Research Association, Huntsville, AL 35805, USA

²NASA Marshall Space Flight Center, Huntsville, AL 35812, USA

³Department of Space Science, University of Alabama in Huntsville, Huntsville, AL 35899, USA

⁴Center for Space Plasma and Aeronomic Research, University of Alabama in Huntsville, Huntsville, AL 35899, USA

⁵Université Paris-Saclay, CNRS/IN2P3, IJCLab, 91405 Orsay, France

⁶Dipartimento Interateneo di Fisica, Politecnico di Bari, Via E. Orabona 4, 70125, Bari, Italy

⁷INFN - Sezione di Bari, Via E. Orabona 4, 70125, Bari, Italy

⁸Department of Physics & Astronomy, Louisiana State University, Baton Rouge, LA 70803, USA

⁹Jacobs Space Exploration Group, Huntsville, AL 35806, USA

¹⁰Center for Space Plasma and Aeronomic Research, The University of Alabama in Huntsville, Huntsville, AL 35899

¹¹Department of Space Science, University of Alabama in Huntsville, 320 Sparkman Drive, Huntsville, AL 35899, USA

¹²Department of Aerospace, Physics and Space Sciences, Florida Institute of Technology, Melbourne, FL 32901, USA

¹³International Space Science Institute (ISSI), Hallerstrasse 6, 3012 Bern, Switzerland

¹⁴Max-Planck-Institut für extraterrestrische Physik, Giessenbachstrasse 1, D-85748 Garching, Germany

¹⁵Department of Astronomy, University of Maryland, College Park, MD 20742, USA

¹⁶Center for Research and Exploration in Space Science and Technology, NASA Goddard Space Flight Center, Greenbelt, MD 20771, USA

¹⁷Stockholm University and The Oskar Klein Centre for Cosmoparticle Physics, Alba Nova, 10691 Stockholm, Sweden

¹⁸Department of Physics and Astronomy, University of Alabama, Tuscaloosa, AL 35487, USA

¹⁹Department of Physics, Pennsylvania State University, University Park, PA 16802, USA

²⁰Center for Multimessenger Astrophysics, Institute for Gravitation and the Cosmos, Pennsylvania State University, University Park, PA 16802, USA

²¹Department of Astronomy & Astrophysics, University of Toronto, Toronto, Ontario M5S 1A1, Canada

²²Astrophysics Science Division, NASA Goddard Space Flight Center, MC 661, Greenbelt, MD 20771, USA

²³Joint Space-Science Institute, University of Maryland, College Park, MD 20742, USA

²⁴Astrophysics Science Division, NASA Goddard Space Flight Center, Greenbelt, MD 20771, USA

²⁵Center for Space Science and Technology, University of Maryland Baltimore County, 1000 Hilltop Circle, Baltimore, MD 21250, USA

²⁶LIGO Laboratory, California Institute of Technology, Pasadena, CA 91125, USA

²⁷Graduate School of Science, Tokyo Institute of Technology, Meguro-ku, Tokyo 152-8551, Japan

²⁸Dipartimento di Farmacia, Università di Salerno, I-84084 Fisciano, Salerno, Italy

²⁹INFN, Sezione di Napoli, Complesso Universitario di Monte S. Angelo, I-80126 Napoli, Italy

³⁰OzGrav, School of Physics & Astronomy, Monash University, Clayton 3800, Victoria, Australia

³¹University of Wisconsin-Milwaukee, Milwaukee, WI 53201, USA

³²Louisiana State University, Baton Rouge, LA 70803, USA

³³OzGrav, Australian National University, Canberra, Australian Capital Territory 0200, Australia

³⁴Max Planck Institute for Gravitational Physics (Albert Einstein Institute), D-30167 Hannover, Germany

³⁵Leibniz Universität Hannover, D-30167 Hannover, Germany

³⁶Inter-University Centre for Astronomy and Astrophysics, Pune 411007, India

³⁷University of Cambridge, Cambridge CB2 1TN, United Kingdom

³⁸Theoretisch-Physikalisches Institut, Friedrich-Schiller-Universität Jena, D-07743 Jena, Germany

³⁹University of Birmingham, Birmingham B15 2TT, United Kingdom

⁴⁰Northwestern University, Evanston, IL 60208, USA

⁴¹Instituto Nacional de Pesquisas Espaciais, 12227-010 São José dos Campos, São Paulo, Brazil

⁴²Cardiff University, Cardiff CF24 3AA, United Kingdom

⁴³INFN, Sezione di Pisa, I-56127 Pisa, Italy

- ⁴⁴International Centre for Theoretical Sciences, Tata Institute of Fundamental Research, Bengaluru 560089, India
- ⁴⁵Gravitational Wave Science Project, National Astronomical Observatory of Japan (NAOJ), Mitaka City, Tokyo 181-8588, Japan
- ⁴⁶Advanced Technology Center, National Astronomical Observatory of Japan (NAOJ), Mitaka City, Tokyo 181-8588, Japan
- ⁴⁷Dipartimento di Fisica, Università degli Studi di Torino, I-10125 Torino, Italy
- ⁴⁸INFN Sezione di Torino, I-10125 Torino, Italy
- ⁴⁹SUPA, University of Glasgow, Glasgow G12 8QQ, United Kingdom
- ⁵⁰Università di Napoli “Federico II”, Complesso Universitario di Monte S. Angelo, I-80126 Napoli, Italy
- ⁵¹Université de Lyon, Université Claude Bernard Lyon 1, CNRS, Institut Lumière Matière, F-69622 Villeurbanne, France
- ⁵²Department of Physics, The University of Tokyo, Bunkyo-ku, Tokyo 113-0033, Japan
- ⁵³Research Center for the Early Universe (RESCEU), The University of Tokyo, Bunkyo-ku, Tokyo 113-0033, Japan
- ⁵⁴Institut de Ciències del Cosmos (ICCUB), Universitat de Barcelona, C/ Martí i Franquès 1, Barcelona, 08028, Spain
- ⁵⁵Univ. Savoie Mont Blanc, CNRS, Laboratoire d’Annecy de Physique des Particules - IN2P3, F-74000 Annecy, France
- ⁵⁶Institut de Física d’Altes Energies (IFAE), Barcelona Institute of Science and Technology, and ICREA, E-08193 Barcelona, Spain
- ⁵⁷Gran Sasso Science Institute (GSSI), I-67100 L’Aquila, Italy
- ⁵⁸SUPA, University of Strathclyde, Glasgow G1 1XQ, United Kingdom
- ⁵⁹Dipartimento di Scienze Matematiche, Informatiche e Fisiche, Università di Udine, I-33100 Udine, Italy
- ⁶⁰INFN, Sezione di Trieste, I-34127 Trieste, Italy
- ⁶¹Embry-Riddle Aeronautical University, Prescott, AZ 86301, USA
- ⁶²Artemis, Université Côte d’Azur, Observatoire de la Côte d’Azur, CNRS, F-06304 Nice, France
- ⁶³GRAPPA, Anton Pannekoek Institute for Astronomy and Institute for High-Energy Physics, University of Amsterdam, Science Park 904, 1098 XH Amsterdam, Netherlands
- ⁶⁴National and Kapodistrian University of Athens, School of Science Building, 2nd floor, Panepistimiopolis, 15771 Ilissia, Greece
- ⁶⁵INFN, Sezione di Perugia, I-06123 Perugia, Italy
- ⁶⁶Università di Camerino, Dipartimento di Fisica, I-62032 Camerino, Italy
- ⁶⁷American University, Washington, D.C. 20016, USA
- ⁶⁸Earthquake Research Institute, The University of Tokyo, Bunkyo-ku, Tokyo 113-0032, Japan
- ⁶⁹California State University Fullerton, Fullerton, CA 92831, USA
- ⁷⁰Université de Paris, CNRS, Astroparticule et Cosmologie, F-75006 Paris, France
- ⁷¹Université Paris-Saclay, CNRS/IN2P3, IJCLab, 91405 Orsay, France
- ⁷²European Gravitational Observatory (EGO), I-56021 Cascina, Pisa, Italy
- ⁷³Georgia Institute of Technology, Atlanta, GA 30332, USA
- ⁷⁴Chennai Mathematical Institute, Chennai 603103, India
- ⁷⁵Department of Mathematics and Physics, Graduate School of Science and Technology, Hirosaki University, 3 Bunkyo-cho, Hirosaki, Aomori 036-8561, Japan
- ⁷⁶Columbia University, New York, NY 10027, USA
- ⁷⁷University of Portsmouth, Portsmouth, PO1 3FX, United Kingdom
- ⁷⁸Kamioka Branch, National Astronomical Observatory of Japan (NAOJ), Kamioka-cho, Hida City, Gifu 506-1205, Japan
- ⁷⁹The Graduate University for Advanced Studies (SOKENDAI), Mitaka City, Tokyo 181-8588, Japan
- ⁸⁰Università degli Studi di Urbino “Carlo Bo”, I-61029 Urbino, Italy
- ⁸¹INFN, Sezione di Firenze, I-50019 Sesto Fiorentino, Firenze, Italy
- ⁸²LIGO Livingston Observatory, Livingston, LA 70754, USA
- ⁸³INFN, Sezione di Roma, I-00185 Roma, Italy
- ⁸⁴Université catholique de Louvain, B-1348 Louvain-la-Neuve, Belgium
- ⁸⁵Nikhef, Science Park 105, 1098 XG Amsterdam, Netherlands
- ⁸⁶King’s College London, University of London, London WC2R 2LS, United Kingdom
- ⁸⁷Korea Institute of Science and Technology Information, Daejeon 34141, Republic of Korea
- ⁸⁸National Institute for Mathematical Sciences, Daejeon 34047, Republic of Korea
- ⁸⁹Christopher Newport University, Newport News, VA 23606, USA
- ⁹⁰School of High Energy Accelerator Science, The Graduate University for Advanced Studies (SOKENDAI), Tsukuba City, Ibaraki 305-0801, Japan
- ⁹¹Institute for Gravitational and Subatomic Physics (GRASP), Utrecht University, Princetonplein 1, 3584 CC Utrecht, Netherlands
- ⁹²University of Oregon, Eugene, OR 97403, USA
- ⁹³Syracuse University, Syracuse, NY 13244, USA
- ⁹⁴Université de Liège, B-4000 Liège, Belgium
- ⁹⁵Università degli Studi di Milano-Bicocca, I-20126 Milano, Italy
- ⁹⁶INFN, Sezione di Milano-Bicocca, I-20126 Milano, Italy
- ⁹⁷INAF, Osservatorio Astronomico di Brera sede di Merate, I-23807 Merate, Lecco, Italy

- ⁹⁸ *LIGO Hanford Observatory, Richland, WA 99352, USA*
- ⁹⁹ *Dipartimento di Medicina, Chirurgia e Odontoiatria “Scuola Medica Salernitana”, Università di Salerno, I-84081 Baronissi, Salerno, Italy*
- ¹⁰⁰ *LIGO Laboratory, Massachusetts Institute of Technology, Cambridge, MA 02139, USA*
- ¹⁰¹ *Wigner RCP, RMKI, H-1121 Budapest, Konkoly Thege Miklós út 29-33, Hungary*
- ¹⁰² *University of Florida, Gainesville, FL 32611, USA*
- ¹⁰³ *Stanford University, Stanford, CA 94305, USA*
- ¹⁰⁴ *Università di Pisa, I-56127 Pisa, Italy*
- ¹⁰⁵ *Università di Perugia, I-06123 Perugia, Italy*
- ¹⁰⁶ *Università di Padova, Dipartimento di Fisica e Astronomia, I-35131 Padova, Italy*
- ¹⁰⁷ *INFN, Sezione di Padova, I-35131 Padova, Italy*
- ¹⁰⁸ *Bard College, Annandale-On-Hudson, NY 12504, USA*
- ¹⁰⁹ *Montana State University, Bozeman, MT 59717, USA*
- ¹¹⁰ *Institute for Plasma Research, Bhat, Gandhinagar 382428, India*
- ¹¹¹ *Universiteit Gent, B-9000 Gent, Belgium*
- ¹¹² *Nicolaus Copernicus Astronomical Center, Polish Academy of Sciences, 00-716, Warsaw, Poland*
- ¹¹³ *Dipartimento di Ingegneria, Università del Sannio, I-82100 Benevento, Italy*
- ¹¹⁴ *OzGrav, University of Adelaide, Adelaide, South Australia 5005, Australia*
- ¹¹⁵ *The University of Texas Rio Grande Valley, Brownsville, TX 78520, USA*
- ¹¹⁶ *California State University, Los Angeles, Los Angeles, CA 90032, USA*
- ¹¹⁷ *Departamento de Matemáticas, Universitat Autònoma de Barcelona, Edificio C Facultad de Ciencias 08193 Bellaterra (Barcelona), Spain*
- ¹¹⁸ *INFN, Sezione di Genova, I-16146 Genova, Italy*
- ¹¹⁹ *OzGrav, University of Western Australia, Crawley, Western Australia 6009, Australia*
- ¹²⁰ *RRCAT, Indore, Madhya Pradesh 452013, India*
- ¹²¹ *Missouri University of Science and Technology, Rolla, MO 65409, USA*
- ¹²² *Vrije Universiteit Amsterdam, 1081 HV Amsterdam, Netherlands*
- ¹²³ *Lomonosov Moscow State University, Moscow 119991, Russia*
- ¹²⁴ *Università di Trento, Dipartimento di Fisica, I-38123 Povo, Trento, Italy*
- ¹²⁵ *INFN, Trento Institute for Fundamental Physics and Applications, I-38123 Povo, Trento, Italy*
- ¹²⁶ *SUPA, University of the West of Scotland, Paisley PA1 2BE, United Kingdom*
- ¹²⁷ *Bar-Ilan University, Ramat Gan, 5290002, Israel*
- ¹²⁸ *Dipartimento di Fisica “E.R. Caianiello”, Università di Salerno, I-84084 Fisciano, Salerno, Italy*
- ¹²⁹ *INFN, Sezione di Napoli, Gruppo Collegato di Salerno, Complesso Universitario di Monte S. Angelo, I-80126 Napoli, Italy*
- ¹³⁰ *Università di Roma “La Sapienza”, I-00185 Roma, Italy*
- ¹³¹ *Univ Rennes, CNRS, Institut FOTON - UMR6082, F-3500 Rennes, France*
- ¹³² *Indian Institute of Technology Bombay, Powai, Mumbai 400 076, India*
- ¹³³ *INFN, Laboratori Nazionali del Gran Sasso, I-67100 Assergi, Italy*
- ¹³⁴ *Laboratoire Kastler Brossel, Sorbonne Université, CNRS, ENS-Université PSL, Collège de France, F-75005 Paris, France*
- ¹³⁵ *Astronomical Observatory Warsaw University, 00-478 Warsaw, Poland*
- ¹³⁶ *University of Maryland, College Park, MD 20742, USA*
- ¹³⁷ *Max Planck Institute for Gravitational Physics (Albert Einstein Institute), D-14476 Potsdam, Germany*
- ¹³⁸ *L2IT, Laboratoire des 2 Infinis - Toulouse, Université de Toulouse, CNRS/IN2P3, UPS, F-31062 Toulouse Cedex 9, France*
- ¹³⁹ *Villanova University, Villanova, PA 19085, USA*
- ¹⁴⁰ *IGFAE, Universidad de Santiago de Compostela, 15782 Spain*
- ¹⁴¹ *Stony Brook University, Stony Brook, NY 11794, USA*
- ¹⁴² *Center for Computational Astrophysics, Flatiron Institute, New York, NY 10010, USA*
- ¹⁴³ *NASA Goddard Space Flight Center, Greenbelt, MD 20771, USA*
- ¹⁴⁴ *Dipartimento di Fisica, Università degli Studi di Genova, I-16146 Genova, Italy*
- ¹⁴⁵ *Department of Astronomy, Beijing Normal University, Beijing 100875, China*
- ¹⁴⁶ *OzGrav, University of Melbourne, Parkville, Victoria 3010, Australia*
- ¹⁴⁷ *Università degli Studi di Sassari, I-07100 Sassari, Italy*
- ¹⁴⁸ *INFN, Laboratori Nazionali del Sud, I-95125 Catania, Italy*
- ¹⁴⁹ *Università di Roma Tor Vergata, I-00133 Roma, Italy*
- ¹⁵⁰ *INFN, Sezione di Roma Tor Vergata, I-00133 Roma, Italy*
- ¹⁵¹ *University of Sannio at Benevento, I-82100 Benevento, Italy and INFN, Sezione di Napoli, I-80100 Napoli, Italy*
- ¹⁵² *Departamento de Astronomía y Astrofísica, Universitat de València, E-46100 Burjassot, València, Spain*

- ¹⁵³ *Universität Hamburg, D-22761 Hamburg, Germany*
- ¹⁵⁴ *Rochester Institute of Technology, Rochester, NY 14623, USA*
- ¹⁵⁵ *National Tsing Hua University, Hsinchu City, 30013 Taiwan, Republic of China*
- ¹⁵⁶ *The Chinese University of Hong Kong, Shatin, NT, Hong Kong*
- ¹⁵⁷ *Department of Applied Physics, Fukuoka University, Jonan, Fukuoka City, Fukuoka 814-0180, Japan*
- ¹⁵⁸ *OzGrav, Charles Sturt University, Wagga Wagga, New South Wales 2678, Australia*
- ¹⁵⁹ *Department of Physics, Tamkang University, Danshui Dist., New Taipei City 25137, Taiwan*
- ¹⁶⁰ *Department of Physics, Center for High Energy and High Field Physics, National Central University, Zhongli District, Taoyuan City 32001, Taiwan*
- ¹⁶¹ *CaRT, California Institute of Technology, Pasadena, CA 91125, USA*
- ¹⁶² *Dipartimento di Ingegneria Industriale (DIIN), Università di Salerno, I-84084 Fisciano, Salerno, Italy*
- ¹⁶³ *Institute of Physics, Academia Sinica, Nankang, Taipei 11529, Taiwan*
- ¹⁶⁴ *Université Lyon, Université Claude Bernard Lyon 1, CNRS, IP2I Lyon / IN2P3, UMR 5822, F-69622 Villeurbanne, France*
- ¹⁶⁵ *INAF, Osservatorio Astronomico di Padova, I-35122 Padova, Italy*
- ¹⁶⁶ *OzGrav, Swinburne University of Technology, Hawthorn VIC 3122, Australia*
- ¹⁶⁷ *Université libre de Bruxelles, Avenue Franklin Roosevelt 50 - 1050 Bruxelles, Belgium*
- ¹⁶⁸ *IAC3-IEEC, Universitat de les Illes Balears, E-07122 Palma de Mallorca, Spain*
- ¹⁶⁹ *Université Libre de Bruxelles, Brussels 1050, Belgium*
- ¹⁷⁰ *Departamento de Matemáticas, Universitat de València, E-46100 Burjassot, València, Spain*
- ¹⁷¹ *Texas Tech University, Lubbock, TX 79409, USA*
- ¹⁷² *University of Minnesota, Minneapolis, MN 55455, USA*
- ¹⁷³ *The Pennsylvania State University, University Park, PA 16802, USA*
- ¹⁷⁴ *University of Rhode Island, Kingston, RI 02881, USA*
- ¹⁷⁵ *Bellevue College, Bellevue, WA 98007, USA*
- ¹⁷⁶ *Scuola Normale Superiore, Piazza dei Cavalieri, 7 - 56126 Pisa, Italy*
- ¹⁷⁷ *Eötvös University, Budapest 1117, Hungary*
- ¹⁷⁸ *Maastricht University, P.O. Box 616, 6200 MD Maastricht, Netherlands*
- ¹⁷⁹ *The University of Sheffield, Sheffield S10 2TN, United Kingdom*
- ¹⁸⁰ *Université Lyon, Université Claude Bernard Lyon 1, CNRS, Laboratoire des Matériaux Avancés (LMA), IP2I Lyon / IN2P3, UMR 5822, F-69622 Villeurbanne, France*
- ¹⁸¹ *Dipartimento di Scienze Matematiche, Fisiche e Informatiche, Università di Parma, I-43124 Parma, Italy*
- ¹⁸² *INFN, Sezione di Milano Bicocca, Gruppo Collegato di Parma, I-43124 Parma, Italy*
- ¹⁸³ *The University of Utah, Salt Lake City, UT 84112, USA*
- ¹⁸⁴ *Carleton College, Northfield, MN 55057, USA*
- ¹⁸⁵ *University of Zurich, Winterthurerstrasse 190, 8057 Zurich, Switzerland*
- ¹⁸⁶ *Perimeter Institute, Waterloo, ON N2L 2Y5, Canada*
- ¹⁸⁷ *Université de Strasbourg, CNRS, IPHC UMR 7178, F-67000 Strasbourg, France*
- ¹⁸⁸ *West Virginia University, Morgantown, WV 26506, USA*
- ¹⁸⁹ *University of Chicago, Chicago, IL 60637, USA*
- ¹⁹⁰ *Montclair State University, Montclair, NJ 07043, USA*
- ¹⁹¹ *Colorado State University, Fort Collins, CO 80523, USA*
- ¹⁹² *Institute for Nuclear Research, Bem tér 18/c, H-4026 Debrecen, Hungary*
- ¹⁹³ *University of Texas, Austin, TX 78712, USA*
- ¹⁹⁴ *CNR-SPIN, c/o Università di Salerno, I-84084 Fisciano, Salerno, Italy*
- ¹⁹⁵ *Scuola di Ingegneria, Università della Basilicata, I-85100 Potenza, Italy*
- ¹⁹⁶ *Osservatori Astronomic, Universitat de València, E-46980 Paterna, València, Spain*
- ¹⁹⁷ *Centro de Física das Universidades do Minho e do Porto, Universidade do Minho, Campus de Gualtar, PT-4710 - 057 Braga, Portugal*
- ¹⁹⁸ *Department of Astronomy, The University of Tokyo, Mitaka City, Tokyo 181-8588, Japan*
- ¹⁹⁹ *Faculty of Engineering, Niigata University, Nishi-ku, Niigata City, Niigata 950-2181, Japan*
- ²⁰⁰ *Department of Physics, Graduate School of Science, Osaka City University, Sumiyoshi-ku, Osaka City, Osaka 558-8585, Japan*
- ²⁰¹ *Vanderbilt University, Nashville, TN 37235, USA*
- ²⁰² *State Key Laboratory of Magnetic Resonance and Atomic and Molecular Physics, Innovation Academy for Precision Measurement Science and Technology (APM), Chinese Academy of Sciences, Xiao Hong Shan, Wuhan 430071, China*
- ²⁰³ *University of Szeged, Dóm tér 9, Szeged 6720, Hungary*
- ²⁰⁴ *Cornell University, Ithaca, NY 14850, USA*
- ²⁰⁵ *University of British Columbia, Vancouver, BC V6T 1Z4, Canada*
- ²⁰⁶ *INAF, Osservatorio Astronomico di Capodimonte, I-80131 Napoli, Italy*

- ²⁰⁷ *The University of Mississippi, University, MS 38677, USA*
- ²⁰⁸ *University of Michigan, Ann Arbor, MI 48109, USA*
- ²⁰⁹ *Texas A&M University, College Station, TX 77843, USA*
- ²¹⁰ *Ulsan National Institute of Science and Technology, Ulsan 44919, Republic of Korea*
- ²¹¹ *Shanghai Astronomical Observatory, Chinese Academy of Sciences, Shanghai 200030, China*
- ²¹² *Institute for Cosmic Ray Research (ICRR), KAGRA Observatory, The University of Tokyo, Kashiwa City, Chiba 277-8582, Japan*
- ²¹³ *Faculty of Science, University of Toyama, Toyama City, Toyama 930-8555, Japan*
- ²¹⁴ *Institute for Cosmic Ray Research (ICRR), KAGRA Observatory, The University of Tokyo, Kamioka-cho, Hida City, Gifu 506-1205, Japan*
- ²¹⁵ *University of California, Berkeley, CA 94720, USA*
- ²¹⁶ *Maastricht University, 6200 MD, Maastricht, Netherlands*
- ²¹⁷ *Lancaster University, Lancaster LA1 4YW, United Kingdom*
- ²¹⁸ *College of Industrial Technology, Nihon University, Narashino City, Chiba 275-8575, Japan*
- ²¹⁹ *Rutherford Appleton Laboratory, Didcot OX11 0DE, United Kingdom*
- ²²⁰ *Department of Astronomy & Space Science, Chungnam National University, Yuseong-gu, Daejeon 34134, Republic of Korea*
- ²²¹ *Department of Physical Sciences, Aoyama Gakuin University, Sagami-hara City, Kanagawa 252-5258, Japan*
- ²²² *Kavli Institute for Astronomy and Astrophysics, Peking University, Haidian District, Beijing 100871, China*
- ²²³ *Aristotle University of Thessaloniki, University Campus, 54124 Thessaloniki, Greece*
- ²²⁴ *Graduate School of Science and Engineering, University of Toyama, Toyama City, Toyama 930-8555, Japan*
- ²²⁵ *Nambu Yoichiro Institute of Theoretical and Experimental Physics (NITEP), Osaka City University, Sumiyoshi-ku, Osaka City, Osaka 558-8585, Japan*
- ²²⁶ *Directorate of Construction, Services & Estate Management, Mumbai 400094, India*
- ²²⁷ *Universiteit Antwerpen, Prinsstraat 13, 2000 Antwerpen, Belgium*
- ²²⁸ *University of Białystok, 15-424 Białystok, Poland*
- ²²⁹ *Ewha Womans University, Seoul 03760, Republic of Korea*
- ²³⁰ *National Astronomical Observatories, Chinese Academic of Sciences, Chaoyang District, Beijing, China*
- ²³¹ *School of Astronomy and Space Science, University of Chinese Academy of Sciences, Chaoyang District, Beijing, China*
- ²³² *University of Southampton, Southampton SO17 1BJ, United Kingdom*
- ²³³ *Institute for Cosmic Ray Research (ICRR), The University of Tokyo, Kashiwa City, Chiba 277-8582, Japan*
- ²³⁴ *Institute for High-Energy Physics, University of Amsterdam, Science Park 904, 1098 XH Amsterdam, Netherlands*
- ²³⁵ *Chung-Ang University, Seoul 06974, Republic of Korea*
- ²³⁶ *University of Washington Bothell, Bothell, WA 98011, USA*
- ²³⁷ *Institute of Applied Physics, Nizhny Novgorod, 603950, Russia*
- ²³⁸ *Inje University Gimhae, South Gyeongsang 50834, Republic of Korea*
- ²³⁹ *Department of Physics, Myongji University, Yongin 17058, Republic of Korea*
- ²⁴⁰ *Institute of Particle and Nuclear Studies (IPNS), High Energy Accelerator Research Organization (KEK), Tsukuba City, Ibaraki 305-0801, Japan*
- ²⁴¹ *School of Physics and Astronomy, Cardiff University, Cardiff, CF24 3AA, UK*
- ²⁴² *Institute of Mathematics, Polish Academy of Sciences, 00656 Warsaw, Poland*
- ²⁴³ *National Center for Nuclear Research, 05-400 Świerk-Otwock, Poland*
- ²⁴⁴ *Instituto de Física Teórica, 28049 Madrid, Spain*
- ²⁴⁵ *Department of Physics, Nagoya University, Chikusa-ku, Nagoya, Aichi 464-8602, Japan*
- ²⁴⁶ *Université de Montréal/Polytechnique, Montreal, Quebec H3T 1J4, Canada*
- ²⁴⁷ *Laboratoire Lagrange, Université Côte d'Azur, Observatoire Côte d'Azur, CNRS, F-06304 Nice, France*
- ²⁴⁸ *Seoul National University, Seoul 08826, Republic of Korea*
- ²⁴⁹ *Sungkyunkwan University, Seoul 03063, Republic of Korea*
- ²⁵⁰ *NAVIER, École des Ponts, Univ Gustave Eiffel, CNRS, Marne-la-Vallée, France*
- ²⁵¹ *Università di Firenze, Sesto Fiorentino I-50019, Italy*
- ²⁵² *Department of Physics, National Cheng Kung University, Tainan City 701, Taiwan*
- ²⁵³ *School of Physics and Technology, Wuhan University, Wuhan, Hubei, 430072, China*
- ²⁵⁴ *National Center for High-performance computing, National Applied Research Laboratories, Hsinchu Science Park, Hsinchu City 30076, Taiwan*
- ²⁵⁵ *Department of Physics, National Taiwan Normal University, sec. 4, Taipei 116, Taiwan*
- ²⁵⁶ *NASA Marshall Space Flight Center, Huntsville, AL 35811, USA*
- ²⁵⁷ *INFN, Sezione di Roma Tre, I-00146 Roma, Italy*
- ²⁵⁸ *ESPCI, CNRS, F-75005 Paris, France*
- ²⁵⁹ *Kenyon College, Gambier, OH 43022, USA*

- ²⁶⁰ *School of Physics Science and Engineering, Tongji University, Shanghai 200092, China*
- ²⁶¹ *Dipartimento di Fisica, Università di Trieste, I-34127 Trieste, Italy*
- ²⁶² *Institute for Photon Science and Technology, The University of Tokyo, Bunkyo-ku, Tokyo 113-8656, Japan*
- ²⁶³ *Indian Institute of Technology Madras, Chennai 600036, India*
- ²⁶⁴ *Saha Institute of Nuclear Physics, Bidhannagar, West Bengal 700064, India*
- ²⁶⁵ *Institute of Space and Astronautical Science (JAXA), Chuo-ku, Sagami-hara City, Kanagawa 252-0222, Japan*
- ²⁶⁶ *Institut des Hautes Etudes Scientifiques, F-91440 Bures-sur-Yvette, France*
- ²⁶⁷ *Faculty of Law, Ryukoku University, Fushimi-ku, Kyoto City, Kyoto 612-8577, Japan*
- ²⁶⁸ *Indian Institute of Science Education and Research, Kolkata, Mohanpur, West Bengal 741252, India*
- ²⁶⁹ *Department of Physics, University of Notre Dame, Notre Dame, IN 46556, USA*
- ²⁷⁰ *Graduate School of Science and Technology, Niigata University, Nishi-ku, Niigata City, Niigata 950-2181, Japan*
- ²⁷¹ *Consiglio Nazionale delle Ricerche - Istituto dei Sistemi Complessi, Piazzale Aldo Moro 5, I-00185 Roma, Italy*
- ²⁷² *Korea Astronomy and Space Science Institute (KASI), Yuseong-gu, Daejeon 34055, Republic of Korea*
- ²⁷³ *Hobart and William Smith Colleges, Geneva, NY 14456, USA*
- ²⁷⁴ *International Institute of Physics, Universidade Federal do Rio Grande do Norte, Natal RN 59078-970, Brazil*
- ²⁷⁵ *Museo Storico della Fisica e Centro Studi e Ricerche "Enrico Fermi", I-00184 Roma, Italy*
- ²⁷⁶ *Dipartimento di Matematica e Fisica, Università degli Studi Roma Tre, I-00146 Roma, Italy*
- ²⁷⁷ *University of Arizona, Tucson, AZ 85721, USA*
- ²⁷⁸ *Università di Trento, Dipartimento di Matematica, I-38123 Povo, Trento, Italy*
- ²⁷⁹ *University of California, Riverside, Riverside, CA 92521, USA*
- ²⁸⁰ *University of Washington, Seattle, WA 98195, USA*
- ²⁸¹ *Indian Institute of Technology, Palaj, Gandhinagar, Gujarat 382355, India*
- ²⁸² *Department of Electronic Control Engineering, National Institute of Technology, Nagaoka College, Nagaoka City, Niigata 940-8532, Japan*
- ²⁸³ *Departamento de Matemática da Universidade de Aveiro and Centre for Research and Development in Mathematics and Applications, Campus de Santiago, 3810-183 Aveiro, Portugal*
- ²⁸⁴ *Marquette University, Milwaukee, WI 53233, USA*
- ²⁸⁵ *Faculty of Science, Toho University, Funabashi City, Chiba 274-8510, Japan*
- ²⁸⁶ *Graduate School of Science and Technology, Gunma University, Maebashi, Gunma 371-8510, Japan*
- ²⁸⁷ *Institute for Quantum Studies, Chapman University, Orange, CA 92866, USA*
- ²⁸⁸ *Accelerator Laboratory, High Energy Accelerator Research Organization (KEK), Tsukuba City, Ibaraki 305-0801, Japan*
- ²⁸⁹ *Faculty of Information Science and Technology, Osaka Institute of Technology, Hirakata City, Osaka 573-0196, Japan*
- ²⁹⁰ *INAF, Osservatorio Astrofisico di Arcetri, Largo E. Fermi 5, I-50125 Firenze, Italy*
- ²⁹¹ *Indian Institute of Technology Hyderabad, Sangareddy, Khandi, Telangana 502285, India*
- ²⁹² *Indian Institute of Science Education and Research, Pune, Maharashtra 411008, India*
- ²⁹³ *Istituto di Astrofisica e Planetologia Spaziali di Roma, Via del Fosso del Cavaliere, 100, 00133 Roma RM, Italy*
- ²⁹⁴ *Department of Space and Astronautical Science, The Graduate University for Advanced Studies (SOKENDAI), Sagami-hara City, Kanagawa 252-5210, Japan*
- ²⁹⁵ *Andrews University, Berrien Springs, MI 49104, USA*
- ²⁹⁶ *Research Center for Space Science, Advanced Research Laboratories, Tokyo City University, Setagaya, Tokyo 158-0082, Japan*
- ²⁹⁷ *Institute for Cosmic Ray Research (ICRR), Research Center for Cosmic Neutrinos (RCCN), The University of Tokyo, Kashiwa City, Chiba 277-8582, Japan*
- ²⁹⁸ *Department of Physics, Kyoto University, Sakyou-ku, Kyoto City, Kyoto 606-8502, Japan*
- ²⁹⁹ *Yukawa Institute for Theoretical Physics (YITP), Kyoto University, Sakyou-ku, Kyoto City, Kyoto 606-8502, Japan*
- ³⁰⁰ *Dipartimento di Scienze Aziendali - Management and Innovation Systems (DISA-MIS), Università di Salerno, I-84084 Fisciano, Salerno, Italy*
- ³⁰¹ *Van Swinderen Institute for Particle Physics and Gravity, University of Groningen, Nijenborgh 4, 9747 AG Groningen, Netherlands*
- ³⁰² *Faculty of Science, Department of Physics, The Chinese University of Hong Kong, Shatin, N.T., Hong Kong*
- ³⁰³ *Vrije Universiteit Brussel, Pleinlaan 2, 1050 Brussel, Belgium*
- ³⁰⁴ *Applied Research Laboratory, High Energy Accelerator Research Organization (KEK), Tsukuba City, Ibaraki 305-0801, Japan*
- ³⁰⁵ *Department of Communications Engineering, National Defense Academy of Japan, Yokosuka City, Kanagawa 239-8686, Japan*
- ³⁰⁶ *Department of Physics, University of Florida, Gainesville, FL 32611, USA*
- ³⁰⁷ *Department of Information and Management Systems Engineering, Nagaoka University of Technology, Nagaoka City, Niigata 940-2188, Japan*
- ³⁰⁸ *Tata Institute of Fundamental Research, Mumbai 400005, India*
- ³⁰⁹ *Eindhoven University of Technology, Postbus 513, 5600 MB Eindhoven, Netherlands*
- ³¹⁰ *Department of Physics and Astronomy, Sejong University, Gwangjin-gu, Seoul 143-747, Republic of Korea*
- ³¹¹ *Concordia University Wisconsin, Mequon, WI 53097, USA*

³¹²*Department of Electrophysics, National Yang Ming Chiao Tung University, Hsinchu, Taiwan*
³¹³*Department of Physics, Rikkyo University, Toshima-ku, Tokyo 171-8501, Japan*

(Dated: August 29, 2023)

ABSTRACT

We present *Fermi* Gamma-ray Burst Monitor (*Fermi*-GBM) and *Swift* Burst Alert Telescope (*Swift*-BAT) searches for gamma-ray/X-ray counterparts to gravitational wave (GW) candidate events identified during the third observing run of the Advanced LIGO and Advanced Virgo detectors. Using *Fermi*-GBM on-board triggers and sub-threshold gamma-ray burst (GRB) candidates found in the *Fermi*-GBM ground analyses, the Targeted Search and the Untargeted Search, we investigate whether there are any coincident GRBs associated with the GWs. We also search the *Swift*-BAT rate data around the GW times to determine whether a GRB counterpart is present. No counterparts are found. Using both the *Fermi*-GBM Targeted Search and the *Swift*-BAT search, we calculate flux upper limits and present joint upper limits on the gamma-ray luminosity of each GW. Given these limits, we constrain theoretical models for the emission of gamma-rays from binary black hole mergers.

1. INTRODUCTION

The detection of GW170817 (Abbott et al. 2017) coincident with the short gamma-ray burst GRB 170817A (Goldstein et al. 2017; Savchenko et al. 2017) was a ground-breaking discovery for the multimessenger era. Not only was it the first binary neutron star (BNS) merger detected by the gravitational-wave (GW) instruments Advanced LIGO (Aasi et al. 2015) and Advanced Virgo (Acernese et al. 2014), it was also the first, and to date only, GW detection with a confirmed electromagnetic (EM) counterpart. Since then, the search for EM emission from more of these extreme events has been at the forefront of multimessenger astronomy, particularly in the gamma-ray energy band since GRB 170817A demonstrated that BNS mergers are a progenitor of short gamma-ray bursts (GRBs) (Abbott et al. 2017). GWs have also been observed from the mergers of other compact objects, such as binary black hole (BBH) and neutron star–black hole (NSBH) systems (Abbott et al. 2019; Abbott et al. 2021; Abbott et al. 2021; Abbott et al. 2021); however, no additional EM counterparts have been confirmed as they have been inconclusive (Connaughton et al. 2016; LSC and Virgo and Fermi-GBM Team 2019a,b) or are still under debate (Graham et al. 2020; Ashton et al. 2021; Bustillo et al. 2021; De Paolis et al. 2020; Palmese et al. 2021).

GRB 170817A was first reported by the *Fermi* Gamma-ray Burst Monitor (GBM; Meegan et al. 2009), a space-based gamma-ray instrument sensitive from 8 keV to 40 MeV. This wide energy range of *Fermi*-GBM combined with its large field-of-view (FoV) and rapid alert abilities make it an ideal platform to search

for gamma-ray counterparts to GWs in real time. *Fermi*-GBM also provides continuous time tagged event (CTTE) data with a 6-hour latency that enables sensitive searches for short GRBs on the ground. Two of these searches are the Untargeted Search, a blind search of *Fermi*-GBM data for short GRBs, and the Targeted Search, which uses an external time to search for a short GRB (Blackburn et al. 2015; Goldstein et al. 2019). Both were previously used to look for sub-threshold GRBs coincident with GWs from the first two LIGO-Virgo observing runs.

Additionally, the Burst Alert Telescope (BAT; Barthelmy et al. 2005) on-board the *Neil Gehrels Swift Observatory* (hereafter referred to as *Swift*) provides excellent sensitivity to detecting hard X-ray and gamma-ray transients (Gehrels et al. 2004). *Swift*-BAT primarily runs in a survey mode that continuously evaluates photon rate increases and potential GRB triggers. An increase in the observed photon rate can trigger the on-board image-processing algorithms which can yield \sim arcminute GRB localizations.

Ideally, *Swift*-BAT would detect and localize a GRB produced by a binary merger independently of the GW detection. If a GRB does not trigger an on-board detection, continuous count rate lightcurves are still available for offline ground searches. Although *Swift*-BAT has been used to search for public and sub-threshold GWs during the LIGO-Virgo observing runs, this work presents the first systematic search of *Swift*-BAT data from a LIGO-Virgo observing run.

The first observing run (O1) operated from September 2015 to January 2016, producing the first detection of GWs from a BBH merger (GW150914; Abbott et al. 2016). Burns et al. (2019) used the *Fermi*-GBM Targeted Search to identify both triggered and sub-threshold GRB candidates in coincidence with GW

* Deceased, August 2020.

† Deceased, April 2021.

candidates from O1. The most significant gamma-ray candidate found by the search was within 0.4 s of GW150914; however, it could not be confirmed as a counterpart due to its weak signal and poor localization (Connaughton et al. 2016; Greiner et al. 2016; Connaughton et al. 2018).

The second observing run (O2) took place from November 2016 to August 2017, resulting in the detections of GW170817, GRB 170817A, and the kilonova AT2017gfo (Chornock et al. 2017; Cowperthwaite et al. 2017; Nicholl et al. 2017; Soares-Santos et al. 2017; Tanvir et al. 2017; Margutti & Chornock 2021). Following O2, the LIGO Scientific and Virgo Collaboration published its first catalog of GW signals called the Gravitational-Wave Transient Catalog 1 (GWTC-1; Abbott et al. 2019) using a re-analysis of data from both O1 and O2. Hamburg et al. (2020) searched for GRBs coincident to the GWs reported in GWTC-1, using *Fermi*-GBM triggers as well as sub-threshold GRB candidates from the Untargeted and Targeted Searches, but found no additional counterparts beyond GRB 170817A.

The third observing run (O3) occurred from April 2019 to March 2020 with a month-long commissioning break during October 2019. It benefited from improvements to the sensitivity and duty cycle of the GW detectors made after O2 (Buikema et al. 2020; Abbott et al. 2021; Acernese et al. 2019). This observing run provided 56 public GW candidates in real-time with information from their preliminary analysis. More detailed analyses were published by the LIGO, Virgo, and KAGRA (LVK) Collaboration in a series of GWTCs (GWTC-2; Abbott et al. 2021, GWTC-2.1; Abbott et al. 2021, GWTC-3; Abbott et al. 2021) with GWTC-3 providing a cumulative list of 79 GW signals from O3 with a probability of astrophysical origin ($p_{\text{astro}} > 0.5$) – an 8-fold increase relative to O2. Among these candidates was the detection of a second confident signal classified as a BNS merger, GW190425, whose total mass is larger than that known from Galactic neutron star binaries (Abbott et al. 2020).

Additionally, GW191219.163120 and GW200115.042309 provided the first detections of NSBH systems with $p_{\text{astro}} > 0.5$. Another possible NSBH, GW200105.162426, fell just outside the $p_{\text{astro}} > 0.5$ criterion in the GWTC-3 analysis (Abbott et al. 2021). There were also two confident detections with ambiguous classifications, GW190814 (Abbott et al. 2020b) and GW200210.092254, that represent a black hole merging with either a light black hole or a heavy neutron star. An overwhelming majority of the remaining candidates are most likely BBH in origin.

In this paper, we search *Fermi*-GBM and *Swift*-BAT data for short GRB counterparts to GW candidates from O3, discussed in Section 2.1. Section 2.2 provides an overview of the *Fermi*-GBM Untargeted Search as well as improvements made to the *Fermi*-GBM Targeted Search. Section 2.3 describes the *Swift*-BAT sub-threshold search. We present the results of the search with *Fermi*-GBM triggers and the Untargeted Search in Section 3.1; with the *Fermi*-GBM Targeted Search, including a new joint ranking statistic that takes the spatial coincidence into account, in Section 3.2; and with the *Swift*-BAT sub-threshold search in 3.3. Section 3.4 presents the results from both *Fermi*-GBM and *Swift*-BAT for the marginal GWs identified in Section 2.1. Furthermore, Section 4 divides the discussion of GWs with $p_{\text{astro}} > 0.5$ into two groups depending on their estimated secondary component mass m_2 . For mergers with a possible neutron star component, we present the flux and isotropic equivalent luminosity upper limits from both *Fermi*-GBM and *Swift*-BAT (Section 4.1). For the BBH mergers, we compare the lack of observed gamma-ray emission to that predicted by theoretical models (Section 4.2). We discuss upper limits to the marginal GWs in Section 4.3. Finally, in Section 5 we summarize our results and discuss future plans for using the sub-threshold searches for GWs.

2. METHOD

In this section, we summarize the set of GW signals that we analyze from O3. We also present the search methods used to find coincident gamma-ray and hard X-ray emission with *Fermi*-GBM and *Swift*-BAT.

2.1. GW Trigger Selection

The analysis reported here focuses on GW candidates identified during O3. These were selected by four separate analysis pipelines (i.e., GstLAL, Multi-Band Template Analysis (MBTA), PyCBC, and cWB) and published in GWTC-3 (Abbott et al. 2021). Each pipeline calculates both a false alarm rate (FAR) from a background noise hypothesis and a p_{astro} for each candidate assuming a compact binary coalescence source. Candidate signals with $p_{\text{astro}} > 0.5$ in any pipeline are selected for detailed analysis with a full estimation of the potential astrophysical source parameters. The one exception is GW candidates identified by the minimally modeled cWB pipeline, which requires a time-matched confirmation with $p_{\text{astro}} > 0.1$ in one of the other pipelines in order to ensure they originated from a compact binary coalescence. In total, there were 79 GWs identified with $p_{\text{astro}} > 0.5$ during O3. Table 1 shows the candidate identifier, date, time, and p_{astro} for these GWs.

The remaining subset of GW signals with a FAR below 2 yr^{-1} and $p_{\text{astro}} \leq 0.5$ in a given pipeline are considered marginal GW candidates. As of GWTC-3, there are 6 marginal candidates which cannot be attributed to instrumental or environmental causes (Table 2). We exclude these candidates from our main analysis; however, since the existence of a gamma-ray counterpart could potentially prove an astrophysical origin, we perform separate searches around each marginal candidate.

2.2. Fermi-GBM Searches

Fermi-GBM has 12 sodium iodide (NaI) and 2 bismuth germanate (BGO) detectors that are strategically positioned to cover the full sky, unoccluded by the Earth (Meegan et al. 2009). The flight software on-board *Fermi*-GBM triggers on an event when there is an influx of gamma rays at a level greater than 4.5σ above the background rate in at least two NaI detectors (Paciesas et al. 2012). Additionally, the downlink of CTTE data enables searches for GRBs below *Fermi*-GBM’s on-board triggering threshold using ground-based computing resources. With $2 \mu\text{s}$ timing resolution and full coverage of the unoccluded sky over the energy range from 8 keV to 40 MeV, CTTE data has significantly expanded the sensitivity of the *Fermi*-GBM instrument and its sub-threshold searches.

2.2.1. Untargeted Search

The *Fermi*-GBM Untargeted Search is a blind search that automatically scans the CTTE data for significant count rate increases in at least two NaI detectors. The algorithm was originally developed for detecting terrestrial gamma-ray flashes (Briggs et al. 2013) and has since been adapted to search for short GRBs with fluxes below the on-board triggering threshold. The Untargeted Search runs through eighteen timescales ranging from 64 ms to 31 s and five energy bins from 27 keV to 985 keV, and short GRB candidates are identified when at least two detectors exceed 2.5σ and 1.25σ above the background rate. Each candidate is given a reliability score based on whether the geometry of the detectors with significant flux is consistent with the observation of a distant astrophysical source. Currently, short GRB candidates with durations less than 2.8 s and reliability classifications of low, medium, and high are publicly distributed via GCN.¹

In this work, we combine short GRB candidates detected by the Untargeted Search with GBM-triggered GRBs and examine their temporal offsets from the GWs listed in Table 1. Theoretical models predict the tem-

poral offset between merger time and the production of gamma-rays to range from 0.01 s to 10 s depending on the conditions producing the gamma-ray emission (Zhang 2019). For GRB 170817A, the only known short GRB associated with a GW, the temporal offset was 1.7 s with a duration (T_{90}) over which 5–95% of the GRB flux (50–300 keV) was detected of 2 s (Abbott et al. 2017). This is consistent with a range of physically viable scenarios (e.g., Lin et al. 2018; Salafia et al. 2018; Zhang et al. 2018) where the temporal offset is correlated with burst duration. We therefore choose to subtract the burst duration timescale from the temporal offset when performing our analysis. Doing so increases the observed significance of simulated short GRB counterparts and yields no loss in detection sensitivity at the 3σ level in alternative scenarios where the temporal offset is the same for all simulated GRBs.

After calculating the time offsets for each GW–GRB pair minus the burst duration, the smallest resulting time offset for each GW is taken. For GBM-triggered GRBs, we use the T_{90} as a measure of the duration. For GRB candidates from the Untargeted Search, we use the most significant timescale over which the GRB candidate was detected, which scales linearly with T_{90} for on-board triggered GRBs. A background distribution is produced in the same way by replacing the observed GW times with random times during which there are no reported GW signals. This yields a distribution of temporal offsets minus the burst duration between unrelated GWs and the GRB sample. In both the search and background samples, positive and negative time offsets are allowed, with no maxima imposed. GW triggers occurring during *Fermi* passage through South Atlantic Anomaly (SAA) are also included. See the results presented in Section 3.1 for a comparison of the cumulative signal and background distributions.

2.2.2. GBM Targeted Search

The *Fermi*-GBM Targeted Search was developed for multimessenger follow-up observations (Blackburn et al. 2015). It uses CTTE data to scan around an external trigger time for gamma-ray emission typical of a short GRB. For follow-up of the GWs in Table 1, we search from -1 s to $+30$ s around the GW time to ensure we do not miss unexpectedly delayed gamma-ray emission from a counterpart short GRB, even after accounting for temporal offsets up to 10 s relative to the GW time. Starting 1 s before the GW time provides a comfortable buffer to account for the fact that the trigger times can vary by a few milliseconds for GW signals that are identified by multiple pipelines. The scan is repeated for eight characteristic emission timescales which increase

¹ https://gcn.gsfc.nasa.gov/fermi_gbm_subthresh_archive.html

Table 1. GW candidates from O3 with $p_{\text{astro}} > 0.5$ (Abbott et al. 2021).

Event Name	Date	Time (UTC)	p_{astro}	Event Name	Date	Time (UTC)	p_{astro}
GW190403_051519	04-03-2019	05:15:19	0.60	GW191103_012549	11-03-2019	01:25:49	0.94
GW190408_181802	04-08-2019	18:18:02	>0.99	GW191105_143521	11-05-2019	14:35:21	>0.99
GW190412	04-12-2019	05:30:44	>0.99	GW191109_010717	11-09-2019	01:07:17	>0.99
GW190413_052954	04-13-2019	05:29:54	0.92	GW191113_071753	11-13-2019	07:17:53	0.68
GW190413_134308	04-13-2019	13:43:08	0.99	GW191126_115259	11-26-2019	11:52:59	0.70
GW190421_213856	04-21-2019	21:38:56	>0.99	GW191127_050227	11-27-2019	05:02:27	0.74
GW190425	04-25-2019	08:18:05	0.69	GW191129_134029	11-29-2019	13:40:29	>0.99
GW190426_190642	04-26-2019	19:06:42	0.73	GW191204_110529	12-04-2019	11:05:29	0.74
GW190503_185404	05-03-2019	18:54:04	>0.99	GW191204_171526	12-04-2019	17:15:26	>0.99
GW190512_180714	05-12-2019	18:07:14	>0.99	GW191215_223052	12-15-2019	22:30:52	>0.99
GW190513_205428	05-13-2019	20:54:28	>0.99	GW191216_213338	12-16-2019	21:33:38	>0.99
GW190514_065416	05-14-2019	06:54:16	0.75	GW191219_163120	12-19-2019	16:31:20	0.82
GW190517_055101	05-17-2019	05:51:01	>0.99	GW191222_033537	12-22-2019	03:35:37	>0.99
GW190519_153544	05-19-2019	15:35:44	>0.99	GW191230_180458	12-30-2019	18:04:58	0.96
GW190521	05-21-2019	03:02:29	>0.99	GW200112_155838	01-12-2020	15:58:38	>0.99
GW190521_074359	05-21-2019	07:43:59	>0.99	GW200115_042309	01-15-2020	04:23:09	>0.99
GW190527_092055	05-27-2019	09:20:55	0.83	GW200128_022011	01-28-2020	02:20:11	>0.99
GW190602_175927	06-02-2019	17:59:27	>0.99	GW200129_065458	01-29-2020	06:54:58	>0.99
GW190620_030421	06-20-2019	03:04:21	0.99	GW200202_154313	02-02-2020	15:43:13	>0.99
GW190630_185205	06-30-2019	18:52:05	>0.99	GW200208_130117	02-08-2020	13:01:17	>0.99
GW190701_203306	07-01-2019	20:33:06	>0.99	GW200208_222617	02-08-2020	22:26:17	0.70
GW190706_222641	07-06-2019	22:26:41	>0.99	GW200209_085452	02-09-2020	08:54:52	0.97
GW190707_093326	07-07-2019	09:33:26	>0.99	GW200210_092254	02-10-2020	09:22:54	0.54
GW190708_232457	07-08-2019	23:24:57	>0.99	GW200216_220804	02-16-2020	22:08:04	0.77
GW190719_215514	07-19-2019	21:55:14	0.91	GW200219_094415	02-19-2020	09:44:15	>0.99
GW190720_000836	07-20-2019	00:08:36	>0.99	GW200220_061928	02-20-2020	06:19:28	0.62
GW190725_174728	07-25-2019	17:47:28	0.96	GW200220_124850	02-20-2020	12:48:50	0.83
GW190727_060333	07-27-2019	06:03:33	>0.99	GW200224_222234	02-24-2020	22:22:34	>0.99
GW190728_064510	07-28-2019	06:45:10	>0.99	GW200225_060421	02-25-2020	06:04:21	>0.99
GW190731_140936	07-31-2019	14:09:36	0.83	GW200302_015811	03-02-2020	01:58:11	0.91
GW190803_022701	08-03-2019	02:27:01	0.97	GW200306_093714	03-06-2020	09:37:14	0.81
GW190805_211137	08-05-2019	21:11:37	0.95	GW200308_173609	03-08-2020	17:36:09	0.86
GW190814	08-14-2019	21:10:39	>0.99	GW200311_115853	03-11-2020	11:58:53	>0.99
GW190828_063405	08-28-2019	06:34:05	>0.99	GW200316_215756	03-16-2020	21:57:56	>0.99
GW190828_065509	08-28-2019	06:55:09	>0.99	GW200322_091133	03-22-2020	09:11:33	0.62
GW190910_112807	09-10-2019	11:28:07	>0.99				
GW190915_235702	09-15-2019	23:57:02	>0.99				
GW190916_200658	09-16-2019	20:06:58	0.62				
GW190917_114630	09-17-2019	11:46:30	0.74				
GW190924_021846	09-24-2019	02:18:46	>0.99				
GW190925_232845	09-25-2019	23:28:45	0.99				
GW190926_050336	09-26-2019	05:03:36	0.51				
GW190929_012149	09-29-2019	01:21:49	0.86				
GW190930_133541	09-30-2019	13:35:41	>0.99				

Table 2. Marginal GWs from O3 without clear instrumental or environmental causes (Abbott et al. 2021; Abbott et al. 2021)

Event Name	Date	Time (UTC)	p_{astro}
GW190426_152155	04-26-2019	15:21:55	0.14
GW190531_023648	05-31-2019	02:36:48	0.28
GW191118_212859	11-18-2019	21:28:59	0.05
GW200105_162426	01-05-2020	16:24:26	0.36
GW200201_203549	02-01-2020	20:35:49	0.12
GW200311_103121	03-11-2020	10:31:21	0.19

by factors of 2 from 64 ms to 8.192 s. Each emission timescale begins the search centered at the start of the scan window and then advances until the end using a fixed time step size. Emission timescales greater than 256 ms use a time step equal to one-eighth the total emission duration. The remaining emission timescales use a 64 ms step size to limit both the additional trials and the additional computational time associated with the shorter emission timescales.

The Targeted Search achieves greater sensitivity than the on-board triggering algorithm by processing the data from all 14 detectors coherently rather than focusing on significant signals present in detector pairs. This allows for the detection of weaker signals below the *Fermi*-GBM on-board triggering threshold (Kocevski et al. 2018). To do this, three spectral templates representing spectrally hard, normal, and soft GRBs (Table 3) are folded through the GBM detector responses to produce an expected count rate for a given astrophysical source location and flux. This expected count rate is then compared to the observed counts through a log-likelihood ratio,

$$\mathcal{L}_j(d, s) = \sum_i \left[\ln \frac{\sigma_{n_i}}{\sigma_{d_i}} + \frac{\tilde{d}_i^2}{2\sigma_{n_i}^2} - \frac{(\tilde{d}_i - r_{i,j}s)^2}{2\sigma_{d_i}^2} \right], \quad (1)$$

where \tilde{d}_i represents the background-subtracted measurements in each detector, σ_n is the standard deviation of the background measurement, σ_{d_i} is the standard deviation of the expected data (background+signal), $r_{i,j}$ is the location-dependent instrumental response for the spectrum denoted by index j , and s is the intrinsic source photon flux at the Earth. See Blackburn et al. (2015) for a full derivation.

The log-likelihood ratio quantifies the probability that an astrophysical source is present versus a background-only hypothesis. It is first computed separately for each point on the sky and spectral template at a given time and emission duration. During this process we estimate the best-fit photon flux for each spectral template by finding the value s_{best} that maximizes the log-likelihood ratio. Since the best-fit photon flux maximizes the likelihood, which is effectively a product of Gaussian dis-

tributions, the variance on this photon flux equals the variance of the likelihood:

$$\sigma_{\mathcal{L}_j}^2 = \frac{1}{\sum r_{i,j}^2 / \sigma_{d_i}^2}, \quad (2)$$

where σ_{d_i} includes both background and source contributions, with the latter evaluated at s_{best} . Signal injection studies using the normal spectral template demonstrated that this formulation yields the expected error coverage levels for true source fluxes near 1×10^{-7} erg cm $^{-2}$ s $^{-1}$ and below, which is the relevant flux range for this sub-threshold analysis in *Fermi*-GBM.

We marginalize the log-likelihood ratio over all possible source amplitudes using a modified power law prior designed to both avoid divergence and to produce a luminosity distribution for the observed source flux that is invariant with respect to source distance (Blackburn et al. 2015):

$$P(s) = \left[1 - e^{-(s/2.5\sigma_{\mathcal{L}})^{-1}} \right] s^{-1}. \quad (3)$$

The net result is a hypothesis test formulation following Bayes' theorem.

The amplitude-marginalized log-likelihood ratios for individual spectral templates, $\mathcal{L}'_j(d)$, at each time and duration are then averaged over all sky positions and templates using a uniform prior to formulate the full marginal log-likelihood ratio,

$$\Lambda = \sum_{j=1}^3 \frac{1}{3} \int \frac{\mathcal{L}'_j(d)}{4\pi} d\Omega, \quad (4)$$

where the sum over j covers the hard, normal, and soft spectral templates. The marginal results from all scanned times and durations are then sorted according to the largest value of Λ after filtering out known detector effects.

Localization maps estimating the probability of finding the true source location at each point on the sky are produced for the top ranking candidates using the log-likelihood ratio of the best-fitting spectrum for each candidate. This is done by noting that the log-likelihood

Table 3. Spectral templates used by the *Fermi*-GBM Targeted Search.

Template	Type	Parameters
hard	Cut-off Power-law (Goldstein et al. 2016)	$E_{\text{peak}} = 1500 \text{ keV}, \alpha = -1.5$
normal	Band (Band et al. 1993)	$E_{\text{peak}} = 230 \text{ keV}, \alpha = -1.0, \beta = -2.3$
soft	Band (Band et al. 1993)	$E_{\text{peak}} = 70 \text{ keV}, \alpha = -1.9, \beta = -3.7$

ratio asymptotically approaches the behavior of a χ^2 distribution according to Wilks’ theorem (Wilks 1938) with a statistical probability given by

$$P \propto \exp[\mathcal{L}'_j(d)]. \quad (5)$$

The statistical probability is then convolved with Gaussian kernels to account for systematic errors, which are predominantly induced by the difference between the true source spectrum and the three spectral templates, imperfect knowledge of the detector response, and whether atmospheric scattering is taken into account for a given spacecraft rocking angle. As a final step, we set the region blocked by the Earth in *Fermi*-GBM to zero and re-normalize the map to account for the fact that gamma-ray sources are not visible through the Earth and an implicit assumption that the signal has a non-terrestrial origin.

The Targeted Search method was previously used to search for sub-threshold counterparts to GWs identified during the O1 and O2 observing runs (Hamburg et al. 2020). A number of improvements were made to it in preparation for O3 (Goldstein et al. 2019):

1. Removal of the lowest 4–12 keV energy channel in the NaI detector data helped remove detector noise as well as Galactic transients.
2. Better background fitting during approach and exit from the SAA. This reduces local particle background triggers that were present in about 1% of searches and formed the dominant non-GRB background in the high log-likelihood ratio parameter space.
3. Better detector response models with a more complete treatment of the effects from the back-scattering of high energy gamma-ray photons off the Earth’s atmosphere. The atmospheric scattering effects are currently applied when the zenith of *Fermi*-GBM is within $\pm 5^\circ$ of its nominal rocking angle of 130° with respect to the Earth’s geocenter, which occurs for $\sim 70\%$ of measurements.
4. Decreasing the resolution from 1° to 5° for the grid of sky positions analyzed during the search. This provided an order of magnitude improvement in execution time with no notable loss in sensitivity or degradation of localization capability.

These changes necessitated a recalculation of the estimated systematic uncertainty applied to the localization maps generated for the top-ranking search candidates. An initial study of 34 sub-threshold short GRB detections modeled this uncertainty as a 2.7° Gaussian systematic (Goldstein et al. 2019). A more detailed model was developed for this work using a larger sample of 3,000 simulated short GRB detections. It consists of a weighted pair of Gaussian shapes normalized over the sky with the standard deviation σ_1 of the first Gaussian always smaller than that of the second Gaussian, σ_2 . The parameters of each Gaussian were determined as functions of the most probable zenith angle for each candidate and the spacecraft rocking angle relative to the Earth. They range from 1.6° – 6.0° for σ_1 and 6.4° – 60.4° for σ_2 , with the fractional contribution of the first Gaussian spanning 0.42–0.77.

2.2.3. GBM Targeted Search Ranking Statistic

We use a ranking statistic R to characterize the significance of a coincidence between the GW candidates from the catalog and the short GRB candidates found by the Targeted Search. Following the formulation in Hamburg et al. (2020), the statistic takes into account the probability of astronomical origin of the GW, p_{astro} ; the fraction of the GW localization not occulted by the Earth for *Fermi*-GBM, p_{visible} ; the time offset of the GRB candidate from the GW time, Δt ; and the FAR from the best-fitting spectral template of the GRB candidate, FAR_{GBM} . We update the formulation to include the spatial association probability p_{assoc} and the duration D of the gamma-ray emission:

$$R = \frac{p_{\text{astro}} \times p_{\text{visible}} \times p_{\text{assoc}}}{|\Delta t - D| \times \text{FAR}_{\text{GBM}}}. \quad (6)$$

The spatial association probability p_{assoc} quantifies whether the localizations of a sub-threshold gamma-ray candidate and GW are consistent with being produced by the same source. It is computed according to

$$S = \int \rho_{\text{GBM}} \rho_{\text{GW}} d\Omega, \quad B = \int \rho_{\text{GBM}} \rho_{\text{uniform}} d\Omega, \quad (7)$$

$$p_{\text{assoc}} = \frac{S}{S + B}, \quad (8)$$

where S represents a signal hypothesis with both localizations produced by the same source and B denotes a

background hypothesis where the localizations are unrelated. Both S and B are constructed from integrals over all sky positions. In this context, ρ_{GBM} is the probability density per unit area reported by the localization maps produced for gamma-ray candidates identified by the Targeted Search. Likewise, ρ_{GW} is the probability density of the localization maps produced for each GW and $\rho_{\text{uniform}} = 1/4\pi$ is the unit density of a uniform spatial distribution on the sky.

The duration of gamma-ray emission D is incorporated into the temporal weight,

$$\frac{1}{|\Delta t - D|}, \quad (9)$$

where Δt is the temporal offset between the GW time and the start of the candidate gamma-ray emission identified by the Targeted Search and D is the candidate emission timescale. As discussed in Section 2.2.1, this is designed to account for scenarios where the observed temporal offset scales with burst duration, which is expected from a broad range of models describing the observations of GW170817/GRB 170817A. The best-fit value of D , given by the candidate with the largest value of Λ , is a good proxy for burst duration because it scales proportionally with T_{90} when the Targeted Search is applied to confirmed short GRBs in *Fermi*-GBM.

We enforce a minimum value of $|\Delta t - D| = 1$ ms to avoid divergence and account for the millisecond scale uncertainty between the GW merger times of signals identified by multiple pipelines. We also apply a minimum value of $\text{FAR}_{\text{GBM}} = 6.43 \times 10^{-6}$ Hz. This is equal to observing a single GRB candidate over the length of the background sample used to compute FAR_{GBM} .

We tested the impact of these updates to the ranking statistic by using the *Fermi*-GBM response generator² to inject short GRBs into CTTE data from the locations of modeled BNS mergers in Abbott et al. (2020a). The start time of each GRB was offset from the GW time using the duration of each burst, as given by T_{90} . We then applied the Targeted Search to this dataset and ranked the candidates according to Equation 6 as well as the older method from Hamburg et al. (2020). Doing so resulted in a factor of 1.7 increase in the number of joint detections relative to the ranking statistic formulation from our older method.

Since the true time offset model is not known, we repeated the GRB injection study using the following alternative models for the start time of the injected GRB relative to the GW:

1. Offset of half T_{90} to test a scaling factor less than the total burst duration.
2. No time offset to bound emission scenarios where the GRB occurs a few ms after the GW (Zhang 2019).
3. Fixed offset of 0.5 s assuming most gamma-ray counterparts have a characteristic time delay which is half the median T_{90} of short GRBs observed in *Fermi*-GBM.

These models were chosen with a bias towards testing time offsets shorter than the typical duration of a short GRB since the inclusion of D in the updated temporal weight naturally performs better at longer time offsets than the $1/|\Delta t|$ weight used in Hamburg et al. (2020). The updated ranking statistic outperformed the older method in all scenarios, albeit with a smaller increase in the relative number of joint detections compared to the scenario where temporal offset scales with burst duration.

2.2.4. *Fermi*-GBM Flux Upper Limits

For GW signals without a significant counterpart detection in *Fermi*-GBM we compute the gamma-ray flux upper limits as a function of sky position using the Targeted Search because it is the most sensitive analysis method employed by *Fermi*-GBM. To do this, we use the normal spectral template from Table 3 and the 1 s gamma-ray emission duration from the Targeted Search since they are characteristic of typical short GRBs (von Kienlin et al. 2020; Poolakkil et al. 2021). This results in a set of upper limits for each sky position at times ranging from -1 s to $+30$ s around the GW time. We then choose the maximum observed upper limit measurement for each sky position, guaranteeing that the specified confidence level of the upper limit applies over the entire search period.

We construct the upper limits from the best-fit photon flux amplitude s_{best} and its Gaussian error $\sigma_{\mathcal{L}}$ discussed in Section 2.2.2 according to

$$S_{\text{UL}} = s_{\text{best}} + N \times \sigma_{\mathcal{L}}, \quad (10)$$

where N is the significance level of the upper limit. We use a 3σ upper limit level for reporting upper limits over the full 10–1000 keV energy range of standard GRB flux measurements in *Fermi*-GBM following the convention established in Goldstein et al. (2019). We also compute a second 5σ upper limit over a 15–350 keV range to match the convention used by *Swift*-BAT (see Section 2.3.3) when combining the upper limits from both instruments.

² <https://fermi.gsfc.nasa.gov/ssc/data/analysis/rmfit/DOCUMENTATION.html>

2.3. Swift-BAT Searches

Swift-BAT is a coded-aperture, large FoV (2.2 sr at 10% coding fraction), hard X-ray instrument on-board *Swift*. Its detector plane contains 32,768 CZT detector elements, positioned under a coded aperture mask and a graded-Z fringe shield that helps lower the background rate (Barthelmy et al. 2005). The BAT covers an energy range from 15 keV to 350 keV and monitors large portions of the sky with the goal of detecting GRBs. Once triggered, the BAT can localize a GRB to 1–3 arcmin accuracy, prompting the *Swift* spacecraft to slew and point its two narrow-field instruments—the X-ray Telescope (XRT; Burrows et al. 2005) and the Ultraviolet/Optical Telescope (UVOT; Roming et al. 2005)—for follow-up observations. The BAT’s localization accuracy is quantified by the instrument’s partial coding fraction, i.e. the fraction of detectors exposed to an event at a given time and sky position. If the coding fraction for a given trigger is 0%, then BAT will not be able to localize the event. The BAT averages ~ 90 GRB on-board triggers per year, among which $\sim 10\%$ are short in duration (Gehrels et al. 2009). The on-board GRB triggers are complemented by subsequent on-ground rates and image data processing, in turn allowing for dedicated searches for GRB emission. With no GWs from Table 1 triggering an on-board BAT detection, we conduct an offline follow-up analysis from the ground to search for the corresponding hard X-ray counterpart emission.

2.3.1. Swift-BAT Rates Data Search

The BAT flight software continuously assesses the signal-to-noise ratio (SNR) of the observed count rates. If an SNR exceeds the given threshold value determined by a number of rate-trigger criteria (Fenimore et al. 2004), the triggering algorithm subsequently checks the corresponding image data for the final confirmation and the localization of the potential burst. The detection is confirmed only if the image SNR threshold is surpassed ($\gtrsim 6.5$) and no other sources have been previously reported at the event localization. For every confirmed detection, BAT records event data containing counts’ arrival times, location on the detector plane, and energy. With its large effective area (~ 2600 cm² for 100 keV photon detection at launch), the event data volume collected by BAT is too big to be stored on-board and, due to the limitations of the *Swift* downlink bandwidth, it is not possible to transfer all the event data to the ground. As such, until recently, the only way to conduct an offline, on-ground follow-up analysis of untriggered and sub-threshold events relied upon the rates light curves in four energy channels (15–25 keV, 25–50 keV, 50–100 keV, and 100–350 keV) with three time binnings

(64 ms, 1 s, and 1.6 s) and their corresponding 64 s images in a single energy bin (15–50 keV). The recently developed Gamma-ray Urgent Archiver for Novel Opportunities (GUANO) technique circumvents this issue by retrieving BAT event data extending to ~ 200 s long windows surrounding the trigger times from various astrophysical events (e.g., GWs, GRBs, fast radio bursts, neutrinos, etc.; Tohuvavohu et al. 2020). However, in this paper we do not use the GUANO technique since a significant number of the considered GW triggers were detected prior to the GUANO deployment in December 2019. Instead, we conduct the analysis using the regular rates data from BAT and leave the analogous study using the GUANO data for the future GW observing runs.

To conduct the untriggered and sub-threshold search for hard X-ray counterparts coincident with the LVK triggers in Table 1, we developed a code analogous to Lien et al. (2014). The search process begins by extracting the raw light curves from within the central region of the BAT FoV binned in 64 ms, 1 s, and 1.6 s time intervals. We opt to use the 1 s binned data to calculate the average background rate and standard deviation, σ_{bg} , starting at -1 s before the GW trigger time, and extending to $+30$ s after. Using the raw light curves, we compute the average background rate, r_{bg} , spanning a time window outside the signal interval, and spanning ~ 800 s (excluding the instrument slews or SAA). The signal significance, S , is then computed from σ_{bg} , using

$$S = (r_{\text{sig}} - r_{\text{bg}})/\sigma_{\text{bg}}, \quad (11)$$

where r_{sig} is the threshold signal rate. The background uncertainty is estimated as $\sigma_{\text{bg}} = \sqrt{\frac{1}{N} \sum_{i=1}^N (r_{\text{bg},i} - \bar{r}_{\text{bg}})^2}$, where N is the number of data points in the considered portion of the lightcurve, $r_{\text{bg},i}$ is the i^{th} background rate measurement, and \bar{r}_{bg} is the mean background rate over the considered time interval. Furthermore, we visually inspect each light curve to ensure that no peaks originate from detector noise. Once this is done, we check whether there are any potential counterparts to the GW, defined as a $\geq 5\sigma$ detection above background.

2.3.2. NITRATES Response Functions

To produce the BAT instrument response functions appropriate for converting from photon counts to a source flux in the rate data domain, we use the Non-Imaging Transient Reconstruction And TEmporal Search (NITRATES; DeLaunay & Tohuvavohu 2021). The NITRATES response modeling takes into account both coded and uncoded parts of the detector, and thus includes responses appropriate for all counts recorded in the rates data. In addition, these responses allow for

potential GRB detection from outside the BAT’s coded FoV, as well as higher sensitivity across the entire FoV. The instrument responses were created by simulating photon beams onto the *Swift* Mass Model (SwiMM) using GEANT4, a particle-interaction simulator software toolkit (Allison et al. 2016). We produce Detector Response Matrices (DRMs) for 31 different incident directions, covering the ~ 2.2 sr sky area (corresponding to the 10-% coding fraction) where the responses are well calibrated. For a complete description of the BAT instrument response modeling, see Sec. 5 and Appendix A in DeLaunay & Tohuavohu (2021).

2.3.3. *Swift-BAT Flux Upper Limits*

For GWs without a 5σ detection above background in *Swift*-BAT, we estimate the flux upper limit from the observed photon counts. We compute these limits for each time bin in the search by calculating the necessary number of counts that would result in a 5σ detection at that time from the estimated background uncertainty σ_{bg} , assuming a 1 s emission duration. We then select the largest counts value obtained in the search bins for each GW since this is guaranteed to satisfy the 5σ criteria over the full search window. We convert the photon counts to flux upper limits within the partially coded BAT FoV, over a 15–350 keV energy range as a function of sky position by applying the NITRATES instrument response functions using the normal spectral template (Table 3) employed for upper limits computed with the *Fermi*-GBM Targeted Search in Section 2.2.4. This is done over 31 locations in a grid covering the ~ 2.2 sr BAT FoV.

2.4. *Combined & Marginal Flux Upper Limits*

For GWs without a detected counterpart in *Fermi*-GBM or *Swift*-BAT, we combine the 5σ confidence level flux upper limits described in Sections 2.2.4 & 2.3.3 to produce joint flux upper limits as a function of sky position using both instruments. We do this by selecting the more constraining upper limit at each position since the individual limits result from independent measurements. This allows us to provide a single upper limit map for each GW that simultaneously leverages the wide FoV provided by *Fermi*-GBM as well as the additional coverage and enhanced sensitivity of *Swift*-BAT.

We also provide marginalized flux upper limits ($S_{\text{UL,marg}}$) that we compute by integrating the upper limits over the sky using the probability density of the GW localization as a prior

$$S_{\text{UL,marg}} = \int S_{\text{UL}} \tilde{\rho}_{\text{GW}} d\Omega, \quad (12)$$

where S_{UL} is the position-dependent upper limit at a given confidence level and $\tilde{\rho}_{\text{GW}}$ is the probability density of the GW localization normalized over the visible portion of the sky. This reduces the set of upper limits for each GW to a single, characteristic upper limit that accounts for the most likely location of the GW source.

2.5. *Isotropic-Equivalent Luminosity Upper Limits*

We compute upper limits on the isotropic-equivalent gamma-ray luminosity L_{iso} in the cosmological rest-frame energy range of 1 keV–10 MeV for GWs without a detected counterpart in *Fermi*-GBM or *Swift*-BAT according to

$$L_{\text{iso}} = 4\pi D_{\text{L}}^2 S_{\text{UL,marg}}, k, \quad (13)$$

where D_{L} is the median luminosity distance of the GW, $S_{\text{UL,marg}}$ is the marginalized confidence level flux upper limit described in Section 2.4, and k is the standard bolometric correction factor given by

$$k \equiv \frac{\int_{1 \text{ keV}/(1+z)}^{10 \text{ MeV}/(1+z)} E \frac{dN}{dE}(E) dE}{\int_{15 \text{ keV}}^{350 \text{ keV}} E \frac{dN}{dE}(E) dE}, \quad (14)$$

where z is the redshift inferred from D_{L} . In this case, $\frac{dN}{dE}(E)$ represents the normal spectral shape from Table 3, which is used to generate the marginalized flux upper limit. We chose to use the median D_{L} and the marginalized flux upper limit for each GW rather than marginalizing L_{iso} from the values estimated at each sky position in order to exclude the low-likelihood modes of the distance luminosity posteriors for GW200308_173609 and GW200322_091133, as discussed in Abbott et al. (2021). All other GWs yield similar values for L_{iso} regardless of whether we use the individual or median values for D_{L} in the calculation.

3. RESULTS

This section presents the results for the searches from *Fermi*-GBM and *Swift*-BAT for coincident gamma-ray emission to the GW candidates presented in Tables 1 and 2.

3.1. *Triggered and Untargeted Search Results*

We compare the distribution of temporal offsets between the GWs listed in Table 1 and the closest gamma-ray signal in *Fermi*-GBM, minus its burst duration, shown in Figure 1. The GRB sample here comprises 214 GRBs triggered by *Fermi*-GBM during O3 and 479 short GRB candidates detected by the Untargeted Search. The background distribution was composed by choosing $\sim 10^4$ random times in O3 during which there were no reported GWs. Confidence intervals for the

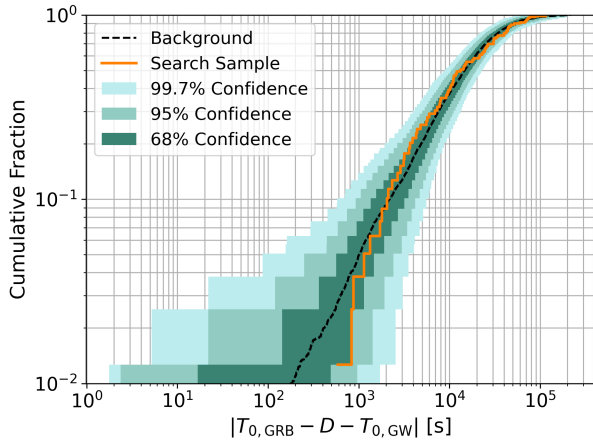


Figure 1. The cumulative distribution for the minimum time offsets between the O3 GW triggers and GRBs found by either the GBM on-board triggering algorithms or the Untargeted Search. Confidence intervals for the search sample were determined by Monte Carlo sampling of the background.

search sample were determined empirically by Monte Carlo sampling of the background distribution.

There are no significant deviations from the background, with the search sample lying largely within the 68% confidence interval. The shortest temporal offset given by the sample distribution is approximately 10 minutes and is within the 95% confidence interval. Such large offsets are not expected for on-axis prompt emission from GRBs associated with binary mergers (Vedrenne & Atteia 2009; Zhang 2019); therefore, we find no further evidence for a GW/gamma-ray association.

3.2. Targeted Search Results

We ran the Targeted Search on the 79 GWs shown in Table 1. *Fermi*-GBM was in the SAA for 15 of those times, therefore the detectors were turned off and no data were obtained. Figure 2 shows the cumulative rate above a given value of the marginalized log-likelihood ratio Λ separated according to the best-fitting spectral template. The background distribution is determined by randomly selecting times during the O3 livetime without known GW triggers. This represents the FAR of the search and describes the frequency of expected false positives as a function of Λ . No significant gamma-ray signals were found in coincidence with GWs.

Figure 3 shows the ranking statistic R from Section 2.2.3 mapped to a p-value, defined as the number of more highly ranked background candidates as compared to the total number of background candidates or $p_i = N(R > R_i)/N$, where N is the number of background gamma-ray candidates and i is the candidate index within the search sample. The plots show no signif-

icant deviations from background, yielding no evidence for a GRB counterpart to the GW signals.

3.3. Swift Results

We ran the pipeline described in Section 2.3 on the 1 s binned light curves from *Swift*-BAT for the 79 candidates listed in Table 1. The goal of the pipeline is to examine whether any emission surpasses the 5σ threshold above the observed background rate level. We visually inspect each light curve to ensure that no detector noise or malfunction affects the reported results. We identify detector noise as a fast duration peak seen only in some of the energy channels. Once identified, the detector noise is subtracted down to the level of the average background rate. There are 14 GWs for which the data are either unavailable or background dominated because they occurred during either the *Swift*-BAT SAA passage or a slew. Separately, 13 GWs were within the BAT FoV ($>10\%$ partial coding) and had image survey data available at the time of interest. We report no significant hard X-ray detection in the *Swift*-BAT rate data coincident with the reported GW triggers at the 5σ level. We also ran the standard BAT analysis on the survey data (longer timescales, ~ 300 s) for the 13 inside-BAT-FoV candidates and also report no excess X-ray emission.³

3.4. Results for Marginal GW Candidates

The *Fermi*-GBM and *Swift*-BAT searches were applied separately to the 6 marginal GW signals from Table 2 in an effort to identify EM counterparts, that could prove an astrophysical origin. The closest time offset from the GBM Triggered and Untargeted Searches was observed for GW191118_212859, which occurred 42 minutes before the on-board trigger of GRB 191118A and corresponds to a p-value of 0.1. The most significant Targeted Search candidate was found for GW200105_162426 using the hard spectral template. It has a pre-trial p-value of 0.1 as estimated by the ranking statistic distribution for background described in Section 2.2.3. Applying a trials factor of 3 to account for the 3 spectral templates used by the Targeted Search increases the p-value to 0.3. No 5σ detections were found for any marginal candidates using the *Swift*-BAT rates data search.

4. SCIENCE DISCUSSION

Compact binary mergers containing a neutron star component are likely candidates for gamma-ray emis-

³ <https://heasarc.gsfc.nasa.gov/ftools/caldb/help/batsurvey.html>

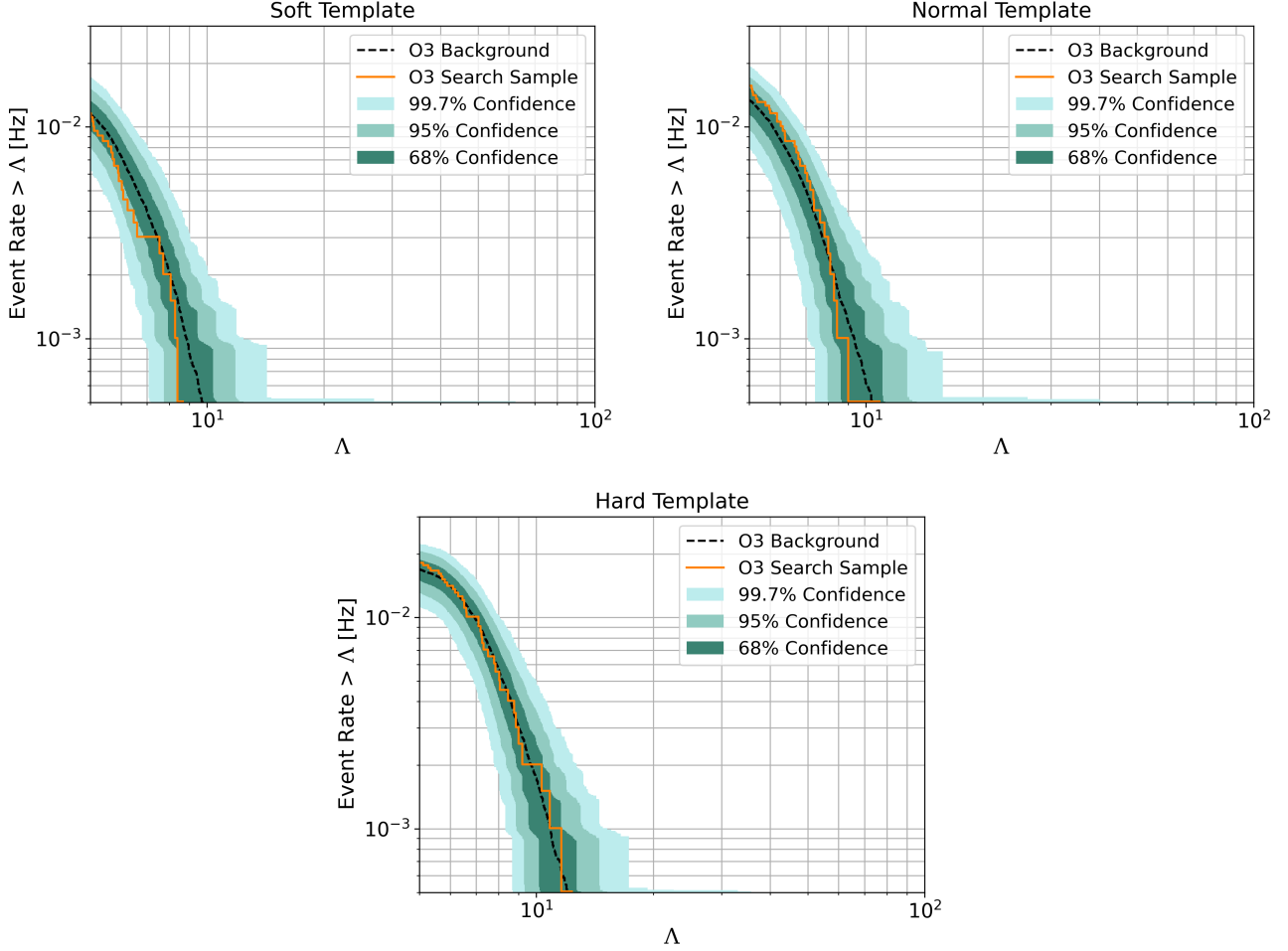


Figure 2. The cumulative rate above a given value of the marginalized log-likelihood ratio Λ , separated into three plots according to the best fitting spectral template, found in the Targeted Search. The orange line is the foreground distribution of GRB candidates found with the Targeted Search around the given GW merger time. The black dotted line is the randomly selected background sample and the green shading represents the 68%, 95% and 99.7% confidence intervals around it.

sion, particularly if the inspiral process results in tidal disruption of the neutron star (Burns 2020). In contrast, BBH mergers are not expected to produce gamma-rays outside of a few exotic scenarios (e.g., Loeb 2016a; Perna et al. 2016; Zhang 2016; Dai et al. 2017). Therefore, using the standard convention of $m_1 > m_2$, we divide our discussion into two sections based on the secondary component mass m_2 :

1. **Mergers with a possible neutron star:** $m_2 \leq 3 M_\odot$ (5% credible level)
2. **Probable BBH mergers:** $m_2 > 3 M_\odot$ (95% credible level)

The cut $m_2 \leq 3 M_\odot$ was chosen to include all systems with at least one neutron star component up to the maximal allowed neutron star mass of 2.16–3.0 M_\odot (Bombaci 1996; Kalogera & Baym 1996; Margalit & Metzger 2017; Rezzolla et al. 2018). It may include a few ambiguous

BBH mergers due to the uncertainty on the maximum allowed neutron star mass. We favor this approach over a stricter cut due to the limited number of systems in O3 with light secondary component masses. Additionally, the discussion of possible BBH mergers does not suffer from the loss of a few ambiguous candidates, particularly given the large number of systems with $m_2 > 3 M_\odot$.

In Section 4.1 we discuss the absence of GRB detections in coincidence with the 6 GWs classified with a possible neutron star component and present flux upper limits from *Fermi*-GBM and *Swift*-BAT. In Section 4.2 we discuss the BBH mergers, providing flux upper limits and exploring how these limits may rule out certain theoretical models.

4.1. Possible Neutron Star in the System

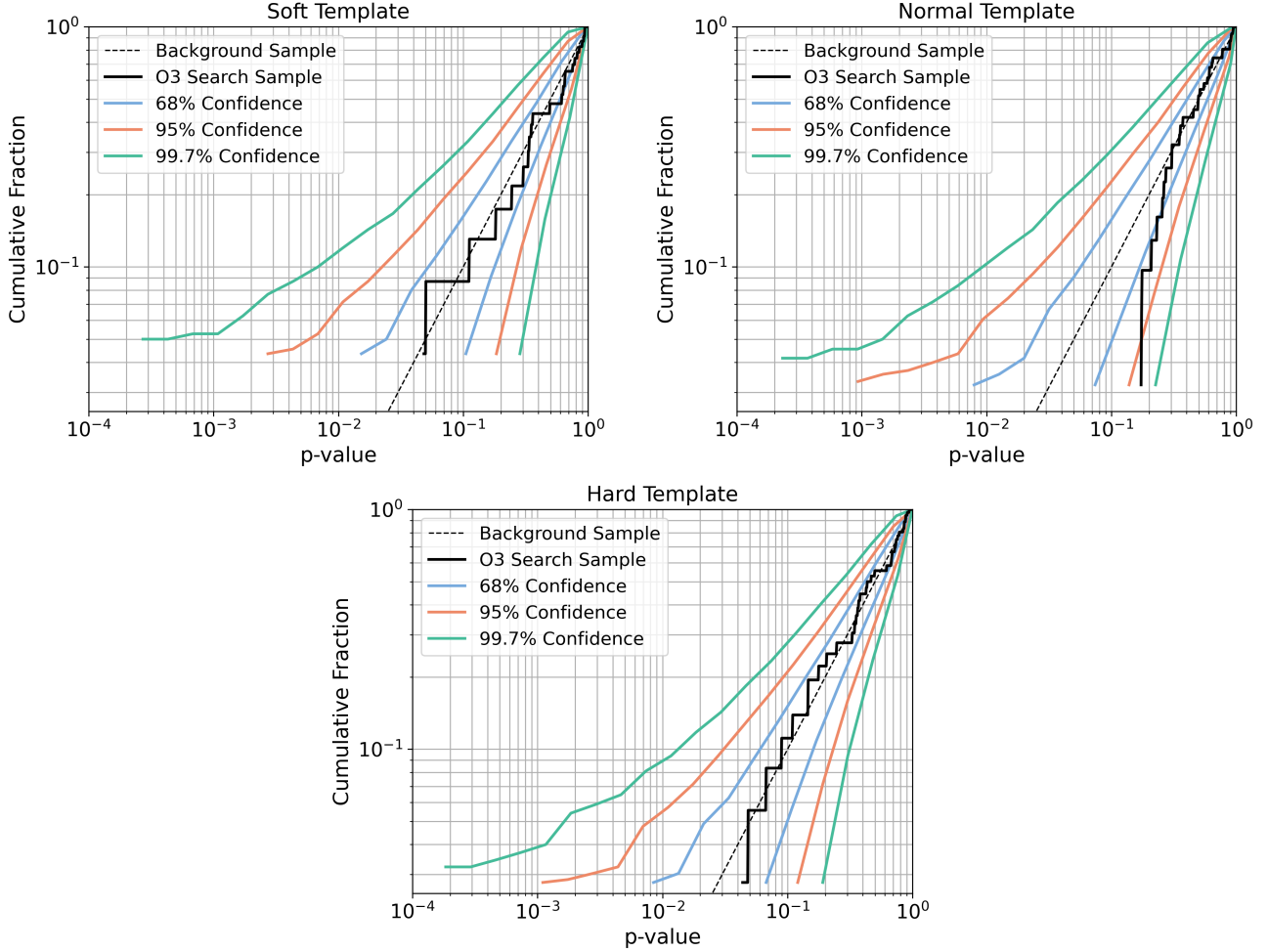


Figure 3. Cumulative fraction versus p-value of the updated ranking statistic R . The solid black line is the foreground distribution of GRB candidates found with the Targeted Search around the given GW merger time. The dashed black line is the randomly selected background sample and the blue, green and orange lines represent the 68%, 95% and 99.7% confidence intervals for background, respectively.

There are 6 GWs (i.e., GW190425, GW190814, GW190917_114630, GW191219_163120, GW200115_042309, and GW200210_092254) where $\geq 5\%$ of posterior probability lies below the dashed red line in Figure 4. GW190425 is the least massive system from O3 and the second BNS merger detected by LIGO-Virgo. It has a primary mass $m_1 = 2.1^{+0.5}_{-0.4} M_\odot$ and a secondary mass of $m_2 = 1.3^{+0.3}_{-0.2} M_\odot$ (Abbott et al. 2021, 2020). GW190814 has a low mass secondary component, estimated at $m_2 = 2.6^{+0.1}_{-0.1} M_\odot$, while its primary component has an estimated mass of $m_1 = 23.3^{+1.4}_{-1.4} M_\odot$. It is unclear whether this source is a BBH or a NSBH merger, since the secondary component could either be a light black hole or a heavy neutron star (Abbott et al. 2021). GW190917_114630 was identified as a BBH merger by the GstLAL pipeline, but its secondary component mass of $m_2 = 2.1^{+1.1}_{-0.4} M_\odot$ is a strong indicator for a NSBH origin (Abbott et al. 2021). GW191219_163120 has a large

primary component mass of $m_1 = 31.1^{+2.2}_{-2.8} M_\odot$ and the lowest secondary component mass $m_2 = 1.17^{+0.07}_{-0.06} M_\odot$ of all the GWs with a possible neutron star (Abbott et al. 2021); it represents a potential NSBH merger. GW200115_042309 has a primary mass of $m_1 = 5.9^{+2.0}_{-2.5} M_\odot$ suggesting a low-mass black hole, and a secondary mass of $m_2 = 1.44^{+0.85}_{-0.29} M_\odot$ which is consistent with a neutron star (Abbott et al. 2021). GW200210_092254 possesses a primary component mass of $m_1 = 24.1^{+7.5}_{-4.6} M_\odot$ and a secondary component mass of $m_2 = 2.83^{+0.47}_{-0.42} M_\odot$ that could either be a light black hole or a heavy neutron star (Abbott et al. 2021). It is unclear if this source is a BBH or NSBH merger.

All GWs except GW191219_163120 were observable by both *Fermi*-GBM and *Swift*-BAT (Table 4). GW191219_163120 was observed by *Fermi*-GBM but no *Swift*-BAT data are available due to a slewing behavior of the spacecraft at the GW time. Neither instrument

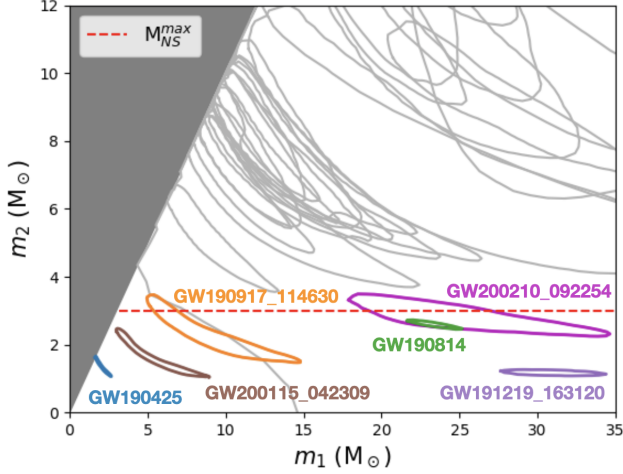


Figure 4. The inferred 90% credible regions of the component masses for all GWs with $p_{\text{astro}} > 0.5$ from O3 are shown in grey (Abbott et al. 2021; Abbott et al. 2021; Abbott et al. 2021). The red dashed line marks the upper bound of m_2 allowed for our classification of systems with a possible neutron star component, which are marked by colored contours.

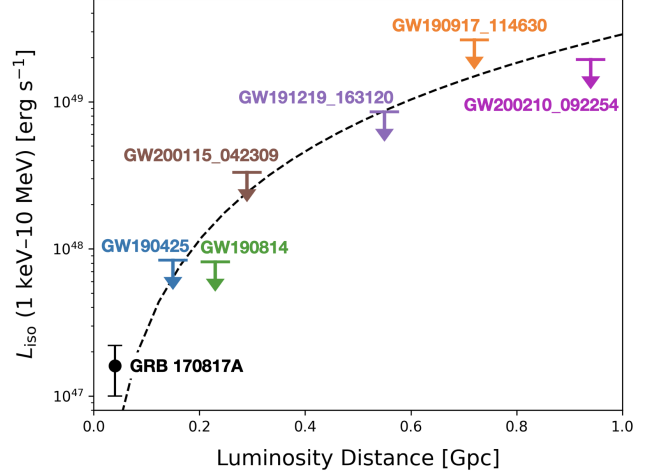


Figure 5. The 5σ upper-limits on isotropic-equivalent luminosity L_{iso} for the 6 GWs in O3 identified with a possible neutron star component and $p_{\text{astro}} > 0.5$. The black data point is the measured L_{iso} from GRB 170817A and the black dashed line is the approximate lower bound for L_{iso} of GRBs detected on-board *Fermi*-GBM (Abbott et al. 2017).

Table 4. Flux upper limits for the 6 GWs from O3 with $p_{\text{astro}} > 0.5$ that are classified with a possible neutron star component. The 3σ upper limits are computed for the 10–1000 keV energy range over the FoV of *Fermi*-GBM. The 5σ upper limits are computed for the combined coverage of *Fermi*-GBM and *Swift*-BAT with both instruments matched to the 15–350 keV energy range of *Swift*-BAT. The columns labeled Min and Max correspond, respectively, to the minimum and maximum upper limits obtained for points within the 90% credible region of the GW localization. The Marginal upper limit is computed by integrating the upper limits produced at individual locations over the full sky using the GW localization as a weighted prior, normalized to the visible portion of the sky. Also shown is the visible coverage percentage of the full GW localization for *Fermi*-GBM alone, *Swift*-BAT alone, and the combined FoV from both instruments.

Event Name	Coverage [%]			3σ Flux U.L. [erg s ⁻¹ cm ⁻²]			5σ Flux U.L. [erg s ⁻¹ cm ⁻²]		
	GBM	BAT	Combined	10–1000 keV			15–350 keV		
				Min	Max	Marginal	Min	Max	Marginal
GW190425	56.70	10.81	57.81	1.37×10^{-7}	2.47×10^{-7}	1.66×10^{-7}	6.12×10^{-8}	2.31×10^{-7}	1.51×10^{-7}
GW190814	100.00	100.00	100.00	1.17×10^{-7}	1.26×10^{-7}	1.21×10^{-7}	4.71×10^{-8}	7.64×10^{-8}	6.26×10^{-8}
GW190917_114630	88.92	6.56	95.07	1.48×10^{-7}	4.33×10^{-7}	2.33×10^{-7}	5.26×10^{-8}	3.83×10^{-7}	2.08×10^{-7}
GW191219_163120	61.06	N/A	61.06	1.03×10^{-7}	2.36×10^{-7}	1.20×10^{-7}	1.00×10^{-7}	2.27×10^{-7}	1.15×10^{-7}
GW200115_042309	96.26	4.80	96.26	1.31×10^{-7}	2.83×10^{-7}	1.78×10^{-7}	8.53×10^{-8}	2.56×10^{-7}	1.60×10^{-7}
GW200210_092254	61.79	50.55	65.85	1.28×10^{-7}	3.13×10^{-7}	2.01×10^{-7}	4.41×10^{-8}	1.47×10^{-7}	9.00×10^{-8}

detected an EM counterpart to these GWs. Therefore, we compute flux upper limits for each GW using the methods described in Section 2. Table 4 presents the minimum and maximum flux upper limits from *Fermi*-GBM and *Swift*-BAT over the 90% credible regions of the GW localizations, as well as sky-marginalized flux upper limits. Incorporating the combined measurements from *Fermi*-GBM and *Swift*-BAT, we also use the sky-marginalized 5σ flux limits to generate upper limits on the isotropic-equivalent luminosity (Figure 5). The combined 5σ flux upper limits over the 15–350 keV energy range can be seen in Figure 6.

The lack of a gamma-ray counterpart to BNS merger GW190425 has three plausible explanations. First, the combined coverage of $\sim 60\%$ of the total GW localization implies that the GW source may not have been visible to *Fermi*-GBM and *Swift*-BAT. Second, GW190425 has an estimated luminosity distance of $D_L = 0.15^{+0.08}_{-0.06}$ Gpc which is 4 times larger than that to GW170817 (Abbott et al. 2019). At this distance, the luminosity of GW170817 would fall well below the upper limit for GW190425⁴ (Fletcher et al. 2019). (Figure 5), indicat-

⁴ Note, the luminosity upper limit for GW190425 is also consistent with that found in Hosseinzadeh et al. 2019, which uses

ing that a counterpart similar to the one for GW170817 would have been unobservable to *Fermi*-GBM or *Swift*-BAT. Finally, the inclination angle of this GW is poorly constrained, with the 90% credible level extending to a viewing angle of 70° with respect to the jet axis. This encompasses scenarios where the observed off-axis flux would be below the detection limits, even if the central engine of GW190425 was powerful enough to be detected on-axis by *Fermi*-GBM and *Swift*-BAT at its measured distance.

4.2. Probable BBH Mergers

There are a total of 73 GWs with the criterion of $m_2 > 3 M_\odot$ in $> 95\%$ of the posterior probability. All of these have estimated primary and secondary component masses much larger than the maximum expected neutron star mass of $3 M_\odot$. Therefore, they are most likely GW signals from BBH mergers.

Of these GWs, 10 occurred during SAA for *Fermi*-GBM, but had data from *Swift*-BAT. Likewise, *Swift*-BAT does not have data for 9 GWs, either because *Swift*-BAT was in the SAA or slewing, but data are available from *Fermi*-GBM. Finally, there are 5 GWs that do not have data from either *Fermi*-GBM or *Swift*-BAT due to being in the SAA and/or slewing. Neither instrument identified an EM counterpart for the GWs with data coverage. As a result, we compute flux upper limits for each GW according to the methods described in Section 2. Table 5 presents the minimum and maximum upper limits over the 90% credible region of the GW localization as well as the marginalized flux upper limits. Joint flux upper limits as a function of sky position and the corresponding isotropic-equivalent luminosity limits for the GWs that have data coverage are provided in a separate data release (Wood et al. 2023). For the GWs with *Fermi*-GBM data, we look into constraining theoretical models of gamma-ray emission from BBHs using the 3σ flux upper limits, as they provide broad spectral coverage over the 10–1000 keV energy range.

4.2.1. Constraining gamma-ray emission models from BBH mergers

EM radiation from BBH mergers is not expected due to the challenges associated with forming an accretion disk during the merger process. Nevertheless, Connaughton et al. (2016) reported GW150914-GBM, a weak gamma-ray signal following the first LIGO–Virgo detection of BBH GW150914 (Abbott et al. 2016), and,

more recently, the Zwicky Transient Facility identified a potential EM counterpart to GW190521 (Graham et al. 2020). While the associations between these detections and the corresponding GWs remain nebulous (Connaughton et al. 2018; Ashton et al. 2021; Bustillo et al. 2021; De Paolis et al. 2020; Palmese et al. 2021), a wide spectrum of models have been developed to invoke EM emission from BBH-mergers, all with non-negligible difficulties (e.g., Loeb 2016b; Perna et al. 2016; Zhang 2016; Perna et al. 2018).

To test the association between GW150914 and GW150914-GBM, Veres et al. (2019) assumed some of these BBH emission models and derived a model-dependent BBH-to-GRB ratio which represents the expected number of BBH mergers to be detected by LVK before a gamma-ray counterpart might be observed by *Fermi*-GBM. Since the number of LVK BBH merger detections has reached the BBH-to-GRB ratio for a few models reported by Veres et al. (2019), we attempt to constrain them by computing gamma-ray flux upper limits for each model and examining the implications with respect to individual BBH mergers.

We consider four models for relating potential gamma-ray emission to the energy present in BBH mergers: a neutrino–antineutrino annihilation powered jet mechanism ($\nu\bar{\nu}$; Ruffert & Janka 1998), a charged BH (Q; Zhang 2016), the Blandford–Znajek mechanism (BZ; Blandford & Znajek 1977), and a model where the gamma-ray energy is proportional to the emitted GW energy (E_{GW}). A detailed summary of these models and their parameters can be found in Veres et al. (2019). We note that all of the above scenarios suffer from non-trivial critiques but are used here to be widely-inclusive of the broad spectrum of proposed mechanisms for gamma-ray production. The intrinsic properties of each model (e.g., magnetic field strength, charge of the black hole, etc.) are determined by setting them to values consistent with the observed luminosity of GW150914-GBM (Connaughton et al. 2016).

For each GW, we use the posterior distributions of BBH parameters (e.g., final mass, distance, inclination, rotation parameter, etc.) from GWTC-3 and derive a distribution of gamma-ray fluxes for the different models. We then compare the distribution of fluxes to the 3σ marginalized flux upper limit from *Fermi*-GBM, shown in Table 5. This is performed for three GRB jet geometries: an isotropic emitter (i.e., an opening angle of 90°), an opening angle distributed uniformly between 10 – 40° , and a fixed 20° opening angle. All jets are assumed to have a top-hat angular structure and are assigned pointing directions by sampling from the inclination posterior of each GW. Due to relativistic beaming, emission is

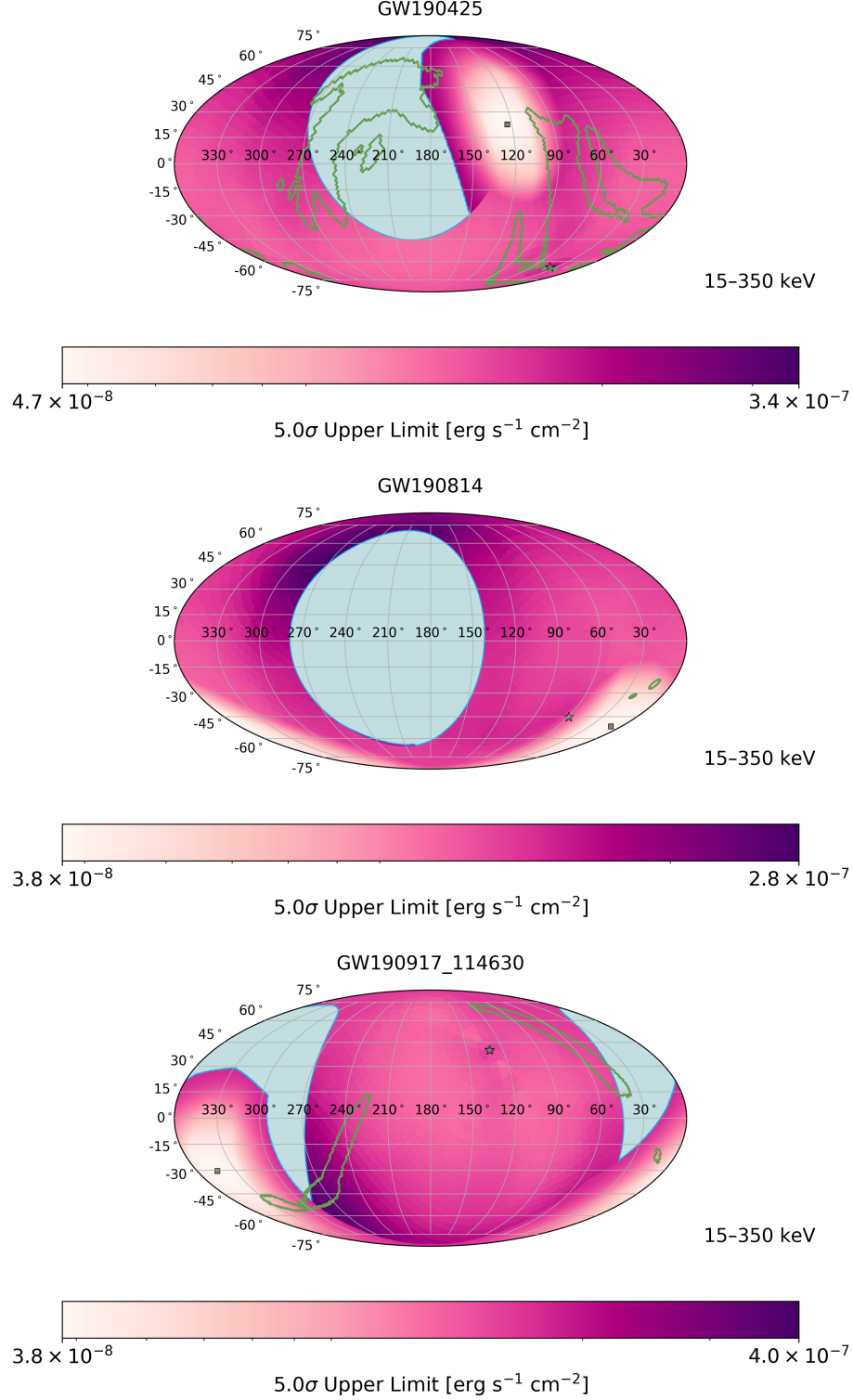


Figure 6. The 5σ flux upper-limit as a function of sky position for the 6 GWs from O3 identified with a possible neutron star component and $p_{\text{astro}} > 0.5$. The purple gradient represents the combined *Fermi*-GBM and *Swift*-BAT flux upper limits for source positions at each point on the sky. The star symbol represents the zenith direction of *Fermi*-GBM, the square symbol represents the center of the *Swift*-BAT FoV, and the green contour represents the 90% credible area of the LVK localization. The blue region is the non-visible portion of the sky which is occulted by the Earth for *Fermi*-GBM and outside the *Swift*-BAT FoV.

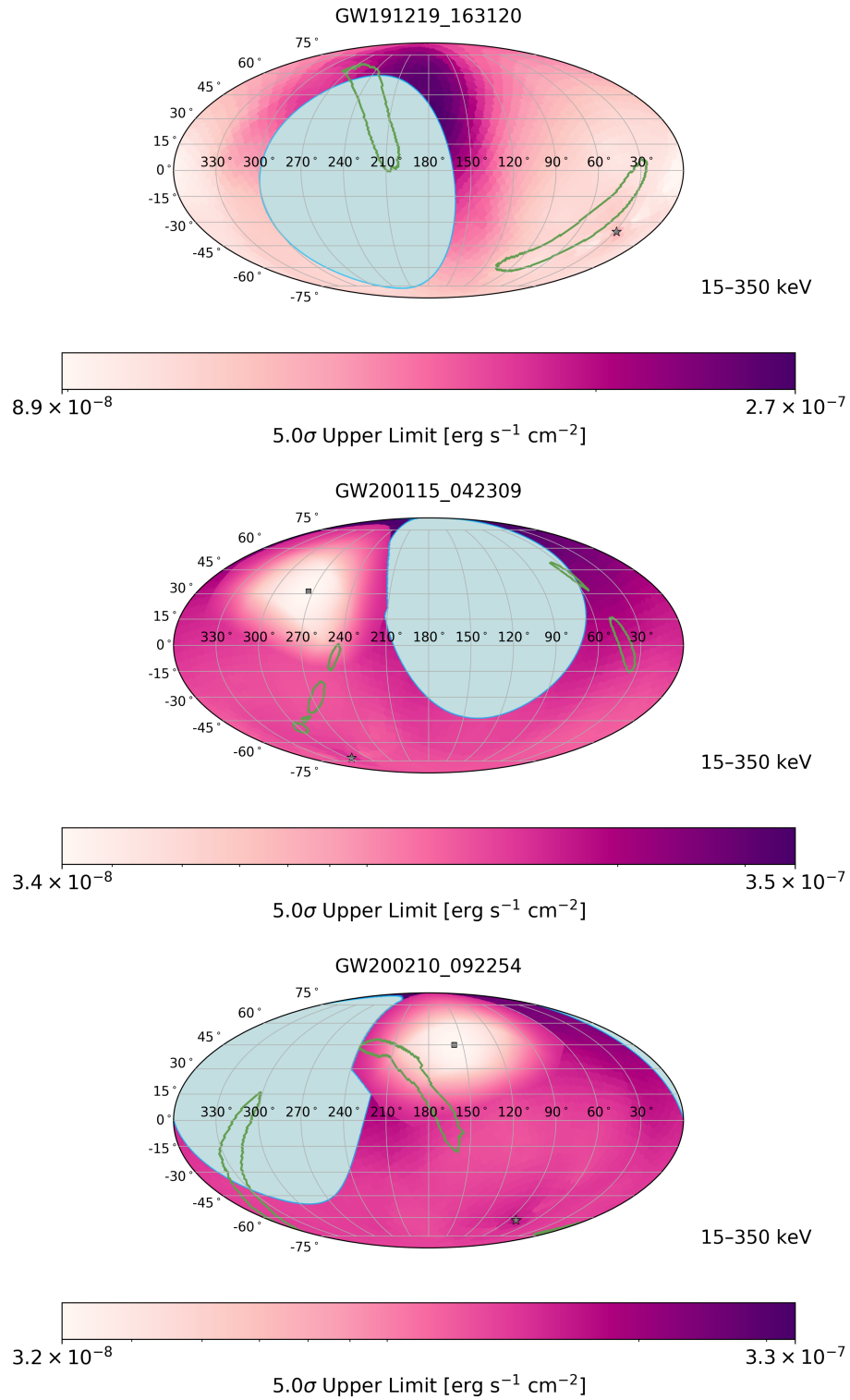


Figure 5 continued.

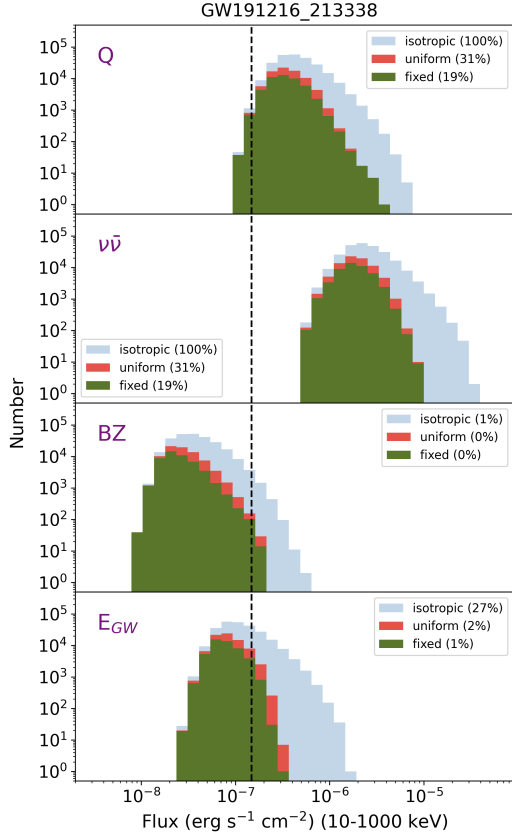


Figure 7. Example of gamma-ray flux expected for the 4 different models: charged BH model (Q), neutrino–antineutrino annihilation powered jet model ($\nu\bar{\nu}$), Blandford–Znajek (BZ), and gamma-ray energy as a fraction of GW energy (E_{GW}) in the case of GW191216.213338. The 3σ (10–1000 keV) marginalized flux upper limit is indicated by the vertical line. The legend contains the fraction of cases above the 3σ upper limit; note that for the jetted emission models (uniform, fixed), cases with zero expected flux are not shown. Here the limit is violated in 100% and >99% of cases for the $\nu\bar{\nu}$ and Q models, respectively (assuming isotropic emission).

strongly suppressed for GRBs with jet opening angles smaller than the viewing angle. In order to simplify the treatment of such cases, we assign zero flux to jets whose inclination is larger than the opening angle.

Figure 7 shows an example of the flux distribution for the four different models and the three jet geometries compared to the GBM upper limits for GW191216.213338. There is a dearth of jetted cases (green, red) compared to isotropic emission (light blue) at higher fluxes. This is explained by the inclination angle–distance degeneracy of the GW parameter estimation. Point estimates with smaller distances and thus higher flux will preferentially have jets pointed away from our line of sight. When we impose a jet

opening angle $\lesssim 40^\circ$ on such systems, they will not include the observer within their aperture in most of the cases. Conversely, the point estimates with largest distances point preferentially towards the observer, thus there will be no strong differences between the jetted and isotropic cases at low flux values.

We classify GW191216.213338 as noteworthy because the predicted gamma-ray flux distribution from at least one model violates the GBM flux upper limit by more than 10%. The 10% limit in the rest of this section refers to the isotropic emission model. Of the 58 probable BBH mergers with *Fermi*-GBM data coverage described in Section 4.2, 18 are considered noteworthy according to this criterion. The remaining 40 did not yield the necessary number of cases above the GBM flux upper limit in any of the models.

Out of the four models considered here, the $\nu\bar{\nu}$ model violates the *Fermi*-GBM flux upper limit in most of the cases. Of the noteworthy GWs (denoted by * in Table 7, Appendix A), 15 exceed the GBM limit in more than 10% of cases for this model. In particular, GW190924.021846, GW191216.213338 (Figure 7) and GW200202.154313 exceed the GBM limit in {100, 30, 20}%, {100, 31, 19}% and {100, 36, 24}% of the cases respectively (the 3 numbers represent the 3 different opening angle choices). Interestingly, for these three events, in the isotropic emission scenario the $\nu\bar{\nu}$ can be ruled out, and the non-detection in gamma-rays can constrain the jet geometry. This is due to GW191216.213338 and GW200202.154313 being the two closest BBH signals observed during O3 with luminosity distances of $0.34_{-0.13}^{+0.12}$ Gpc and $0.41_{-0.16}^{+0.15}$ Gpc, respectively (Abbott et al. 2021). In addition to being nearby (luminosity distance of 0.55 ± 0.22 Gpc), GW190924.021846 has a relatively low final mass ($13.9_{-0.9}^{+2.8} M_\odot$), which leads to higher flux in the $\nu\bar{\nu}$ model.

For the Q model, the most constraining GWs are also GW191216.213338 and GW200202.154313. They violate the GBM flux upper limit for the different jet geometries in {100, 31, 19}% and {96, 33, 22}% of cases, respectively. In total, 12 of the probable BBH mergers have larger than 10% of their flux estimates above the upper limit for this model.

GW191109.010717 is the most constraining for the BZ scenario. It violates the gamma-ray upper limit in {26, <0.1, <0.1}% of cases for the 3 different opening angle choices. It has the fourth-highest total mass $M = 112_{-16}^{+20} M_\odot$ in O3 and is reasonably close at $D_L = 1.29_{-0.65}^{+1.13}$ Gpc (Abbott et al. 2021). The only other GW with more than 10% of the flux estimates above the upper limit for the BZ mechanism is GW190521.074359.

For the E_{GW} scenario, GW191216_213338 is again the most constrained. It violates the gamma-ray upper limit in $\{27, 1.8, 0.7\}\%$ of the cases for the three jet opening angle choices. There are 3 GWs with 10% of the flux estimates from this model above the GBM flux upper limit (Table 7 continued, Appendix A).

In summary, we provide constraints on theoretical models of gamma-ray emission from BBH mergers using the flux upper limits from *Fermi*-GBM. We find that for most BBH mergers the models considered here do not predict gamma-ray flux over the upper limit. Under our model assumptions, this can be understood as a consequence of the larger average distance of BBH mergers during O3 compared to that of GW150914. We also find that the $\nu\bar{\nu}$ model is the most constrained. This model has the lowest BBH-to-GRB ratio in Veres et al. (2016), and indeed, observations reveal that 18 out of 58 cases for the $\nu\bar{\nu}$ model yield an appreciable flux above the upper limit. The expected flux in this model is inversely proportional with the final mass; the average BBH merger in O3 was less massive than GW150914, resulting in larger predicted gamma-ray flux.

4.3. Marginal GWs

Although all 6 marginal GWs from Table 2 have $p_{\text{astro}} < 0.5$ they are of interest for EM follow-up. This is because GW200311_103121 may have a possible BNS origin and the remaining 5 candidates have possible NSBH origins (Abbott et al. 2021; Abbott et al. 2021). In particular, the possible NSBH merger GW200105_162426 was noted as a clear outlier from experimental backgrounds despite not satisfying the $p_{\text{astro}} > 0.5$ criteria used to identify GW signals with a likely astrophysical origin. It also has the highest observed p_{astro} of all the marginal GWs.

The 5 marginal GWs with possible NSBH origins were visible to *Fermi*-GBM while the remaining one, GW200311_103121, occurred when *Fermi*-GBM was in the SAA. None of the marginal GWs have appreciable coverage in *Swift*-BAT. No significant counterparts were found. As with GW190425, this may be due to unfavorable viewing angles with respect to the jet axis, larger observational distances such as the $0.27^{+0.12}_{-0.11}$ Gpc distance to GW200105_162426 (Abbott et al. 2021), and partial sky coverage for candidates other than GW190426_152155. It therefore remains ambiguous as to whether these signals are real compact binary coalescences. Nevertheless, we provide in Table 6 the flux upper limits for each marginal GW calculated according to the same methods described in Section 4.1 since they may provide emission model constraints if future analyses can identify an astrophysical progeni-

tor with a favorable viewing angle with respect to the jet axis. Figure 8 displays the 5σ confidence level flux upper limit map for GW200105_162426 since it is the marginal GW with the highest probability of having an astrophysical origin. The marginalized 5σ flux upper limit of GW200105_162426 yields an isotropic-equivalent luminosity upper limit of $L_{\text{iso}} = 2.1 \times 10^{48}$ erg s $^{-1}$ when combined with its 0.27 Gpc distance. The data release (Wood et al. 2023) associated with this work provides flux upper-limits as a function of sky position for the remaining marginal GWs.

5. SUMMARY AND FUTURE DIRECTIONS

Using the 79 GW candidates with $p_{\text{astro}} > 0.5$ from O3 that were reported in GWTC-3, we searched for coincident EM counterparts with *Fermi*-GBM and *Swift*-BAT. This represents the most comprehensive follow-up to date of the O3 run in the hard X-ray and gamma-ray regime. We found no significant counterparts in either instrument. For the one BNS merger, GW190425, with $p_{\text{astro}} > 0.5$ there are several possible reasons for the non-detection of a counterpart:

- The combined *Fermi*-GBM and *Swift*-BAT coverage of the GW localization area was $\sim 60\%$, meaning that the GW source may have been outside the FoV for both instruments.
- The distance to GW190425 was four times larger than the estimated distance for GW170817, causing the observed flux to be below the detection threshold in both instruments if it had the same intrinsic luminosity and viewing angle as GW170817.
- The viewing angle may have been too far away from the jet axis to detect emission under scenarios with a clean or structured jet.

GW190425 is therefore unconstrained by our observations.

In contrast to GW190425, the large number of BBH detections in this sample allowed us to begin placing constraints on certain models of gamma-ray emission from BBH mergers, despite the larger average distance for this class compared to the BNS mergers. The most constrained model was the $\nu\bar{\nu}$ model where two GWs, GW191216_213338 and GW200202_154313, were predicted to produce an observable flux in *Fermi*-GBM. With the number of GWs from BBH mergers to increase in the fourth LVK observing run (O4), we expect this model to become more constrained and ruled out as a potential explanation of EM emission from BBH mergers.

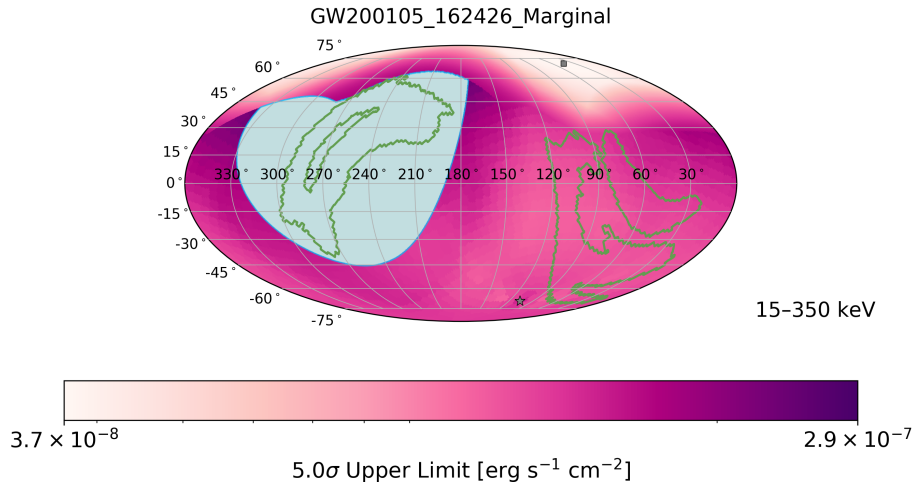


Figure 8. The 5σ upper-limits as a function of sky position for GW200105_162426, the marginal GW with the highest p_{astro} . The purple gradient represents the combined *Fermi*-GBM and *Swift*-BAT flux upper limits for source positions at each point on the sky. The star symbol represents the zenith direction of *Fermi*-GBM, the square symbol represents the center of the *Swift*-BAT field-of-view, and the green contour represents the 90% credible area of the LVK localization. The blue region is the non-visible portion of the sky which is occulted by the Earth for *Fermi*-GBM and outside the *Swift*-BAT FoV.

With O4 having begun on May 24, 2023, we expect an increase in GW detections by a factor of 5 (Abbott et al. 2018; Petrov et al. 2022) and a bountiful regime of EM follow-up data. This will greatly increase the need for further instantaneous, wide FoV gamma-ray/X-ray observations in order to detect the EM counterparts to these GWs and localize them, especially given the absence of a counterpart detection during O3. Towards this end, the *Fermi*-GBM Targeted Search updates presented in this paper will be used in future LVK observing runs. In the absence of detections, flux upper limits, both marginalized and as a function of sky position, will be provided to the community. Additionally, *Swift*-BAT GUANO and NITRATES will be used during the next observing run.

ACKNOWLEDGEMENTS

The USRA co-authors gratefully acknowledge NASA funding through contract 80MSFC17M0022. R.H. acknowledges funding from the European Union’s Horizon 2020 research and innovation programme under the Marie Skłodowska-Curie grant agreement No 945298-ParisRegionFP. The UAH co-authors gratefully acknowledge NASA funding from co-operative agreement 80MSFC22M0004. The NASA authors gratefully acknowledge NASA funding through the Fermi GBM project. This research also made use of Astropy, a community developed core Python package for Astronomy (Astropy Collaboration et al. 2022); NumPy (Harris et al. 2020); SciPy (Virtanen et al. 2020) and matplotlib, a Python library for publication quality graphics (Hunter 2007).

The *Swift* authors acknowledge the use of public data from the *Swift* data archive. MC acknowledges support from NASA under award number 80GSFC21M0002 and from Vetenskapsrådet through project number 31004019. JD acknowledges support by the NSF under award numbers PHY-1913607 and PHY-2209445.

This material is based upon work supported by NSF’s LIGO Laboratory which is a major facility fully funded by the National Science Foundation. The authors also gratefully acknowledge the support of the Science and Technology Facilities Council (STFC) of the United Kingdom, the Max-Planck-Society (MPS), and the State of Niedersachsen/Germany for support of the construction of Advanced LIGO and construction and operation of the GEO 600 detector. Additional support for Advanced LIGO was provided by the Australian Research Council. The authors gratefully acknowledge the Italian Istituto Nazionale di Fisica Nucleare (INFN), the French Centre National de la Recherche Scientifique (CNRS) and the Netherlands Organization for Scientific Research (NWO), for the construction and operation of the Virgo detector and the creation and support of the EGO consortium. The authors also gratefully acknowledge research support from these agencies as well as by the Council of Scientific and Industrial Research of India, the Department of Science and Technology, India, the Science & Engineering Research Board (SERB), India, the Ministry of Human Resource Development, India, the Spanish Agencia Estatal de Investigación (AEI), the Spanish Ministerio de Ciencia e Innovación and Ministerio de Universidades, the Con-

Table 5. Flux upper limits for possible EM counterparts to probable BBH candidates detected during O3 with $p_{\text{astro}} > 0.5$. The 3σ upper limits are computed for the 10–1000 keV energy range over the FoV of *Fermi*-GBM. The 5σ upper limits are computed for the combined coverage of the *Fermi*-GBM and *Swift*-BAT with both instruments matched to the 15–350 keV energy range of *Swift*-BAT. The columns labeled Min and Max correspond, respectively, to the minimum and maximum upper limit values obtained for points within the 90% credible level of the GW localization. The Marginal upper limit is computed by integrating the upper limits produced at individual locations over the full sky using the GW localization as a weighted prior, normalized to the visible portion of the sky.

Event Name	Coverage [%]			3σ Flux U.L. [erg s ⁻¹ cm ⁻²]			5σ Flux U.L. [erg s ⁻¹ cm ⁻²]		
	GBM	BAT	Combined	10–1000 keV			15–350 keV		
				Min	Max	Marginal	Min	Max	Marginal
GW190403.051519	76.61	24.76	82.91	1.07×10^{-7}	3.09×10^{-7}	1.78×10^{-7}	3.67×10^{-8}	2.80×10^{-7}	1.50×10^{-7}
GW190408.181802	SAA	0.00	0.00	-	-	-	-	-	3.50×10^{-7}
GW190412	97.27	3.45	99.80	1.00×10^{-7}	1.22×10^{-7}	1.11×10^{-7}	9.81×10^{-8}	1.15×10^{-7}	1.07×10^{-7}
GW190413.052954	33.38	0.05	33.42	1.21×10^{-7}	1.97×10^{-7}	1.36×10^{-7}	1.15×10^{-7}	2.12×10^{-7}	1.28×10^{-7}
GW190413.134308	SAA	6.94	6.94	-	-	-	7.40×10^{-8}	2.10×10^{-7}	1.25×10^{-7}
GW190421.213856	65.97	40.81	99.97	1.38×10^{-7}	1.58×10^{-7}	1.44×10^{-7}	5.02×10^{-8}	2.04×10^{-7}	1.30×10^{-7}
GW190426.190642	88.70	SAA	88.70	1.10×10^{-7}	2.48×10^{-7}	1.34×10^{-7}	1.09×10^{-7}	2.29×10^{-7}	1.31×10^{-7}
GW190503.185404	96.59	SAA	96.59	1.32×10^{-7}	1.36×10^{-7}	1.33×10^{-7}	1.25×10^{-7}	1.28×10^{-7}	1.26×10^{-7}
GW190512.180714	30.95	0.00	30.95	1.65×10^{-7}	1.79×10^{-7}	1.76×10^{-7}	1.54×10^{-7}	1.66×10^{-7}	1.64×10^{-7}
GW190513.205428	84.97	0.00	84.97	1.07×10^{-7}	1.31×10^{-7}	1.13×10^{-7}	1.06×10^{-7}	1.19×10^{-7}	1.09×10^{-7}
GW190514.065416	83.33	68.64	83.75	1.09×10^{-7}	3.03×10^{-7}	1.35×10^{-7}	3.89×10^{-8}	2.79×10^{-7}	8.77×10^{-8}
GW190517.055101	6.81	4.07	10.57	1.32×10^{-7}	1.35×10^{-7}	1.34×10^{-7}	4.41×10^{-8}	1.26×10^{-7}	1.02×10^{-7}
GW190519.153544	40.53	0.00	40.53	1.13×10^{-7}	1.61×10^{-7}	1.26×10^{-7}	1.06×10^{-7}	1.54×10^{-7}	1.18×10^{-7}
GW190521	58.61	61.27	99.98	1.64×10^{-7}	3.54×10^{-7}	2.19×10^{-7}	4.20×10^{-8}	3.20×10^{-7}	1.35×10^{-7}
GW190521.074359	100.00	0.00	100.00	1.20×10^{-7}	1.61×10^{-7}	1.51×10^{-7}	1.16×10^{-7}	1.48×10^{-7}	1.40×10^{-7}
GW190527.092055	72.51	0.05	72.51	1.14×10^{-7}	3.30×10^{-7}	1.91×10^{-7}	1.10×10^{-7}	2.96×10^{-7}	1.74×10^{-7}
GW190602.175927	65.84	SAA	65.84	1.53×10^{-7}	2.08×10^{-7}	1.89×10^{-7}	1.51×10^{-7}	1.92×10^{-7}	1.76×10^{-7}
GW190620.030421	SAA	4.10	4.10	-	-	-	8.21×10^{-8}	1.79×10^{-7}	1.39×10^{-7}
GW190630.185205	78.32	SAA	78.32	1.17×10^{-7}	2.16×10^{-7}	1.30×10^{-7}	1.08×10^{-7}	1.97×10^{-7}	1.20×10^{-7}
GW190701.203306	100.00	99.51	100.00	1.27×10^{-7}	1.33×10^{-7}	1.28×10^{-7}	1.01×10^{-7}	1.20×10^{-7}	1.15×10^{-7}
GW190706.222641	66.90	12.80	73.80	1.03×10^{-7}	2.95×10^{-7}	1.63×10^{-7}	4.66×10^{-8}	2.79×10^{-7}	1.53×10^{-7}
GW190707.093326	42.31	SAA	42.31	1.38×10^{-7}	2.34×10^{-7}	1.60×10^{-7}	1.30×10^{-7}	2.12×10^{-7}	1.48×10^{-7}
GW190708.232457	56.01	SAA	56.01	1.28×10^{-7}	4.24×10^{-7}	1.93×10^{-7}	1.22×10^{-7}	3.77×10^{-7}	1.75×10^{-7}
GW190719.215514	74.97	15.00	89.79	1.17×10^{-7}	3.74×10^{-7}	1.85×10^{-7}	3.65×10^{-8}	3.40×10^{-7}	1.60×10^{-7}
GW190720.000836	87.90	SAA	87.90	1.08×10^{-7}	2.64×10^{-7}	1.19×10^{-7}	1.01×10^{-7}	2.46×10^{-7}	1.12×10^{-7}
GW190725.174728	SAA	SAA	-	-	-	-	-	-	-
GW190727.060333	61.20	0.01	61.20	1.61×10^{-7}	1.93×10^{-7}	1.74×10^{-7}	1.49×10^{-7}	1.72×10^{-7}	1.58×10^{-7}
GW190728.064510	74.03	71.13	74.03	1.07×10^{-7}	2.36×10^{-7}	1.21×10^{-7}	6.33×10^{-8}	2.28×10^{-7}	9.27×10^{-8}
GW190731.140936	61.08	3.17	61.08	1.20×10^{-7}	1.99×10^{-7}	1.40×10^{-7}	1.13×10^{-7}	1.88×10^{-7}	1.32×10^{-7}
GW190803.022701	SAA	47.43	47.43	-	-	-	7.34×10^{-8}	1.47×10^{-7}	1.16×10^{-7}
GW190805.211137	91.07	7.64	98.63	1.15×10^{-7}	1.60×10^{-7}	1.43×10^{-7}	4.04×10^{-8}	1.48×10^{-7}	1.27×10^{-7}
GW190828.063405	90.53	24.93	90.53	1.34×10^{-7}	2.01×10^{-7}	1.81×10^{-7}	8.58×10^{-8}	1.83×10^{-7}	1.56×10^{-7}
GW190828.065509	12.79	8.82	12.79	1.60×10^{-7}	2.98×10^{-7}	2.00×10^{-7}	5.19×10^{-8}	2.67×10^{-7}	1.32×10^{-7}
GW190910.112807	SAA	34.37	34.37	-	-	-	3.85×10^{-8}	1.77×10^{-7}	8.11×10^{-8}
GW190915.235702	94.82	76.04	94.87	1.59×10^{-7}	2.15×10^{-7}	1.86×10^{-7}	5.59×10^{-8}	1.74×10^{-7}	1.13×10^{-7}
GW190916.200658	56.57	0.00	56.57	1.20×10^{-7}	1.61×10^{-7}	1.31×10^{-7}	1.12×10^{-7}	1.42×10^{-7}	1.21×10^{-7}
GW190924.021846	100.00	92.40	100.00	1.39×10^{-7}	1.61×10^{-7}	1.47×10^{-7}	4.25×10^{-8}	1.43×10^{-7}	8.43×10^{-8}
GW190925.232845	SAA	SAA	-	-	-	-	-	-	-
GW190926.050336	60.68	0.02	60.68	1.53×10^{-7}	2.84×10^{-7}	2.10×10^{-7}	1.43×10^{-7}	2.57×10^{-7}	1.88×10^{-7}
GW190929.012149	73.05	34.84	73.05	1.35×10^{-7}	2.25×10^{-7}	1.75×10^{-7}	4.79×10^{-8}	2.14×10^{-7}	1.59×10^{-7}
GW190930.133541	63.05	0.56	63.05	1.55×10^{-7}	2.87×10^{-7}	2.39×10^{-7}	1.46×10^{-7}	2.71×10^{-7}	2.25×10^{-7}

continued on next page

Table 5 continued.

Event Name	Coverage [%]			3σ Flux U.L. [erg s ⁻¹ cm ⁻²]			5σ Flux U.L. [erg s ⁻¹ cm ⁻²]		
	GBM	BAT	Combined	10–1000 keV			15–350 keV		
				Min	Max	Marginal	Min	Max	Marginal
GW191103.012549	76.96	56.21	97.35	1.57×10^{-7}	3.60×10^{-7}	1.98×10^{-7}	1.25×10^{-7}	3.24×10^{-7}	1.65×10^{-7}
GW191105.143521	77.45	8.05	80.39	1.35×10^{-7}	2.01×10^{-7}	1.69×10^{-7}	1.06×10^{-7}	1.91×10^{-7}	1.58×10^{-7}
GW191109.010717	89.38	29.05	89.38	1.29×10^{-7}	2.22×10^{-7}	1.55×10^{-7}	1.25×10^{-7}	2.05×10^{-7}	1.47×10^{-7}
GW191113.071753	72.98	2.27	73.00	1.53×10^{-7}	2.27×10^{-7}	1.72×10^{-7}	1.45×10^{-7}	2.08×10^{-7}	1.61×10^{-7}
GW191126.115259	59.81	7.88	59.81	1.12×10^{-7}	2.09×10^{-7}	1.36×10^{-7}	7.09×10^{-8}	1.96×10^{-7}	1.25×10^{-7}
GW191127.050227	89.03	77.16	89.04	1.12×10^{-7}	2.42×10^{-7}	1.40×10^{-7}	3.94×10^{-8}	2.23×10^{-7}	8.96×10^{-8}
GW191129.134029	SAA	SAA	-	-	-	-	-	-	-
GW191204.110529	48.10	25.20	66.23	1.09×10^{-7}	2.77×10^{-7}	1.42×10^{-7}	3.10×10^{-8}	1.43×10^{-7}	1.07×10^{-7}
GW191204.171526	SAA	87.15	87.15	-	-	-	2.02×10^{-7}	9.13×10^{-7}	3.97×10^{-7}
GW191215.223052	51.87	21.09	51.87	1.41×10^{-7}	1.69×10^{-7}	1.53×10^{-7}	4.40×10^{-8}	1.55×10^{-7}	1.29×10^{-7}
GW191216.213338	94.70	1.76	94.76	1.40×10^{-7}	1.64×10^{-7}	1.48×10^{-7}	1.26×10^{-7}	1.50×10^{-7}	1.33×10^{-7}
GW191222.033537	SAA	0.89	0.89	-	-	-	1.84×10^{-7}	1.92×10^{-7}	1.89×10^{-7}
GW191230.180458	40.80	0.00	40.80	1.09×10^{-7}	1.72×10^{-7}	1.39×10^{-7}	1.09×10^{-7}	1.60×10^{-7}	1.33×10^{-7}
GW200112.155838	SAA	SAA	-	-	-	-	-	-	-
GW200128.022011	45.58	23.04	45.58	1.22×10^{-7}	3.08×10^{-7}	1.42×10^{-7}	3.29×10^{-8}	2.83×10^{-7}	1.07×10^{-7}
GW200129.065458	1.36	1.16	1.36	-	-	1.42×10^{-7}	-	-	6.49×10^{-8}
GW200202.154313	99.99	SAA	99.99	1.18×10^{-7}	1.26×10^{-7}	1.21×10^{-7}	1.10×10^{-7}	1.18×10^{-7}	1.14×10^{-7}
GW200208.130117	99.70	0.00	99.70	1.33×10^{-7}	1.36×10^{-7}	1.36×10^{-7}	1.22×10^{-7}	1.25×10^{-7}	1.25×10^{-7}
GW200208.222617	SAA	5.85	5.85	-	-	-	6.09×10^{-8}	1.77×10^{-7}	1.06×10^{-7}
GW200209.085452	61.47	7.05	61.63	1.27×10^{-7}	1.69×10^{-7}	1.35×10^{-7}	3.71×10^{-8}	1.28×10^{-7}	1.17×10^{-7}
GW200216.220804	SAA	38.42	38.42	-	-	-	8.98×10^{-8}	1.71×10^{-7}	1.47×10^{-7}
GW200219.094415	20.36	SAA	20.36	1.37×10^{-7}	1.73×10^{-7}	1.52×10^{-7}	1.29×10^{-7}	1.58×10^{-7}	1.41×10^{-7}
GW200220.061928	99.63	0.05	99.65	1.33×10^{-7}	2.12×10^{-7}	1.65×10^{-7}	1.22×10^{-7}	1.87×10^{-7}	1.48×10^{-7}
GW200220.124850	63.37	21.46	80.25	1.10×10^{-7}	2.34×10^{-7}	1.28×10^{-7}	3.07×10^{-8}	2.18×10^{-7}	1.10×10^{-7}
GW200224.222234	SAA	98.76	98.76	-	-	-	1.13×10^{-7}	1.40×10^{-7}	1.27×10^{-7}
GW200225.060421	87.61	1.30	87.61	1.37×10^{-7}	3.32×10^{-7}	2.36×10^{-7}	1.28×10^{-7}	3.10×10^{-7}	2.23×10^{-7}
GW200302.015811	67.41	23.35	67.92	1.04×10^{-7}	3.40×10^{-7}	1.62×10^{-7}	3.27×10^{-8}	1.77×10^{-7}	1.19×10^{-7}
GW200306.093714	72.37	30.46	90.36	1.18×10^{-7}	2.54×10^{-7}	1.46×10^{-7}	5.38×10^{-8}	2.40×10^{-7}	1.33×10^{-7}
GW200308.173609	70.53	4.40	70.89	1.19×10^{-7}	3.39×10^{-7}	1.92×10^{-7}	8.13×10^{-8}	3.20×10^{-7}	1.77×10^{-7}
GW200311.115853	SAA	N/A	-	-	-	-	-	-	-
GW200316.215756	15.69	13.49	15.69	1.14×10^{-7}	1.51×10^{-7}	1.34×10^{-7}	1.09×10^{-7}	1.36×10^{-7}	1.22×10^{-7}
GW200322.091133	75.18	13.82	89.00	1.06×10^{-7}	3.70×10^{-7}	1.54×10^{-7}	4.49×10^{-8}	3.38×10^{-7}	1.39×10^{-7}

selleria de Fons Europeus, Universitat i Cultura and the Direcció General de Política Universitaria i Recerca del Govern de les Illes Balears, the Conselleria d’Innovació, Universitats, Ciència i Societat Digital de la Generalitat Valenciana and the CERCA Programme Generalitat de Catalunya, Spain, the National Science Centre of Poland and the European Union – European Regional Development Fund; Foundation for Polish Science (FNP), the Swiss National Science Foundation (SNSF), the Russian Foundation for Basic Research, the Russian Science Foundation, the European Commission, the European Social Funds (ESF), the European Regional Development Funds (ERDF), the Royal Society,

the Scottish Funding Council, the Scottish Universities Physics Alliance, the Hungarian Scientific Research Fund (OTKA), the French Lyon Institute of Origins (LIO), the Belgian Fonds de la Recherche Scientifique (FRS-FNRS), Actions de Recherche Concertées (ARC) and Fonds Wetenschappelijk Onderzoek – Vlaanderen (FWO), Belgium, the Paris Île-de-France Region, the National Research, Development and Innovation Office Hungary (NKFIH), the National Research Foundation of Korea, the Natural Science and Engineering Research Council Canada, Canadian Foundation for Innovation (CFI), the Brazilian Ministry of Science, Technology, and Innovations, the International Center for Theoretic-

Table 6. Flux upper limits for possible EM counterparts to marginal GW candidates with ($FAR < 2 \text{ yr}^{-1}$, $p_{\text{astro}} < 0.5$). The 3σ upper limits are computed for the 10–1000 keV energy range over the FoV of *Fermi*-GBM. The 5σ upper limits are computed for the combined coverage of *Fermi*-GBM and *Swift*-BAT with both instruments matched to the 15–350 keV energy range of *Swift*-BAT. The columns labeled Min and Max correspond, respectively, to the minimum and maximum upper limits obtained for points within the 90% credible level of the GW candidate localization. The Marginal upper limit is computed by integrating the upper limits produced at individual locations over the full sky using the GW localization as a weighted prior, normalized to the visible portion of the sky. Also shown is the visible coverage percentage of the full GW localization for *Fermi*-GBM alone, *Swift*-BAT alone, and the combined FoV from both instruments.

Event Name	Coverage [%]			3σ Flux U.L. [erg s ⁻¹ cm ⁻²]			5σ Flux U.L. [erg s ⁻¹ cm ⁻²]		
	GBM	BAT	Combined	10–1000 keV			15–350 keV		
				Min	Max	Marginal	Min	Max	Marginal
GW190426.152155	100.00	SAA	100.00	1.03×10^{-7}	1.65×10^{-7}	1.30×10^{-7}	1.00×10^{-7}	1.53×10^{-7}	1.21×10^{-7}
GW190531.023648	86.90	0.03	86.91	1.35×10^{-7}	2.63×10^{-7}	1.74×10^{-7}	1.26×10^{-7}	2.42×10^{-7}	1.60×10^{-7}
GW191118.212859	93.63	SAA	93.63	1.07×10^{-7}	2.93×10^{-7}	1.19×10^{-7}	1.05×10^{-7}	2.71×10^{-7}	1.13×10^{-7}
GW200105.162426	53.57	3.01	54.36	1.13×10^{-7}	1.53×10^{-7}	1.26×10^{-7}	1.06×10^{-7}	1.69×10^{-7}	1.18×10^{-7}
GW200201.203549	86.01	SAA	86.01	1.17×10^{-7}	1.80×10^{-7}	1.31×10^{-7}	1.09×10^{-7}	1.64×10^{-7}	1.22×10^{-7}
GW200311.103121	SAA	0.01	0.01	-	-	-	-	-	1.09×10^{-7}

cal Physics South American Institute for Fundamental Research (ICTP-SAIFR), the Research Grants Council of Hong Kong, the National Natural Science Foundation of China (NSFC), the Leverhulme Trust, the Research Corporation, the National Science and Technology Council (NSTC), Taiwan, the United States Department of Energy, and the Kavli Foundation. The authors gratefully acknowledge the support of the NSF, STFC, INFN and CNRS for provision of computational resources.

This work was supported by MEXT, JSPS Leading-edge Research Infrastructure Program, JSPS Grant-in-Aid for Specially Promoted Research 26000005, JSPS Grant-in-Aid for Scientific Research on Innovative Areas 2905: JP17H06358, JP17H06361 and JP17H06364, JSPS Core-to-Core Program A. Advanced Research Networks, JSPS Grant-in-Aid for Scientific Research (S)

17H06133 and 20H05639, JSPS Grant-in-Aid for Transformative Research Areas (A) 20A203: JP20H05854, the joint research program of the Institute for Cosmic Ray Research, University of Tokyo, National Research Foundation (NRF), Computing Infrastructure Project of Global Science experimental Data hub Center (GSDC) at KISTI, Korea Astronomy and Space Science Institute (KASI), and Ministry of Science and ICT (MSIT) in Korea, Academia Sinica (AS), AS Grid Center (ASGC) and the National Science and Technology Council (NSTC) in Taiwan under grants including the Rising Star Program and Science Vanguard Research Program, Advanced Technology Center (ATC) of NAOJ, and Mechanical Engineering Center of KEK.

Additional LSC-Virgo-KAGRA acknowledgements for support of individual authors may be found in the following document:

<https://dcc.ligo.org/LIGO-M2300033/public>.

REFERENCES

- Aasi, J., Abbott, B. P., Abbott, R., et al. 2015, CQGra, 32, 074001, doi: [10.1088/0264-9381/32/7/074001](https://doi.org/10.1088/0264-9381/32/7/074001)
- Abbott, B. P., Abbott, R., Abbott, T. D., et al. 2016, PhRvL, 116, 061102, doi: [10.1103/PhysRevLett.116.061102](https://doi.org/10.1103/PhysRevLett.116.061102)
- Abbott, B. P., Abbott, R., Abbott, T. D., et al. 2017, PhRvL, 119, 161101, doi: [10.1103/PhysRevLett.119.161101](https://doi.org/10.1103/PhysRevLett.119.161101)
- Abbott, B. P., Abbott, R., Abbott, T. D., et al. 2017, ApJL, 848, L13, doi: [10.3847/2041-8213/aa920c](https://doi.org/10.3847/2041-8213/aa920c)
- . 2018, Living Reviews in Relativity, 21, 3, doi: [10.1007/s41114-018-0012-9](https://doi.org/10.1007/s41114-018-0012-9)
- Abbott, B. P., Abbott, R., Abbott, T. D., et al. 2019, PhRvX, 9, 031040, doi: [10.1103/PhysRevX.9.031040](https://doi.org/10.1103/PhysRevX.9.031040)
- Abbott, B. P., et al. 2020, ApJL, 892, L3, doi: [10.3847/2041-8213/ab75f5](https://doi.org/10.3847/2041-8213/ab75f5)
- Abbott, B. P., Abbott, R., Abbott, T. D., et al. 2020a, LRR, 23, 3, doi: [10.1007/s41114-020-00026-9](https://doi.org/10.1007/s41114-020-00026-9)
- Abbott, R., Abbott, T. D., Abraham, S., et al. 2020b, ApJL, 896, L44, doi: [10.3847/2041-8213/ab960f](https://doi.org/10.3847/2041-8213/ab960f)
- . 2021, PhRvX, 11, 021053, doi: [10.1103/PhysRevX.11.021053](https://doi.org/10.1103/PhysRevX.11.021053)
- Abbott, R., et al. 2021. <https://arxiv.org/abs/2108.01045>

- Abbott, R., Abbott, T. D., Acernese, F., et al. 2021, arXiv e-prints, arXiv:2111.03606.
<https://arxiv.org/abs/2111.03606>
- Abbott, R., Abbott, T. D., Abraham, S., et al. 2021, *The Astrophysical Journal Letters*, 915, L5,
doi: [10.3847/2041-8213/ac082e](https://doi.org/10.3847/2041-8213/ac082e)
- Acernese, F., Agathos, M., Agatsuma, K., et al. 2014, *Classical and Quantum Gravity*, 32, 024001,
doi: [10.1088/0264-9381/32/2/024001](https://doi.org/10.1088/0264-9381/32/2/024001)
- Acernese, F., Agathos, M., Aiello, L., et al. 2019, *Phys. Rev. Lett.*, 123, 231108, doi: [10.1103/PhysRevLett.123.231108](https://doi.org/10.1103/PhysRevLett.123.231108)
- Allison, J., Amako, K., Apostolakis, J., et al. 2016, *NIMPA*, 835, 186, doi: <https://doi.org/10.1016/j.nima.2016.06.125>
- Ashton, G., Ackley, K., Hernandez, I. M., & Piotrkowski, B. 2021, *CQGra*, 38, 235004,
doi: [10.1088/1361-6382/ac33bb](https://doi.org/10.1088/1361-6382/ac33bb)
- Astropy Collaboration, Price-Whelan, A. M., Lim, P. L., et al. 2022, *apj*, 935, 167, doi: [10.3847/1538-4357/ac7c74](https://doi.org/10.3847/1538-4357/ac7c74)
- Band, D., Matteson, J., Ford, L., et al. 1993, *ApJ*, 413, 281,
doi: [10.1086/172995](https://doi.org/10.1086/172995)
- Barthelmy, S. D., Barbier, L. M., Cummings, J. R., et al. 2005, *SSRv*, 120, 143, doi: [10.1007/s11214-005-5096-3](https://doi.org/10.1007/s11214-005-5096-3)
- Blackburn, L., Briggs, M. S., Camp, J., et al. 2015, *The ApJS*, 217, 8, doi: [10.1088/0067-0049/217/1/8](https://doi.org/10.1088/0067-0049/217/1/8)
- Blandford, R. D., & Znajek, R. L. 1977, *MNRAS*, 179, 433,
doi: [10.1093/mnras/179.3.433](https://doi.org/10.1093/mnras/179.3.433)
- Bombaci, I. 1996, *A&A*, 305, 871
- Briggs, M. S., Xiong, S., Connaughton, V., et al. 2013, *JGRA*, 118, 3805,
doi: <https://doi.org/10.1002/jgra.50205>
- Buikema, A., Cahillane, C., Mansell, G. L., et al. 2020, *PhRvD*, 102, 062003, doi: [10.1103/PhysRevD.102.062003](https://doi.org/10.1103/PhysRevD.102.062003)
- Burns, E. 2020, *LRR*, 23, 4,
doi: [10.1007/s41114-020-00028-7](https://doi.org/10.1007/s41114-020-00028-7)
- Burns, E., Goldstein, A., Hui, C. M., et al. 2019, *ApJ*, 871, 90, doi: [10.3847/1538-4357/aaf726](https://doi.org/10.3847/1538-4357/aaf726)
- Burrows, D. N., Hill, J. E., Nousek, J. A., et al. 2005, *SSRv*, 120, 165, doi: [10.1007/s11214-005-5097-2](https://doi.org/10.1007/s11214-005-5097-2)
- Bustillo, J. C., Leong, S. H. W., Chandra, K., McKernan, B., & Ford, K. E. S. 2021.
<https://arxiv.org/abs/2112.12481>
- Chornock, R., Berger, E., Kasen, D., et al. 2017, *ApJ*, 848, L19, doi: [10.3847/2041-8213/aa905c](https://doi.org/10.3847/2041-8213/aa905c)
- Connaughton, V., Burns, E., Goldstein, A., et al. 2016, *ApJL*, 826, L6, doi: [10.3847/2041-8205/826/1/L6](https://doi.org/10.3847/2041-8205/826/1/L6)
- Connaughton, V., Burns, E., Goldstein, A., et al. 2018, *ApJ*, 853, L9, doi: [10.3847/2041-8213/aaa4f2](https://doi.org/10.3847/2041-8213/aaa4f2)
- Cowperthwaite, P. S., Berger, E., Villar, V. A., et al. 2017, *ApJ*, 848, L17, doi: [10.3847/2041-8213/aa8fc7](https://doi.org/10.3847/2041-8213/aa8fc7)
- Dai, L., McKinney, J. C., & Miller, M. C. 2017, *MNRAS*, 470, L92, doi: [10.1093/mnras/slx086](https://doi.org/10.1093/mnras/slx086)
- De Paolis, F., Nucita, A. A., Strafella, F., Licchelli, D., & Ingrosso, G. 2020, *MNRAS*, 499, L87,
doi: [10.1093/mnras/slaa140](https://doi.org/10.1093/mnras/slaa140)
- DeLaunay, J., & Tohuvavohu, A. 2021.
<https://arxiv.org/abs/2111.01769>
- Fenimore, E. E., McLean, K., Palmer, D., et al. 2004, *BaltA*, 13, 301. <https://arxiv.org/abs/astro-ph/0408513>
- Fletcher, C., Fermi-GBM Team, & GBM-LIGO/Virgo Group. 2019, *GRB Coordinates Network*, 24185, 1
- Gehrels, N., Ramirez-Ruiz, E., & Fox, D. 2009, *ARA&A*, 47, 567, doi: [10.1146/annurev.astro.46.060407.145147](https://doi.org/10.1146/annurev.astro.46.060407.145147)
- Gehrels, N., Chincarini, G., Giommi, P., et al. 2004, *ApJ*, 611, 1005, doi: [10.1086/422091](https://doi.org/10.1086/422091)
- Goldstein, A., Burns, E., Hamburg, R., et al. 2016, Updates to the Fermi-GBM Short GRB Targeted Offline Search in Preparation for LIGO's Second Observing Run.
<https://arxiv.org/abs/1612.02395>
- Goldstein, A., Veres, P., Burns, E., et al. 2017, *ApJL*, 848, L14, doi: [10.3847/2041-8213/aa8f41](https://doi.org/10.3847/2041-8213/aa8f41)
- Goldstein, A., Hamburg, R., Wood, J., et al. 2019, arXiv e-prints, arXiv:1903.12597.
<https://arxiv.org/abs/1903.12597>
- Graham, M. J., Ford, K. E. S., McKernan, B., et al. 2020, *PhRvL*, 124, 251102,
doi: [10.1103/PhysRevLett.124.251102](https://doi.org/10.1103/PhysRevLett.124.251102)
- Greiner, J., Burgess, J. M., Savchenko, V., & Yu, H.-F. 2016, *ApJ*, 827, L38, doi: [10.3847/2041-8205/827/2/L38](https://doi.org/10.3847/2041-8205/827/2/L38)
- Hamburg, R., Fletcher, C., Burns, E., et al. 2020, *ApJ*, 893, 100, doi: [10.3847/1538-4357/ab7d3e](https://doi.org/10.3847/1538-4357/ab7d3e)
- Harris, C. R., Millman, K. J., van der Walt, S. J., et al. 2020, *Nature*, 585, 357, doi: [10.1038/s41586-020-2649-2](https://doi.org/10.1038/s41586-020-2649-2)
- Hosseinzadeh, G., Cowperthwaite, P. S., Gomez, S., et al. 2019, *The Astrophysical Journal*, 880, L4,
doi: [10.3847/2041-8213/ab271c](https://doi.org/10.3847/2041-8213/ab271c)
- Hunter, J. D. 2007, *Computing in Science & Engineering*, 9, 90, doi: [10.1109/MCSE.2007.55](https://doi.org/10.1109/MCSE.2007.55)
- Kalogera, V., & Baym, G. 1996, *ApJL*, 470, L61,
doi: [10.1086/310296](https://doi.org/10.1086/310296)
- Kocevski, D., Burns, E., Goldstein, A., et al. 2018, *ApJ*, 862, 152, doi: [10.3847/1538-4357/aacb7b](https://doi.org/10.3847/1538-4357/aacb7b)
- Lien, A., Sakamoto, T., Gehrels, N., et al. 2014, *ApJ*, 783, 24, doi: [10.1088/0004-637X/783/1/24](https://doi.org/10.1088/0004-637X/783/1/24)
- Lin, D.-B., Liu, T., Lin, J., et al. 2018, *The Astrophysical Journal*, 856, 90, doi: [10.3847/1538-4357/aab3d7](https://doi.org/10.3847/1538-4357/aab3d7)
- Loeb, A. 2016a, *ApJL*, 819, L21,
doi: [10.3847/2041-8205/819/2/L21](https://doi.org/10.3847/2041-8205/819/2/L21)
- . 2016b, *ApJL*, 819, L21,
doi: [10.3847/2041-8205/819/2/L21](https://doi.org/10.3847/2041-8205/819/2/L21)

- LSC and Virgo and Fermi-GBM Team. 2019a, GRB Coordinates Network, 25406, 1
- . 2019b, GRB Coordinates Network, 25465, 1
- Margalit, B., & Metzger, B. D. 2017, *ApJL*, 850, L19, doi: [10.3847/2041-8213/aa991c](https://doi.org/10.3847/2041-8213/aa991c)
- Margutti, R., & Chornock, R. 2021, *ARA&A*, 59, 155, doi: [10.1146/annurev-astro-112420-030742](https://doi.org/10.1146/annurev-astro-112420-030742)
- Meegan, C., Lichti, G., Bhat, P. N., et al. 2009, *ApJ*, 702, 791, doi: [10.1088/0004-637x/702/1/791](https://doi.org/10.1088/0004-637x/702/1/791)
- Nicholl, M., Berger, E., Kasen, D., et al. 2017, *The Astrophysical Journal Letters*, 848, L18, doi: [10.3847/2041-8213/aa9029](https://doi.org/10.3847/2041-8213/aa9029)
- Paciesas, W. S., Meegan, C. A., von Kienlin, A., et al. 2012, *The ApJS*, 199, 18, doi: [10.1088/0067-0049/199/1/18](https://doi.org/10.1088/0067-0049/199/1/18)
- Palmese, A., Fishbach, M., Burke, C. J., Annis, J., & Liu, X. 2021, *ApJL*, 914, L34, doi: [10.3847/2041-8213/ac0883](https://doi.org/10.3847/2041-8213/ac0883)
- Perna, R., Chruslinska, M., Corsi, A., & Belczynski, K. 2018, *MNRAS*, 477, 4228, doi: [10.1093/mnras/sty814](https://doi.org/10.1093/mnras/sty814)
- Perna, R., Lazzati, D., & Giacomazzo, B. 2016, *ApJL*, 821, L18, doi: [10.3847/2041-8205/821/1/L18](https://doi.org/10.3847/2041-8205/821/1/L18)
- Petrov, P., Singer, L. P., Coughlin, M. W., et al. 2022, *ApJ*, 924, 54, doi: [10.3847/1538-4357/ac366d](https://doi.org/10.3847/1538-4357/ac366d)
- Poolakkil, S., Preece, R., Fletcher, C., et al. 2021, *ApJ*, 913, 60, doi: [10.3847/1538-4357/abf24d](https://doi.org/10.3847/1538-4357/abf24d)
- Rezzolla, L., Most, E. R., & Weih, L. R. 2018, *The Astrophysical Journal Letters*, 852, L25, doi: [10.3847/2041-8213/aaa401](https://doi.org/10.3847/2041-8213/aaa401)
- Roming, P. W. A., Kennedy, T. E., Mason, K. O., et al. 2005, *SSRv*, 120, 95, doi: [10.1007/s11214-005-5095-4](https://doi.org/10.1007/s11214-005-5095-4)
- Ruffert, M., & Janka, H. T. 1998, *A&A*, 338, 535. <https://arxiv.org/abs/astro-ph/9804132>
- Salafia, Ghisellini, G., Ghirlanda, G., & Colpi, M. 2018, *A&A*, 619, A18, doi: [10.1051/0004-6361/201732259](https://doi.org/10.1051/0004-6361/201732259)
- Savchenko, V., Ferrigno, C., Kuulkers, E., et al. 2017, *ApJL*, 848, L15, doi: [10.3847/2041-8213/aa8f94](https://doi.org/10.3847/2041-8213/aa8f94)
- Soares-Santos, M., Holz, D. E., Annis, J., et al. 2017, *The Astrophysical Journal Letters*, 848, L16, doi: [10.3847/2041-8213/aa9059](https://doi.org/10.3847/2041-8213/aa9059)
- Tanvir, N. R., Levan, A. J., González-Fernández, C., et al. 2017, *ApJ*, 848, L27, doi: [10.3847/2041-8213/aa90b6](https://doi.org/10.3847/2041-8213/aa90b6)
- Tohuvavohu, A., Kennea, J. A., DeLaunay, J., et al. 2020, *ApJ*, 900, 35, doi: [10.3847/1538-4357/aba94f](https://doi.org/10.3847/1538-4357/aba94f)
- Vedrenne, G., & Atteia, J.-L. 2009, *Gamma-Ray Bursts: The Brightest Explosions in the Universe* (Berlin, Heidelberg: Springer Berlin Heidelberg), 385–476, doi: [10.1007/978-3-540-39088-6_8](https://doi.org/10.1007/978-3-540-39088-6_8)
- Veres, P., Dal Canton, T., Burns, E., et al. 2019, *ApJ*, 882, 53, doi: [10.3847/1538-4357/ab31aa](https://doi.org/10.3847/1538-4357/ab31aa)
- Veres, P., Preece, R. D., Goldstein, A., et al. 2016, *ApJL*, 827, L34, doi: [10.3847/2041-8205/827/2/L34](https://doi.org/10.3847/2041-8205/827/2/L34)
- Virtanen, P., Gommers, R., Oliphant, T. E., et al. 2020, *Nature Methods*, 17, 261, doi: [10.1038/s41592-019-0686-2](https://doi.org/10.1038/s41592-019-0686-2)
- von Kienlin, A., Meegan, C. A., Paciasas, W. S., et al. 2020, *ApJ*, 893, 46, doi: [10.3847/1538-4357/ab7a18](https://doi.org/10.3847/1538-4357/ab7a18)
- Wilks, S. S. 1938, *The Annals of Mathematical Statistics*, 9, 60, doi: [10.1214/aoms/1177732360](https://doi.org/10.1214/aoms/1177732360)
- Wood, J., Fletcher, C., Crnogorcevic, M., Hamburg, R., & Veres, P. 2023, *Fermi-GBM and Swift-BAT Data Release Related to Analysis of Gravitational-Wave Candidates from the Third Gravitational-wave Observing Run*, v1, Zenodo, doi: [10.5281/zenodo.8101645](https://doi.org/10.5281/zenodo.8101645)
- Zhang, B. 2016, *ApJL*, 827, L31, doi: [10.3847/2041-8205/827/2/L31](https://doi.org/10.3847/2041-8205/827/2/L31)
- Zhang, B. 2019, *FrPhy*, 14, doi: [10.1007/s11467-019-0913-4](https://doi.org/10.1007/s11467-019-0913-4)
- Zhang, B., Zhang, B., Sun, H., et al. 2018, *Nature Communications*, 9, doi: [10.1038/s41467-018-02847-3](https://doi.org/10.1038/s41467-018-02847-3)

APPENDIX

A. FLUX UPPER LIMITS FOR PROBABLE BBH MERGERS

Here we present the sky-marginalized 3σ flux upper limits for the probable BBH mergers described in Section 4.2 as well as the 0.95 percentile fluxes for different models of BBH emission. The upper limits are constructed over a 10–1000 keV energy range according to the method in Section 2. They assume the spectral shape of potential emission follows the normal spectral template from Table 3 with a 1 s emission duration.

Name	Waveform (visible frac.)	F_Q	$F_{\nu\bar{\nu}}$	F_{BZ}	F_{GW}	UL
GW190403_051519	IMRPhenomXPHM (49, 36)	74, 70, 67	7.3, 6.7, 6.4	7.3, 5.8, 5.6	2.5, 1.8, 1.7	178
GW190403_051519	SEOBNRv4PHM (39, 30)	44, 35, 35	5.0, 4.0, 3.8	6.5, 4.6, 4.5	3.4, 1.9, 1.7	178
GW190412	IMRPhenomXPHM (6, 0)	*137, 83, 95	*299, 165, 173	59, 30, 25	64, 28, 22	111
GW190412	SEOBNRv4PHM (12, 4)	*148, 85, 82	*356, 178, 172	48, 25, 23	70, 29, 25	111
GW190413_052954	IMRPhenomXPHM (30, 19)	11, 5.8, 5.2	10, 5.7, 5.2	10, 4.4, 4.0	10, 4.2, 3.6	136
GW190421_213856	IMRPhenomXPHM (23, 14)	21, 8.1, 7.5	14, 6.1, 5.8	36, 13, 12	27, 10, 9.6	144
GW190426_190642	IMRPhenomXPHM (22, 14)	32, 31, 29	2.7, 2.3, 2.1	75, 24, 22	26, 8.0, 7.1	134
GW190503_185404	IMRPhenomXPHM (30, 20)	50, 20, 18	38, 16, 15	68, 29, 28	54, 20, 18	133
GW190503_185404	SEOBNRv4PHM (25, 16)	42, 22, 21	32, 17, 16	53, 25, 24	44, 19, 18	133
GW190512_180714	IMRPhenomXPHM (27, 17)	49, 24, 24	107, 55, 54	20, 7.2, 6.6	28, 10, 9.2	176
GW190512_180714	SEOBNRv4PHM (22, 13)	45, 18, 17	104, 46, 43	18, 6.1, 5.2	28, 9.5, 8.2	176
GW190513_205428	IMRPhenomXPHM (31, 19)	42, 24, 23	35, 21, 20	16, 9.2, 8.4	17, 8.2, 7.5	113
GW190513_205428	SEOBNRv4PHM (30, 19)	52, 26, 24	36, 20, 19	15, 8.3, 7.9	17, 8.0, 7.0	113
GW190514_065416	IMRPhenomXPHM (24, 15)	12, 5.1, 4.8	7.8, 3.8, 3.7	21, 8.7, 7.3	14, 6.0, 5.4	135
GW190514_065416	SEOBNRv4PHM (21, 13)	12, 6.9, 6.1	7.5, 4.4, 4.2	17, 8.0, 7.8	12, 6.0, 5.5	135
GW190517_055101	IMRPhenomXPHM (10, 5)	*485, 198, 173	*202, 85, 74	48, 10, 7.9	60, 18, 14	134
GW190517_055101	SEOBNRv4PHM (14, 8)	*360, 171, 145	*142, 70, 62	29, 9.3, 7.6	53, 16, 14	134
GW190519_153544	IMRPhenomXPHM (6, 3)	49, 19, 19	14, 6.1, 5.8	47, 12, 9.7	32, 7.1, 5.5	126
GW190519_153544	SEOBNRv4PHM (5, 2)	49, 21, 17	12, 6.3, 4.9	38, 17, 14	26, 9.6, 7.7	126
GW190521_074359	IMRPhenomXPHM (7, 3)	*222, 58, 49	142, 44, 38	*259, 76, 69	*228, 65, 57	151
GW190521_074359	SEOBNRv4PHM (25, 14)	*99, 51, 47	62, 31, 29	*94, 37, 35	*87, 35, 31	151
GW190521	IMRPhenomXPHM (19, 11)	15, 3.4, 3.2	2.9, 0.77, 0.72	121, 21, 18	38, 6.9, 5.9	219
GW190527_092055	IMRPhenomXPHM (21, 13)	44, 16, 15	31, 14, 13	27, 13, 12	23, 9.5, 8.7	191
GW190527_092055	SEOBNRv4PHM (22, 14)	34, 16, 15	29, 15, 14	23, 10, 9.7	24, 10, 10	191
GW190602_175927	IMRPhenomXPHM (31, 20)	24, 14, 13	6.8, 4.2, 3.9	61, 33, 32	29, 13, 12	189
GW190630_185205	IMRPhenomXPHM (21, 14)	*225, 75, 70	*215, 78, 73	145, 56, 51	167, 56, 51	130
GW190630_185205	SEOBNRv4PHM (26, 18)	*195, 93, 88	*185, 89, 83	131, 56, 53	145, 60, 57	130
GW190701_203306	IMRPhenomXPHM (32, 20)	20, 11, 10	10, 6.0, 5.5	51, 26, 24	31, 15, 13	128
GW190701_203306	SEOBNRv4PHM (35, 23)	21, 14, 14	9.7, 6.9, 6.7	48, 29, 26	29, 16, 15	128
GW190706_222641	IMRPhenomXPHM (20, 12)	53, 37, 34	11, 8.4, 8.2	63, 43, 40	31, 19, 18	163
GW190706_222641	SEOBNRv4PHM (19, 10)	41, 27, 29	9.1, 6.9, 7.5	62, 44, 46	33, 22, 23	163
GW190707_093326	IMRPhenomXPHM (37, 26)	174, 114, 109	*961, 632, 602	21, 13, 12	63, 38, 35	160
GW190707_093326	SEOBNRv4PHM (31, 20)	151, 76, 70	*821, 429, 389	20, 9.8, 8.9	57, 27, 24	160
GW190708_232457	IMRPhenomXPHM (39, 26)	152, 96, 91	*415, 260, 248	35, 20, 18	70, 39, 36	193
GW190708_232457	SEOBNRv4PHM (36, 25)	125, 74, 72	*338, 203, 197	37, 19, 19	64, 34, 34	193
GW190719_215514	IMRPhenomXPHM (25, 16)	51, 29, 28	25, 13, 13	16, 10, 9.2	14, 7.2, 6.4	185
GW190720_000836	IMRPhenomXPHM (44, 32)	*261, 234, 266	*1054, 759, 785	19, 12, 12	54, 28, 26	119
GW190720_000836	SEOBNRv4PHM (35, 24)	*194, 126, 119	*852, 555, 515	19, 11, 10	51, 28, 26	119
GW190727_060333	IMRPhenomXPHM (30, 19)	23, 11, 10	14, 7.8, 7.3	16, 6.8, 6.1	15, 6.1, 5.4	174
GW190727_060333	SEOBNRv4PHM (25, 16)	21, 12, 11	12, 7.8, 7.3	14, 6.8, 6.3	14, 6.1, 5.6	174
GW190728_064510	IMRPhenomXPHM (32, 21)	*253, 125, 125	*1130, 462, 459	21, 8.4, 7.6	58, 17, 15	121
GW190728_064510	SEOBNRv4PHM (30, 19)	*208, 79, 75	*1015, 408, 388	17, 6.0, 5.6	54, 18, 16	121
GW190731_140936	IMRPhenomXPHM (28, 18)	20, 11, 10	12, 7.4, 6.8	24, 11, 10	19, 9.3, 8.7	140
GW190731_140936	SEOBNRv4PHM (27, 18)	26, 17, 16	13, 9.4, 9.1	24, 12, 10	20, 11, 9.9	140
GW190805_211137	IMRPhenomXPHM (22, 14)	28, 13, 12	8.7, 4.8, 4.6	7.4, 2.2, 1.9	7.3, 2.2, 1.9	143
GW190805_211137	SEOBNRv4PHM (18, 11)	21, 13, 13	6.6, 4.7, 4.8	7.9, 2.6, 2.2	6.9, 2.4, 2.3	143

Table 7. Table showing the 0.95 percentile fluxes from different models of BBH emission. The two numbers after the waveform names indicate the percentage of the cases where the jet is pointing towards Earth in the uniform 10-40 degree opening angle and in the fixed 20 degrees opening angle case respectively. Flux units are 10^{-9} erg cm^{-2} s^{-1} . The three numbers in each cell represent the isotropic emission, the uniform-distributed jet opening angle and the fixed jet opening angle. The upper limits (UL) are the 3σ , 10–1000 keV range values from Table 5. Stars mark instances where the isotropic emission exceeds the UL in more than 10% of the cases.

Name	Waveform (visible frac.)	F_Q	$F_{\nu\bar{\nu}}$	F_{BZ}	F_{GW}	UL
GW190828.063405	IMRPhenomXPHM (31, 21)	58, 25, 23	48, 22, 21	27, 7.7, 6.8	33, 9.9, 8.5	181
GW190828.065509	IMRPhenomXPHM (22, 12)	43, 19, 18	103, 48, 44	16, 6.4, 5.4	23, 7.6, 6.3	200
GW190915.235702	IMRPhenomXPHM (18, 10)	39, 17, 14	37, 18, 16	28, 11, 10	29, 11, 10	186
GW190915.235702	SEOBNRv4PHM (20, 12)	42, 25, 24	39, 23, 22	31, 12, 10	32, 13, 11	186
GW190916.200658	IMRPhenomXPHM (28, 18)	13, 6.6, 6.2	6.8, 3.5, 3.2	8.4, 4.0, 3.6	6.7, 2.3, 2.0	131
GW190916.200658	SEOBNRv4PHM (25, 16)	12, 6.1, 6.0	6.1, 3.4, 3.4	8.4, 4.9, 4.2	5.9, 2.4, 2.2	131
GW190924.021846	IMRPhenomXPHM (32, 22)	*351, 258, 281	*3217, 1887, 1884	21, 12, 12	78, 31, 28	147
GW190924.021846	SEOBNRv4PHM (25, 16)	*317, 131, 120	*3158, 1364, 1253	17, 6.4, 5.8	75, 28, 25	147
GW190926.050336	IMRPhenomXPHM (10, 6)	14, 2.9, 2.6	11, 3.3, 3.0	21, 3.9, 3.5	13, 2.5, 2.2	210
GW190929.012149	IMRPhenomXPHM (9, 5)	12, 2.8, 2.6	4.9, 1.5, 1.4	34, 14, 12	14, 4.3, 3.7	175
GW190930.133541	IMRPhenomXPHM (34, 23)	*363, 236, 252	*1483, 790, 776	23, 12, 12	69, 26, 23	239
GW190930.133541	SEOBNRv4PHM (32, 21)	*264, 141, 136	*1086, 566, 534	24, 11, 11	60, 26, 24	239
GW191103.012549	IMRPhenomXPHM (34, 23)	*332, 234, 230	*1349, 831, 801	15, 9.3, 8.6	53, 27, 24	198
GW191103.012549	SEOBNRv4PHM (27, 18)	*303, 164, 158	*1355, 764, 710	16, 8.6, 8.3	58, 28, 26	198
GW191105.143521	IMRPhenomXPHM (35, 24)	86, 43, 42	*509, 262, 247	8.5, 3.5, 3.3	26, 10, 9.5	169
GW191105.143521	SEOBNRv4PHM (27, 17)	84, 35, 31	*509, 229, 208	8.3, 3.0, 2.7	26, 9.8, 8.6	169
GW191109.010717	IMRPhenomXPHM (5, 2)	169, 11, 10	43, 5.5, 5.0	*437, 54, 43	217, 27, 22	155
GW191109.010717	SEOBNRv4PHM (16, 10)	47, 24, 22	16, 10.0, 9.5	*198, 113, 102	89, 50, 43	155
GW191113.071753	IMRPhenomXPHM (15, 8)	35, 20, 20	86, 53, 51	25, 8.3, 7.3	16, 5.9, 5.3	172
GW191113.071753	SEOBNRv4PHM (15, 9)	74, 42, 35	118, 72, 62	17, 8.6, 8.0	14, 6.3, 5.7	172
GW191126.115259	IMRPhenomXPHM (36, 25)	103, 68, 68	*394, 252, 244	5.6, 2.9, 2.7	18, 9.1, 8.4	136
GW191126.115259	SEOBNRv4PHM (28, 18)	104, 58, 52	*419, 234, 214	6.5, 3.1, 2.7	21, 9.8, 8.8	136
GW191127.050227	IMRPhenomXPHM (29, 19)	59, 58, 61	15, 11, 11	48, 44, 41	11, 8.8, 8.8	140
GW191127.050227	SEOBNRv4PHM (17, 10)	32, 15, 16	16, 7.4, 7.1	20, 10, 11	13, 4.8, 4.5	140
GW191204.110529	IMRPhenomXPHM (22, 13)	107, 56, 51	118, 68, 64	46, 26, 25	57, 32, 30	142
GW191204.110529	SEOBNRv4PHM (15, 9)	119, 78, 70	121, 84, 82	42, 29, 31	55, 35, 36	142
GW191215.223052	IMRPhenomXPHM (15, 8)	34, 14, 11	54, 22, 18	19, 5.2, 4.1	25, 6.5, 5.4	153
GW191215.223052	SEOBNRv4PHM (14, 8)	31, 13, 12	49, 21, 19	17, 4.9, 4.3	22, 6.7, 5.8	153
GW191216.213338	IMRPhenomXPHM (31, 19)	*1097, 696, 684	*5893, 3599, 3466	96, 60, 54	*287, 152, 140	148
GW191216.213338	SEOBNRv4PHM (25, 15)	*1180, 586, 545	*6516, 3304, 3024	93, 45, 40	*311, 150, 135	148
GW191230.180458	IMRPhenomXPHM (21, 13)	10, 3.2, 2.9	4.6, 1.8, 1.7	18, 5.5, 4.9	11, 3.5, 3.1	139
GW191230.180458	SEOBNRv4PHM (23, 14)	8.4, 4.2, 4.1	3.8, 2.1, 2.1	14, 5.1, 4.5	9.3, 3.5, 3.0	139
GW200128.022011	IMRPhenomXPHM (20, 12)	35, 13, 11	18, 8.1, 7.0	32, 11, 9.8	27, 9.5, 8.3	142
GW200128.022011	SEOBNRv4PHM (26, 15)	36, 29, 21	15, 13, 9.6	26, 18, 11	23, 17, 10	142
GW200129.065458	IMRPhenomXPHM (33, 18)	*220, 149, 145	170, 108, 105	113, 64, 59	128, 62, 57	142
GW200129.065458	SEOBNRv4PHM (18, 9)	*235, 108, 103	211, 96, 88	165, 60, 59	188, 75, 71	142
GW200202.154313	IMRPhenomXPHM (37, 25)	*666, 364, 350	*4383, 2342, 2214	50, 23, 21	*174, 78, 71	121
GW200202.154313	SEOBNRv4PHM (32, 21)	*703, 330, 300	*4700, 2248, 2051	50, 22, 20	*185, 80, 72	121
GW200208.130117	IMRPhenomXPHM (31, 20)	18, 9.3, 8.4	16, 8.7, 7.9	25, 11, 9.6	21, 9.3, 7.8	136
GW200208.130117	SEOBNRv4PHM (31, 20)	17, 11, 11	14, 9.8, 9.2	22, 11, 10	19, 10, 9.0	136
GW200209.085452	IMRPhenomXPHM (22, 13)	21, 4.4, 4.0	16, 4.6, 4.3	25, 4.8, 4.2	21, 4.4, 4.0	135
GW200209.085452	SEOBNRv4PHM (22, 14)	10, 5.7, 5.6	8.4, 4.9, 4.8	12, 4.5, 3.9	10, 4.0, 3.7	135
GW200219.094415	IMRPhenomXPHM (18, 11)	11, 3.1, 2.7	8.9, 3.1, 2.8	16, 3.6, 3.2	13, 3.2, 2.7	152
GW200219.094415	SEOBNRv4PHM (22, 14)	10, 4.9, 4.6	7.7, 3.9, 3.7	11, 4.1, 3.8	9.7, 3.4, 3.2	152
GW200220.061928	IMRPhenomXPHM (22, 14)	8.3, 3.3, 3.1	1.3, 0.63, 0.61	52, 11, 10	12, 4.1, 3.4	165
GW200220.061928	SEOBNRv4PHM (22, 14)	10, 6.2, 5.3	1.4, 0.88, 0.8	34, 12, 10	12, 4.6, 4.1	165
GW200220.124850	IMRPhenomXPHM (20, 13)	13, 4.4, 4.3	8.8, 3.6, 3.5	16, 6.3, 6.0	12, 5.0, 4.8	128
GW200220.124850	SEOBNRv4PHM (17, 12)	11, 4.8, 5.3	8.0, 3.8, 3.9	18, 6.2, 7.5	13, 4.9, 5.5	128

Table 7 continued.

Name	Waveform (visible frac.)	F_Q	$F_{\nu\bar{\nu}}$	F_{BZ}	F_{GW}	UL
GW200225_060421	IMRPhenomXPHM (16, 8)	97, 45, 40	224, 114, 107	33, 16, 14	53, 26, 24	236
GW200225_060421	SEOBNRv4PHM (22, 13)	71, 43, 47	174, 97, 102	25, 12, 12	43, 18, 20	236
GW200302_015811	IMRPhenomXPHM (15, 8)	62, 27, 26	60, 29, 29	62, 27, 26	53, 23, 22	162
GW200302_015811	SEOBNRv4PHM (20, 12)	66, 35, 35	58, 30, 30	54, 22, 21	48, 20, 18	162
GW200306_093714	IMRPhenomXPHM (28, 18)	133, 73, 67	113, 60, 56	19, 10, 9.7	24, 9.9, 9.1	146
GW200306_093714	SEOBNRv4PHM (25, 16)	132, 86, 82	102, 63, 61	20, 9.3, 8.1	23, 10, 9.5	146
GW200308_173609	IMRPhenomXPHM (18, 11)	51, 55, 51	24, 24, 22	74, 19, 12	7.3, 2.2, 2.2	192
GW200308_173609	SEOBNRv4PHM (14, 8)	71, 66, 67	32, 26, 25	13, 2.8, 3.3	4.7, 2.1, 2.1	192
GW200316_215756	IMRPhenomXPHM (21, 11)	112, 68, 62	*482, 258, 237	13, 6.3, 5.3	29, 10, 9.2	134
GW200316_215756	SEOBNRv4PHM (24, 15)	103, 45, 41	*484, 223, 205	10, 3.6, 3.2	28, 10, 9.1	134
GW200322_091133	IMRPhenomXPHM (14, 9)	147, 476, 499	72, 58, 64	42, 26, 27	8.7, 3.3, 3.7	154
GW200322_091133	SEOBNRv4PHM (4, 4)	3.7, 3.3, 0.22	2.0, 0.45, 0.17	4.8, 0.48, 0.37	0.77, 0.27, 0.26	154

Table 7 continued.